DATA-BASED BIFURCATION AND STABILITY ANALYSIS OF FEEDBACK-CONTROLLED LABORATORY EXPERIMENTS

DISSERTATION
zur
Erlangung des akademischen Grades
Doctor rerum naturalium
der Mathematisch-Naturwissenschaftlichen Fakultät
der Universität Rostock

vorgelegt von:
Anna DITTUS

Rostock, im Juni 2023

überarbeitete Fassung vom 19. Dezember 2023

https://doi.org/10.18453/rosdok_id00004538

Gutachter:
Prof. Dr. Jens Starke, Universität Rostock, Institut für Mathematik
Prof. Dr. Jan Sieber, University of Exeter,
College of Engineering, Mathematics and Physical Sciences

Jahr der Einreichung: 2023
Jahr der Verteidigung: 2023

ABSTRACT

Unstable equilibrium points and unstable periodic orbits are not observable by direct simulations or experimental time series of uncontrolled dynamical systems. Feedback control methods allow for finding and stabilizing unstable stationary points and periodic orbits. In this doctoral thesis, data-based methods applied to controlled systems are introduced and presented in order to gain stability information about the originally uncontrolled systems. Complete bifurcation diagrams can be obtained for simulated and laboratory experiments while keeping the noninvasive feedback control active. In particular, the knowledge about the bifurcation points' positions is of great interest in dynamical systems theory since bifurcation points indicate a possible change of qualitative behavior, e. g., a change of stability. Thus, a supplementary control is presented that uses the data-based stability information to continue the curve of bifurcation points for systems depending on an additional parameter. Laboratory experiments of the Zeeman catastrophe machine verify the realizability of the methods.

ZUSAMMENFASSUNG

Instabile Gleichgewichtspunkte und instabile periodische Orbits sind nicht durch direkte Simulationen oder experimentelle Zeitreihen ungeregelter dynamischer Systeme beobachtbar. Regelungsmethoden erlauben das Finden und Stabilisieren von instabilen stationären Punkten und periodischen Orbits. In dieser Dissertation werden datenbasierte Methoden eingeführt und präsentiert, die auf geregelte Systeme angewandt werden, um die Stabilitätsinformationen über das ursprünglich ungeregelte System zu gewinnen. Komplette Bifurkationsdiagramme können für Simulations- und Laborexperimente erhalten werden, während die nichtinvasive Regelung aktiviert bleibt. Insbesondere das Wissen über die Positionen der Bifurkationspunkte ist von großem Interesse für die Theorie dynamischer Systeme, da Bifurkationspunkte eine Änderung des qualitativen Verhaltens wie z. B. der Stabilität anzeigen. Daher wird eine ergänzende Regelung präsentiert, die die datenbasierte Stabilitätsinformation verwendet, um die Kurve der Bifurkationspunkte für Systeme zu berechnen, die von einem zusätzlichen Parameter abhängen. Laborversuche an der Zeemanschen Katastrophenmaschine bestätigen die Realisierbarkeit der Methoden.

ACKNOWLEDGMENTS

First of all, I thank my supervisor Jens Starke who always gave me a sympathetic hearing and who always had great advice and fascinating ideas on how to continue. The fruitful and open discussions kept me curious and made me believe in my abilities.
I would also like to thank the members of the group *Wissenschaftliches Rechnen*, Wolfram Just, Niklas Kruse, and Konstantinos Siettos, for their support and numerous intriguing discussions. In particular, I thank Wolfram for all his extensive, patiently repeated explanations and for pushing on ahead with the stroboscopic control, and Niklas, Konstantinos, and Hannes Wallner for the productive and friendly atmosphere in the office. And, of course, for all of your helpful feedback and proofreading.
I thank the group of Sylvia Speller for the great cooperation and for providing us with all the necessary knowledge about Atomic Force Microscopes (AFM). In particular, I thank Ingo Barke for constructing and repairing the Zeeman catastrophe machine whenever we asked for help. I thank Lukas Böttcher for the measurements at the AFM and for trying out the physical realizations of the theoretical ideas we came up with. This collaboration was also financially supported by the Deutsche Forschungsgemeinschaft (DFG) through the SFB 1270 (Electrically Active Implants) grant number 1270/2-299150580.
I thank my dear friend Maurin Graner for all the wonderful conversations. It helped so much to hear that I was not the only one struggling with the circumstances.
Especially, I thank my parents, Marianne and Hansjörg, for encouraging me the whole way. I know it is not a matter of course.
And last but not least, I want to express my biggest thanks to Olli whose patience is incredible. I thank you for supporting me during the whole time and for making me so happy.

CONTENTS

LIST OF FIGURES

LIST OF TABLES

1 INTRODUCTION

Motion in a physical system can often be described at least approximately by a mathematical rule for the evolution in state space. This rule is called a *dynamical system*. In many cases, e. g. the pendulum or Hooke's law for the motion of a spring, a mathematical model is available. These models concisely depict the system's state at each time, except for some small noise that could be modeled stochastically, too. For other physical systems, no explicit or precise mathematical description is available due to numerous reasons, e. g. missing information on parameter values or insufficient knowledge about the involved forces. Regardless of the accessibility of a mathematical description, dynamical processes occur.
States where no movement is happening, the *equilibrium* or *stationary points*, are of great interest for the analysis of dynamical systems. If a system has reached a stable stationary point, it will remain inside a small neighborhood for some time, even in case of small perturbations. However, small perturbations let the system drift away if the equilibrium point is unstable. Thus, when a dynamical system is not precisely initialized in an unstable stationary point, it will diverge from it. This fact inhibits the detection of unstable equilibrium points by uncontrolled performing or simulation. A well-established tool to gain information about unstable stationary states or their analog in Fourier space, periodic orbits, is to stabilize them by feedback control. In section 1.1, an overview of already existing feedback-control methods is given. In section 1.2, the necessary foundations of dynamical systems and control theory for the results in the following chapters are summarized.
Once a stationary point is stabilized, the stability information of the underlying uncontrolled dynamical system gets lost. The main aim of this dissertation is to stabilize unstable stationary states by feedback control and to detect the original stability of the underlying uncontrolled system for cases where no explicit mathematical equations are available or are hardly achievable, like in the case of laboratory experiments. In many cases, the right-hand side of the dynamical system $\dot{x} = f(x, \mu)$ is dependent on a parameter $\mu \in \mathbb{R}^m$. Hence, the parameter choice influences the qualitative behavior of the stationary points' position, number, and stability. Therefore, the equilibria's parameter dependence is essential for the following considerations. Since it is simple to implement, the proportional control combined with a state observer introduced in [88, 89] is extended such that stability analysis is also possible for unstable stationary states. The stability information of the underlying uncontrolled system can be gained by regulating the controlled system's stability by an additional control law for the first of the two control parameters. Since the second control parameter's sign depends on the equilibrium's original stability, it is not possible to follow the parameter-dependent curve of stationary points around folds. Hence, the gained stability information can serve to identify bifurcation points, investigate their neighborhood, and indicate the distance to bifurcations.

Another class of feedback-control methods is the proportional-derivative (PD) control respecting the derivative additionally to the system's state. Under certain controllability and stabilizability conditions on the system and control parameters, this method allows for following the curve of stationary points even around fold bifurcation points. In chapter 3, a least-squares approach is introduced to gain the original stability information out of the motion data of the PD-controlled system [26]. The applicability of the presented method is demonstrated in a real-life laboratory experiment on the example of the Zeeman catastrophe machine [123]. A comparison between the results for the physical laboratory system with the analytically gained information for the mathematical simulation shows the high reliability of the proposed method for physical systems with little noise.
The least-squares-based stability analysis is taken as a foundation for chapter 4. A second bifurcation parameter is varied by an additional control law based on the gained stability information. By forcing the system to have an eigenvalue with real part (close to) zero, the curve of bifurcation points can be traced. Again, the laboratory example of the Zeeman catastrophe machine demonstrates the method's applicability. Except for two singularities, the curve of bifurcation points has been followed for the simulated model and the physical machine. Also, for the physical machine first results have been obtained.
Besides the development and adaption of the mathematical methods and their algorithmic realization, the practical implementation in the laboratory experiment of the Zeeman machine was a major part of producing the results. The usual difficulties of real-life experiments like measurement noise, friction, and problems like data collection with electronic devices make the realization a major challenge for chapters 3 and 4.
The PD control presented in chapter 3 can also be applied to dynamical systems with periodic orbits. In Fourier space, the periodic orbits appear as stationary points. In chapter 5, this fact is used, and the PD control is applied to an Atomic Force Microscope (AFM) model. The derivative information with respect to time can only be gained by comparing values with a distance of integer multiples of the period. This was taken as a basis for the stroboscopic control of periodic orbits [27] in section 5.5, for which no indirect quantities are needed in contrast to the PD control. This provides new opportunities for challenging future work, especially for simulation models where at least precise numerical derivative information is available.
This dissertation concludes with a synopsis of the results and an outlook on possible further developments in chapter 6.
In appendix D, all variable names and quantities used within this work are summarized.

1.1 ESTABLISHED METHODS BASED ON FEEDBACK CONTROL

As already outlined, one of the general aims of this dissertation is to stabilize unstable states of dynamical systems by a control method. The methods used are based on feedback control since they use output information to adapt the control. That is why these methods are also called *closed-loop control*. This term is often used

to distinguish from *open-loop* or *feedforward control*, where no output information is applied. Furthermore, the herein-presented control methods are all *noninvasive*. This means the control signal vanishes in the original dynamical system's equilibrium point or periodic orbit. The noninvasiveness enables the exploration of the originally uncontrolled system's behavior, one of the major topics discussed in this thesis.
For physical systems usually exists neither an explicit mathematical description of the underlying dynamics nor further knowledge about the periodic orbits or the equilibria's time profile. Hence, methods not relying on one of these prerequisites are highly attractive in physical stabilizing setups.
One of the classes that use information about the state and the integral, the proportional-integral (PI) control methods, are the so-called *washout filter-aided feedback control methods* introduced by Abed et al. [1, 48, 62]. These methods stabilize unstable stationary states $x \in \mathbb{R}^n$ of the system $\dot{x} = f(x)$, $f : \mathbb{R}^n \to \mathbb{R}^n$, by the usage of a scalar control input u and a washout filter w, and can be written as

$$\dot{x} = Mx + Nu + h(x, u) \tag{1.1a}$$
$$\dot{w} = Q(x - w) \tag{1.1b}$$
$$u = K(x - w)\,, \tag{1.1c}$$

with the Jacobian M of the function f evaluated at a given point $\tilde{x}$, the derivative N of f with respect to u, a non-singular matrix Q, the feedback gain matrix K, and a higher-order term $h(\cdot, \cdot)$ with respect to x. The output signal gets filtered for the presented method, and its difference from the actual state is used as a control signal. According to linear stability theory, equilibria and periodic orbits can be stabilized by eq. (1.1) in the linear sense, if M is invertible and if (M, N) is stabilizable (def. 1.11); see [48].
The OGY method introduced by Ott, Gregobi, and Yorke in [78] follows a similar approach. The Poincaré section yields the information to kick the system into the desired direction. Even though using the Poincaré section needs only little knowledge about the dynamical processes, the required high measurement precision can cause problems in physical systems. The OGY method has been successfully applied to dynamical system, e. g. in [70] on a model of an AFM. Another approach to stabilize unstable periodic orbits was followed by Pyragas in [87] by using time-delayed feedback signal. Applications on experiments, e. g. on an oscillatory dissolution of nickel [60], show the practicality of this method.
The washout filter-aided feedback control's structure eq. (1.1) is similar to the one proposed by Pyragas et al. in [88, 89]. See [115] for the details of the similarities. The authors introduce a combination of a proportional control with a state observer of the form

$$\dot{x} = f(x, \mu) + \alpha_1 \cdot (y - x)$$
$$\dot{y} = \alpha_2 \cdot (y - x)\,.$$

Here, $\alpha_1,\ \alpha_2 \neq 0$ denote the scalar control parameters, $\mu \in \mathbb{R}$ is the bifurcation parameter, and $y \in \mathbb{R}$ is a dynamic variable representing the control target. In laboratory experiments, the values of the control parameters are bounded due to physical restrictions. This approach allows for adapting the control target during the control process. This method is the foundation for chapter 2. Due to its

simplicity and the possibility to track curves of equilibrium points that are either all stable or all unstable, this approach has been applied successfully in models [80, 102] and physical systems [79, 88]. For tracking the curve of stationary points around fold bifurcation points, switching the sign of the control parameter α_2 is necessary. Additionally, bifurcation points can only be found implicitly by tracking the stationary points around them.
A well-established method in numerical bifurcation analysis to overcome the problem of the singularity around a fold is the so-called *pseudo-arclength continuation* [28, 29, 58, 59]. An orthogonality condition adds one more dimension to the system of equations, which are then solved by a Newton method. Due to the orthogonality condition, the finally found new equilibrium point must be on a line perpendicular to the one connecting two previously found two equilibria.
In [102], Siettos, Maroudas, and Kevrekidis introduce a method combining the pseudo-arclength control with a feedback control law that drives a microscopically defined dynamical system to stationary states on a coarse scale. Thus, a bifurcation diagram of a macroscopic dynamical system can be produced with knowledge only about the microscopic dynamics.
The ideas presented in [87] served as an inspiration for the first work on *control-based continuation* in [100, 101] by Sieber, Krauskopf et al.; see also [93]. In [101], the authors propose combining a pseudo-arclength continuation with a PD control similar to extended time-delayed feedback control. This allows for tracking periodic orbits even around folds without further knowledge about the underlying dynamics. In the original work, no explicit feedback-control law is given since this is problem dependent, and no test model is given. Nevertheless, the control-based continuation was applied successfully in [100] on the continuation of periodic orbits through a saddle-node bifurcation point for a pendulum.
In [7], another approach to exploring bifurcation diagrams for laboratory experiments has been introduced. The authors propose to first estimate the position of the next equilibrium by a secant prediction in the (x, μ)-plane. The newly predicted parameter value for the stationary point allows for constructing an adequate feedback control on the dynamical system, which has an ω-limit point on the branch of the bifurcation diagram. Once the transients have settled, the reached state is assumed to be a (stabilized) equilibrium of the system.
All of the aforementioned works present feedback control methods for noninvasive stabilization of stationary points or periodic orbits. The introduced control schemes allow for determining bifurcation diagrams under certain controllability and observability conditions on the dynamical system. As mentioned above, chapters 2 to 4 are motivated to gain stability information about the underlying uncontrolled dynamical system. The methods presented in there make use of the above-cited ideas and approaches.

1.2 FOUNDATIONS IN DYNAMICAL SYSTEMS AND CONTROL THEORY

A *dynamical system* is a mathematical model whose rules describe the time evolution in a state space. The system is time-independent, which means that the evolution depends on the initial state but not on the initial time. Besides other notations of the

rule, the most common one is generated by an autonomous ordinary differential equation (ODE) or a system of ODEs

$$\frac{\mathrm{d}x}{\mathrm{d}t} = \dot{x}(t) = f(x(t)), \tag{1.2}$$

where $x \in \mathbb{R}^n$ is the state whose motions are described by the map $f : \mathbb{R}^n \to \mathbb{R}^n$. Note that the state $x = x(t)$ is dependent on the time t. For reasons of clarity, it will be denoted simply by x throughout this dissertation. Additionally, the symbol $\dot{x}$ denotes the derivative of x with respect to time.
The ODE (1.2) is autonomous in time and independent of the initial condition, while the solution of an initial value problem varies by these conditions. To distinguish between these two solutions, we will use the following definitions for the solution [41, 69, 118].

Definition 1.1 (Solution curve, trajectory, phase space, orbit)**.** *If a specific solution $\zeta : I \to \mathbb{R}^n$, $t \mapsto \zeta(t; t_0, x_0)$ on an interval $I \subset \mathbb{R}$ through the initial value x_0 is required, the system (1.2) becomes the initial value problem*

$$\frac{\mathrm{d}x}{\mathrm{d}t} = \dot{x}(t) = f(x), \quad x(t_0) = x_0. \tag{1.3}$$

The graph of a solution of eq. (1.3) *through x_0 is defined by $\{(t, \zeta(t; t_0, x_0)) \in \mathbb{R} \times \mathbb{R}^n | t \in I\}$ and called the* solution curve*. The* phase space *is the space in which the behavior of the variables $x_1, \ldots, x_n$ of $x = (x_1, \ldots, x_n) \in \mathbb{R}^n$ parametrized by the time t is described. The image set*

$$\{\zeta(t; t_0, x_0) \subset \mathbb{R}^n | t \in I\}$$

of a solution $\zeta(t; t_0, x_0)$ is called trajectory in phase space*. It is hence a curve in $\mathbb{R}^n$ parametrized by the function ζ and often named* orbit*.*

When a solution of the initial value problem (1.3) converges to a point or a set of points in forward or backward time, this point or set defines a limit. Determining of the origin and the destination of an orbit is one of the primary concerns in dynamical systems theory. Thus, we will define these sets following [41, 51, 118].

Definition 1.2 (ω/α-limit points and sets)**.** *A point $y \in \mathbb{R}^n$ is called the* ω-limit point *of a solution $\zeta(t; t_0, x_0)$ of eq.* (1.3) *if a time sequence $t_n \to \infty$ as $n \to \infty$ exists and if*

$$\lim_{n\to\infty} \zeta(t_n; t_0, x_0) = y.$$

A point $z \in \mathbb{R}^n$ is called the α-limit point *of a solution $\zeta(t; t_0, x_0)$ of eq.* (1.3) *if a time sequence $t_n \to -\infty$ as $n \to \infty$ exists and*

$$\lim_{n\to\infty} \zeta(t_n; t_0, x_0) = z.$$

The corresponding ω-limit set *consists of all ω-limit points of the solution $\zeta(t_n; t_0, x_0)$, and is hence the sample of points a solution converges to in positive time. Analogously, the* α-limit set *consists of all the points a solution converges to in negative time.*

1.2.1 *Equilibrium points, fixed points, periodic orbits, and stability*

One of the main topics in the following chapters is the position of a dynamical system's equilibrium points and its properties. In many application scenarios, it is of great interest to find the points where the system is stationary, i. e. where the state has no motion ($\dot{x} = 0$) [42, 118].

Definition 1.3 (Equilibrium point, stationary point)**.** *A point $\bar{x}$ is called the* equilibrium point *or the* stationary point *of the dynamical system (1.2) if it holds $f(\bar{x}) = 0$, i. e., $\zeta(t; t_0, \bar{x}) = \bar{x}$ for all $t \in I$.*

As already pointed out, stability is the main object for the consideration of stationary solutions within this dissertation. Throughout the whole work, we will use the definition following those in [42, 118].

Definition 1.4 (Stable, asymptotically stable, and unstable equilibrium points)**.** *An equilibrium point $\bar{x}$ of the system (1.2) is said to be* stable *if for the solution $\zeta(t; t_0, x_0)$ of eq.* (1.2) *and for any given $\epsilon > 0$, there exists a $\delta > 0$ such that*

$$\|x_0 - \bar{x}\| < \delta \Longrightarrow \|\zeta(t; t_0, x_0) - \bar{x}\| < \epsilon\,,$$

for all $t \geq t_0$. The equilibrium $\bar{x}$ is called asymptotically stable *if $\bar{x}$ is stable, if additionally there exists an $r > 0$, and if it satisfies*

$$\|\zeta(t; t_0, x_0) - \bar{x}\| \to 0$$

for $t \to \infty$ and all initial points x_0 satisfying $\|x_0 - \bar{x}\| < r$. If a stationary point $\bar{x}$ is not stable, it is called unstable*.*

Note that in many textbooks, equilibrium points are called "fixed points". Throughout the dissertation, the term *fixed point* is taken in the discrete-time sense following the definition according to [51, 61].

Definition 1.5 (Fixed point)**.** *Let $x_{k+1} = F(x_{k+1})$, x_k, $x_{k+1} \in \mathbb{R}^n$, $F : \mathbb{R}^n \to \mathbb{R}^n$ be a discrete-time dynamical system. Then the point x_* is called a fixed point of $F(x)$ if $f(x_*) = x_*$ holds for all time $t \in I$.*

Analogously to the stationarity of solutions exists the periodicity of orbits. If the values of a solution $\zeta(t; t_0, x_0)$ repeat after a certain period, the solution and hence its orbit are periodic [42, 118].

Definition 1.6 (Periodic solution, periodic orbit, limit cycle)**.** *A solution $\zeta(t; t_0, x_0)$ of eq.* (1.2) *is called a* periodic solution of period T*, with $T > 0$, if $\zeta(t + T; t_0, x_0) = \zeta(t; t_0, x_0)$ for all $t \in I$. If it holds $\zeta(t; t_0, x_0) \neq x_0$ for $0 < t < T$, then T is the* minimal period*. A* periodic orbit of period T *is the orbit $\{\zeta(t; t_0, x_0) | t \in I\}$ of a periodic solution $\zeta(t; t_0, x_0)$ with period T. The periodic orbit, which is the α- or ω-limit set for all points on nearby orbits, is called the* limit cycle*.*

In the general defs. 1.1, 1.3, 1.5 and 1.6, no assumptions were made on the time interval $I \subset \mathbb{R}$. We will assume $I = \mathbb{R}$ in the following chapters.

1.2.2 *Linearization of dynamical systems*

Heretofore, the function f describing the motion of the state x in the dynamical system (1.2) was assumed to be nonlinear. Since nonlinear behavior is difficult to analyze, one of the principal aims for many techniques in analysis and numerics, e. g. derivative and difference quotient, is to describe the behavior locally by a linear approximation. This idea is used for stability, and further *linear stability*, too. Using the stationarity condition $f(\bar{x}) = 0$, the dynamical system (1.2) can be approximated in the neighborhood of the stationary point $\bar{x}$ by the linearized form

$$\dot{(\delta x)} = Df(\bar{x}) \cdot \delta x \quad \text{and} \quad \delta x = x - \bar{x}\,, \tag{1.4}$$

where $Df(\bar{x})$ denotes the Jacobian matrix of f at the stationary point $\bar{x}$ [42, 69] and δx is a notation for the vectors of the tangent space at the point $\bar{x}$. The Jacobian Df can be used to classify those equilibrium points that are either stable or unstable, the so-called *hyperbolic equilibrium points* [61, 69, 118].

Definition 1.7 (Hyperbolic equilibrium point)**.** *If all the eigenvalues of the Jacobian $Df(\bar{x})$ in the stationary point $\bar{x}$ have nonzero real parts, $\bar{x}$ is called a* hyperbolic equilibrium point.

Note that their name comes from the hyperbola-like shape of the phase flow in their neighborhood in the planar case. For higher dimensions, this does not hold, and the term *hyperbolic* is misleading but still standard.
The linearization (1.4) is of great interest concerning the system (1.2)'s stability since the eigenvalues of the Jacobian Df yield the necessary information [42].

Theorem 1.1. *Let $\bar{x}$ be a hyperbolic equilibrium point of the system (1.2), and let f be a C^1 function. If all the eigenvalues of the Jacobian $Df(\bar{x})$ at the point $\bar{x}$ have negative real parts, then $\bar{x}$ is asymptotically stable. If at least one eigenvalue has a positive real part, the equilibrium point $\bar{x}$ is unstable.*

A proof of thm. 1.1 requires the Taylor expansion

$$\dot{x} = Df(\bar{x}) \cdot x + g(x)$$

with a function $g : \mathbb{R}^n \to \mathbb{R}^n$ containing higher-order terms. Since the Taylor expansion is a local approximation, there always exists a neighborhood around the equilibrium point where the dynamics are governed by the ODE $\dot{x} = Df(\bar{x}) \cdot x$ as long as the eigenvalues have a nonvanishing real part. See [42] for further details. The equivalence of the dynamical system and its linearization in the neighborhood around hyperbolic equilibrium points was found independently by Hartman and Grobman [38, 47].

Theorem 1.2 (Hartman-Grobman, 1959/1960)**.** *At a hyperbolic equilibrium point $\bar{x}$, the nonlinear system (1.2) is topologically equivalent to its linearization (1.4), i. e., there exists a homeomorphism $h : \mathbb{R}^n \to \mathbb{R}^n$ mapping orbits of eq.* (1.2) *onto orbits of eq.* (1.4) *under preservation of the direction of time.*

With the result of thm. 1.2, one needs to only consider the eigenvalues' real parts of $Df(\bar{x})$. If all have negative signs, it can be shown by the Mean Value Theorem for the norm of g and Gronwall's inequality [9, 39] that $\|x(t)\| \to 0$ for $t \to \infty$. For one eigenvalue with a positive real part, it can be shown that no constant exists for a finite estimate of $\|x(t)\|$ when $t \to \infty$. For a detailed proof of thm. 1.1, see, e. g., [42, Chapter 9, 51, Chapter 9]. Similar to thm. 1.1, the following result for fixed points of discrete-time systems is known.

Theorem 1.3. *Suppose x_* is a fixed point of the discrete-time system $x_{k+1} = F(x_k)$. Let $DF(x_*)$ denote the Jacobian of $F(x)$ evaluated at the point x_*. Then the fixed point x_* is asymptotically stable if for all eigenvalues $\nu_1, \nu_2, \ldots, \nu_n$ of $DF(x_*)$ holds $|\nu_j| < 1$ with $j = 1, \ldots, n$.*

In [61, Chapter 1], this theorem and further details on fixed points can be found.

1.2.3 *Bifurcation*

A dynamical system's rule can depend not only on time but also on additional quantities. We extend the dynamical system (1.2) by a so-called *bifurcation parameter* $\mu \in \mathbb{R}^k$, and consider from now on the system

$$\frac{\mathrm{d}}{\mathrm{d}t}x(t) = \dot{x}(t) = f(x(t), \mu) \tag{1.5}$$

where $f : \mathbb{R}^n \times \mathbb{R}^k \to \mathbb{R}^n$, $(x, \mu) \mapsto f(x, \mu)$. If the parameter μ is perturbed, the phase portrait changes, too. From the viewpoint of stability, the changes in the topological equivalence of the perturbed system yield the necessary information [61].

Definition 1.8 (Bifurcation point)**.** *Let $(\bar{x}, \bar{\mu})$ be an equilibrium point of the system (1.5). If there exist nonequivalent phase portraits, i. e., partitionings of the state space into orbits, for any small perturbation in $\bar{\mu}$, the point $(\bar{x}, \bar{\mu})$ is called a* bifurcation point.

Throughout this dissertation, we consider a specific type of so-called *codimension-one bifurcations* where the system (1.5) for $\mu = \bar{\mu} + \delta$ for small perturbations δ folds into two topologically nonequivalent systems. See also [15, Chapter 7] for the following observations. To simplify the subsequent considerations and to avoid heavy technical notation, we focus on the case $x, \mu \in \mathbb{R}$. If no local continuation of $f : \mathbb{R}^2 \to \mathbb{R}$ at the bifurcation point $(\bar{x}, \bar{\mu})$ is possible, then according to the Implicite Function Theorem, $\partial_x f(\bar{x}, \bar{\mu}) = 0$ is a necessary condition for a bifurcation point of the system (1.5). Here and throughout the dissertation,

$$\partial_x f(z) \coloneqq \frac{\partial f}{\partial x}(z)$$

denotes the partial derivative of f with respect to x evaluated at the point z. For reasons of legibility, it is often used the short form $\partial_x f$ where no evaluation at a specific point is meant. Furthermore, f is assumed to have no other degeneracies, so it must hold

$$\partial_\mu f(\bar{x}, \bar{\mu}) \neq 0 \quad \text{and} \quad (\partial_x(\partial_x f))(\bar{x}, \bar{\mu}) \neq 0\,.$$

On the branch $x(\mu)$ of equilibria, the vector field vanishes since $f(x,\mu) = 0$ holds for stationary points. Differentiating $f(x,\mu) = 0$ with respect to x yields

$$\partial_x f(\bar{x},\bar{\mu}) + \partial_\mu f(\bar{x},\bar{\mu}) \cdot \frac{\mathrm{d}\mu}{\mathrm{d}x} = 0\,,$$

and hence

$$\frac{\mathrm{d}\mu}{\mathrm{d}x} = 0$$

at the bifurcation point. The second differentiation of $f(x,\mu) = 0$ with respect to x results in

$$\begin{aligned}\left(\partial_x(\partial_x f)\right)(\bar{x},\bar{\mu}) + 2\,\left(\partial_x(\partial_\mu f)\right)(\bar{x},\bar{\mu}) \cdot \frac{\mathrm{d}\mu}{\mathrm{d}x} \\ + \left(\partial_\mu(\partial_\mu f)\right)(\bar{x},\bar{\mu}) \cdot \left(\frac{\mathrm{d}\mu}{\mathrm{d}x}\right)^2 + \partial_\mu f(\bar{x},\bar{\mu}) \cdot \frac{\mathrm{d}^2\mu}{\mathrm{d}x^2} = 0\,,\end{aligned}$$

and so

$$\frac{\mathrm{d}^2\mu}{\mathrm{d}x^2} = -\frac{\left(\partial_x(\partial_x f)\right)(\bar{x},\bar{\mu})}{\partial_\mu f(\bar{x},\bar{\mu})}\,. \tag{1.6}$$

These bifurcation points are often called *nonhyperbolic equilibrium points with quadratic degeneracy* because only the second derivative eq. (1.6) yields information about the type of equilibria. Even though the bifurcations are assumed to have codimension one, throughout the following chapters, the system (1.5) can have one more dimension for $\dot{x}$, the derivative of x with respect to time. Since $\dot{x} = 0$ is a necessary condition for all equilibrium points, all stationary points for the 3-dimensional state $(x,\dot{x},\mu)^T \in \mathbb{R}^3$ of eq. (1.5) lie in the plane with $\dot{x} = 0$, the bifurcation diagram is again 2-dimensional. According to thm. 1.1, an eigenvalue, or a couple for higher dimensions, of the Jacobian $Df(\bar{x})$ of f with zero real part is a necessary condition for an equilibrium $\bar{x}$ to be a bifurcation point. Since the two equilibrium points $(\tilde{x}_1,\bar{\mu}+\delta)$ and $(\tilde{x}_2,\bar{\mu}+\delta)$ collide into a saddle and a node in the point $(\bar{x},\bar{\mu})$ for $\delta \to 0$, the aforementioned bifurcation is called *fold* or *saddle-node* bifurcation [61]. Moreover, a specific case with two saddle-node bifurcation points with bifurcation parameters μ_1 and μ_2 is of great interest for the following chapters. In this case, for bifurcation-parameter values $\mu \in [\mu_1,\,\mu_2]$, two stable equilibrium points and a branch of unstable equilibrium points connecting the two bifurcation points exist. The one-dimensional cubic normal form, used as an example for illustration in chapter 2, has the following form

$$\dot{x} = f(x,\mu) = \mu + x - x^3\,, \quad x,\,\mu \in \mathbb{R}\,. \tag{1.7}$$

A point $(\bar{x},\bar{\mu})$ needs to fulfill $f(\bar{x},\bar{\mu}) = 0$ to be an equilibrium point. Hence, the system (1.7) has the equilibrium points $(\bar{x},\bar{\mu})$ with $\bar{\mu} = \bar{x}^3 - \bar{x}$. According to its definition, a bifurcation point is neither stable nor unstable since it is topologically nonequivalent to the equilibrium points in its neighborhood. In order to find the bifurcation points, one needs to investigate the derivative of f with respect to x. It is

$$\partial_x f = 1 - 3x^2\,.$$

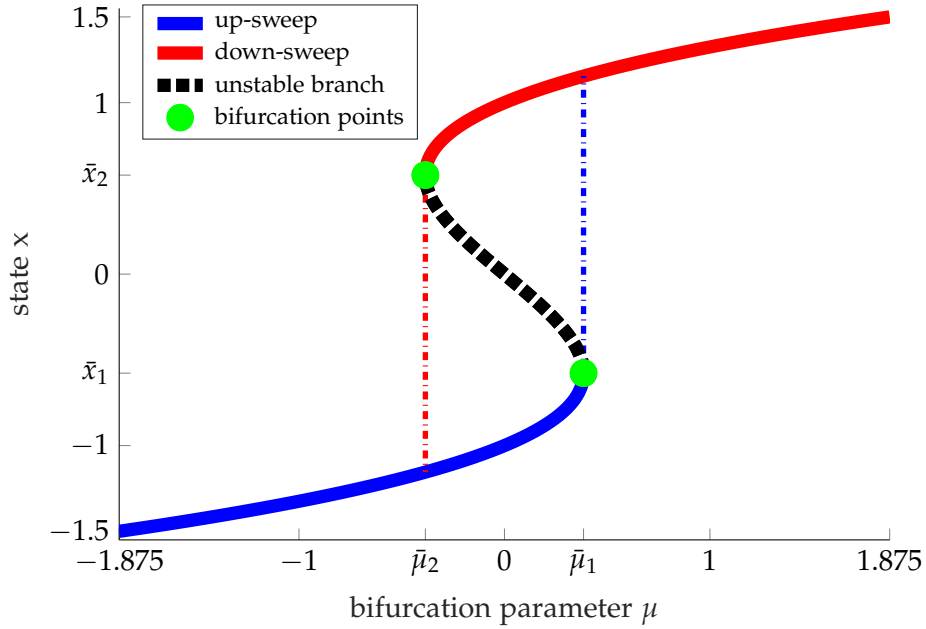

Figure 1.1: Bifurcation diagram of the normal form (1.7). Solid curves mark stable equilibrium points, the green dots illustrate the bifurcation points $(\bar{x}_1, \bar{\mu}_1)$ and $(\bar{x}_2, \bar{\mu}_2)$, and the dashed lines indicate the position of the unstable stationary points.

So, the system has one stable equilibrium point for $\mu < -\sqrt{2/3}$ and $\mu > \sqrt{2/3}$, two equilibria for $\mu = \pm\sqrt{2/3}$ where one is asymptotically stable and one with $\partial_x f(\bar{x}) = 0$, and two stable and one unstable equilibrium point for $\mu \in \left(-\sqrt{2/3}, \sqrt{2/3}\right)$. These two stationary points with $\partial_x f = 0$ are nonhyperbolic equilibrium points. The linearizations of eq. (1.5) are topologically nonequivalent to linearizations in the neighborhood since even small perturbations in $\bar{\mu}$ change the sign of $\partial_x f$ to be either positive or negative. According to thm. 1.2, these equilibrium points are topologically nonequivalent to their surrounding stationary points and hence bifurcation points.
A usual way to visualize the system (1.5)'s dependence on the bifurcation parameter μ is a so-called *bifurcation diagram*. For each value of μ, the corresponding equilibria are plotted. The branch of stable stationary points is a solid curve, whereas the branch of unstable equilibrium points is a dashed line. Note that $\bar{x}(\bar{\mu})$ is not a well-defined function for eq. (1.7) while changing the dependencies allows for finding the equilibrium points $(\bar{x}, \bar{\mu})$ by a function $\bar{\mu}(\bar{x})$. In fig. 1.1 the bifurcation diagram of the normal form (1.7) is shown for illustration.

1.2.4 *Stabilizability, controllability, and observability of dynamical systems*

According to thm. 1.1, a sufficient condition for a linear dynamical system or control system to be stable in the stationary point $\bar{x}$ is that all eigenvalues of the linearization matrix Df in $\bar{x}$ have negative real parts. A common approach to guarantee the stability of a controlled equilibrium point is to test whether all roots of the characteristic polynomial of Df have negative real parts. For the 2-dimensional case, $\mathrm{tr}(Df) < 0$ and $\det(Df) > 0$ are, in combination, sufficient conditions for the

negativity of all eigenvalues' real parts. Alternatively, it is sufficient if all coefficients of the characteristic polynomial are negative. For the higher dimensional case, these conditions require replenishment. Routh and Hurwitz [52, 95] independently found the following criterion, which allows for determining the signs of the roots even for dimensions larger than two.

Theorem 1.4 (Routh-Hurwitz criterion)**.** *The polynomial*

$$p(\nu) = a_n \nu^n + a_{n-1}\nu^{n-1} + \cdots + a_0 \tag{1.8}$$

is a Hurwitz polynomial if all roots ν of eq. (1.8) *have negative real parts. This is fulfilled if $a_n > 0$ and if the* Hurwitz determinant

$$H = \begin{vmatrix} a_{n-1} & a_n & 0 & 0 & \cdots & \cdots \\ a_{n-3} & a_{n-2} & a_{n-1} & a_n & \cdots & \cdots \\ a_{n-5} & a_{n-4} & a_{n-3} & a_{n-2} & \cdots & \cdots \\ a_{n-7} & a_{n-6} & a_{n-5} & a_{n-4} & \cdots & \cdots \\ \vdots & \vdots & \vdots & \vdots & \ddots & a_2 \\ 0 & 0 & \cdots & \cdots & 0 & a_0 \end{vmatrix}$$

and all its north-western minors are positive.

Note that standardization to $a_n = 1 > 0$ is always possible by dividing the original Hurwitz polynomial (1.8) by $a_n \neq 0$.
In the following chapters, we consider control systems Σ for the state $v \in \mathbb{R}^n$ with the *input vector* $u \in \mathbb{R}^m$ of the following form:

$$\Sigma: \quad \dot{v} = \mathsf{C}v(t) + \mathsf{D}u(t)\,, \quad v(t_0) = v_0\,, \tag{1.9}$$

with the state matrix $\mathsf{C} \in \mathbb{R}^{n\times n}$, the input matrix $\mathsf{D} \in \mathbb{R}^{n\times m}$, and the initial value v_0. Often, the system Σ in eq. (1.9) is written as (C, D), which is the case in the following. The input vector u is also known as the *control vector*. The sans-serif notation C, D, and R is chosen for the matrices related to controllability for the visible distinction between the input matrix D and the Jacobian Df.
In control theory, the system (1.9) is said to be a *linear time-invariant* (LTI) system since the matrices C and D are constant over time, and since the time-dependent system functions $v(t)$ and $u(t)$ are no direct functions of time, i. e., they do not depend on the initial time t_0. The system shows the same behavior for the same input at any time. Throughout the following chapters, except for section 5.5, a linearized system of the form (1.9) is assumed to be time-invariant.
When control is applied to a dynamical system, usually the aim is to bring the system to a desired behavior or state; for details, see, e. g., [104]. If a controlled system eq. (1.9) can be brought to any target inside the region of interest, it is *controllable* according to the following definition [68, 104].

Definition 1.9 (Controllability)**.** *A system Σ is* controllable *if it can be moved by an adequate input with $u(t_0) = u_0$ from any initial state v_0 to any final state in finite time. Another term for this system property is* complete state controllability *in order to emphasize the aim of controlling the state.*

Usually, controllability is scrutinized together with its dual, the observability, which is defined as follows [68].

Definition 1.10 (Observability)**.** *A system is called* observable *if the initial state v_0 can be determined by the input $u(t)$ and the measured output signal over a finite time interval $[0, t_e]$.*

Since the herein-mentioned experimental measurements allow accessing directly or, precisely enough, indirectly the desired quantities, observability is assumed for the presented methods. In cases where observability cannot be guaranteed or realized, further considerations could be necessary before applying the control techniques.
Analogously to testing for stability like thm. 1.4, there exist several theorems stating conditions for the controllability of LTI systems. Besides e. g. the so-called *Controllability Gramian* (see, e. g., [68]), a simpler condition concerning the rank was found by Kalman [57].

Theorem 1.5 (Kalman rank criterion)**.** *The system eq.* (1.9) *has the* controllability matrix

$$\mathsf{R} = \left[\begin{array}{c|c|c|c|c} \mathsf{D} & \mathsf{CD} & \mathsf{C}^2\mathsf{D} & \dots & \mathsf{C}^{n-1}\mathsf{D} \end{array} \right] \in \mathbb{R}^{n\times(n\cdot m)} . \tag{1.10}$$

The pair (C, D) of the system (1.9) is controllable if and only if

$$\mathit{rank}(\mathsf{R}) = n ,$$

i. e. if the controllability matrix has full rank.

The proof of thm. 1.5 uses the fact that the initial condition $v(t_0) = v_0$ of the solution

$$v(t_e) = e^{\mathsf{C}t_e} v_0 + \int_{t_0}^{t_e} e^{\mathsf{C}(t_e-\tau)} \mathsf{D} u(\tau) \mathrm{d}\tau$$

of eq. (1.9) has the exponential matrix representation

$$\begin{aligned} -v_0 &= \mathsf{C} \int_{t_0}^{t_e} u(\tau)\mathrm{d}\tau - \mathsf{CD} \int_{t_0}^{t_e} \tau u(\tau)\mathrm{d}\tau + \mathsf{C}^2\mathsf{D} \int_{t_0}^{t_e} \frac{\tau^2}{2!} u(\tau)\mathrm{d}\tau - \dots \\ &= \mathsf{C}u_0 + \mathsf{CD}u_1 + \dots + \mathsf{C}^n\mathsf{D}u_n + \mathsf{C}^{n+1}\mathsf{D}u_{n+1} + \dots , \end{aligned} \tag{1.11}$$

where

$$u_j = (-1)^j \int_{t_0}^{t_e} \frac{\tau^j}{j!} u(\tau)\mathrm{d}\tau \quad \text{for } j = 0,\, 1,\, 2,\, \dots .$$

Only if $\operatorname{span}\left\{\mathsf{C}, \mathsf{CD}, \mathsf{C}^2\mathsf{D}, \dots, \mathsf{C}^n\mathsf{D}, \mathsf{C}^{n+1}\mathsf{D}, \dots\right\} = \mathbb{R}^n$ holds, an arbitrary initial vector $v_0 \in \mathbb{R}^n$ fulfills eq. (1.11). By the Cayley-Hamilton theorem [20, 43–45] (proven completely by Frobenius [33]), every regular quadratic matrix fulfills its own characteristic equation. Hence, it suffices to consider the first n terms in eq. (1.11) to investigate the representability of v_0 in the form (1.11).
An analog result to thm. 1.5 and the *Gilbert criterion* [34] is the *Popov-Belevitch-Hautus test* [8, 50, 84], also known as the *Hautus test*.

Theorem 1.6 (Popov-Belevitch-Hautus test)**.** *Let* $\mathsf{C} \in \mathbb{R}^{n\times n}$ *and* $\mathsf{D} \in \mathbb{R}^{n\times m}$*. Then the following statements are equivalent:*

1. *The pair* (C, D) *is controllable.*
2. *It holds rank* $\left(\left[\begin{array}{c|c} sI - \mathsf{C} & \mathsf{D} \end{array}\right]\right) = n$ *for all* $s \in \mathbb{C}$*.*
3. *It holds rank* $\left(\left[\begin{array}{c|c} sI - \mathsf{C} & \mathsf{D} \end{array}\right]\right) = n$ *for all eigenvalues* $s \in \mathbb{C}$ *of* C*.*

The proof of thm. 1.6 uses the linear independence of the n rows of the controllability matrix eq. (1.10). If this was not the case, a row vector w^T would exist perpendicular to R. This vector w^T would then be orthogonal, particularly to D, and must be a left eigenvector of C. So, no eigenvector of C must be perpendicular to D in order to guarantee controllability. Further details about thms. 1.5 and 1.6 and their proofs can be found, e. g. in [68, 104].
The Popov-Belevitch-Hautus test is preferred to the Kalman condition in many applications since it also provides information about the uncontrollable eigenvalues and their corresponding modes [68]. Nevertheless, we use the Kalman condition due to the minor size of the matrix R that needs to be computed for validation of controllability.
A slightly weaker condition than controllability is stabilizability [68].

Definition 1.11 (Stabilizability)**.** *A system* Σ *is* locally stabilizable *if all uncontrollable state variables are asymptotically stable, i. e. , the linearization matrix of* Σ *in all stationary points has only eigenvalues with negative real parts. Then, the nonlinear system* Σ *is also stabilizable by the control part linearized by* $\mathsf{D}u$ *in* Σ*.*

This means that the second and the third statement of thm. 1.6 must hold for $s \in \mathbb{C}$ with $\Re(s) \geq 0$ if the system Σ is stabilizable. From this definition, it becomes clear that the controllability of a system implies stabilizability. Or in other words, if a system Σ is controllable, the controlled stationary states are stable.
The discrete-time analog of the Routh-Hurwitz criterion (thm. 1.4) is the *Jury stability criterion* for fixed points. In [56], Jury gives several rules that must be satisfied to guarantee stability. For the 2-dimensional case, they can be summarized by the following rules.

Theorem 1.7 (Jury criterion, 2-dimensional case)**.** *Let*

$$q(\nu) = b_2\nu^2 + b_1\nu^1 + b_0 \tag{1.12}$$

be the characteristic polynomial of the Jacobian DF of the right-hand side of the discrete-time system $x_{k+1} = F(x_k)$ *in the fixed point* $x_* \in \mathbb{R}^2$*. Then* x_* *is stable, i. e., all roots of eq.* (1.12) *lie inside the unit circle if*

$$\det(DF(x_*)) < 1 \quad \textit{and} \quad |tr(DF(x_*))| < 1 + \det(DF(x_*))\,.$$

2

STABILITY ESTIMATION BY PROPORTIONAL CONTROL WITH STATE OBSERVER

As shown in section 1.1, the choice of the feedback-control method depends on the prerequisites and the problem itself. Besides stability criteria, the simplicity and the number of prerequisites to apply the control are decisive for the method of choice. This makes the class of proportional-feedback control methods highly attractive for systems where information about the underlying dynamics is rarely known.
In the following, we will consider the dynamical system

$$\dot{x} = f(x, \mu) \tag{2.1}$$

with the state $x \in \mathbb{R}$ whose vector field $f : \mathbb{R} \to \mathbb{R}$ depends on the bifurcation parameter $\mu \in \mathbb{R}$. We assume that, for a fixed parameter value $\bar{\mu}$, there exists at least one stationary point $\bar{x} \in \mathbb{R}$ of the system eq. (2.1). Under certain conditions [53], the point $\bar{x}$ is an asymptotically stable stationary point of the closed-loop system

$$\dot{x} = f(x, \bar{\mu}) + \alpha_1 \cdot (y - x)\,, \tag{2.2}$$

with the control parameter $\alpha_1 \in \mathbb{R}\backslash\{0\}$ and the target $y \in \mathbb{R}$. Here, the difference between the system's state x and the target y affects the system's dynamics proportionally. Even though the control's structure is simple and requires no further knowledge about the dynamics, finding the right target y can be challenging since the equilibrium's position $(\bar{x}, \bar{\mu})$ is generally unknown. Only if the position $\bar{x}$ corresponding to $\bar{\mu}$ is known a priori or reached the proportional feedback control is noninvasive, i. e. vanishes at a stationary state $\bar{x}$. Barton and Sieber [7] propose to adapt the bifurcation parameter $\bar{\mu}$ and the control target y on a line perpendicular to the linear prediction defined by the two previously found equilibrium points. See [28, 29, 58, 59] and section 1.1 for pseudo-arclength continuation. This allows for tracking noninvasively the branch of stationary points even around fold bifurcation points.

2.1 PROPORTIONAL CONTROL WITH STATE OBSERVER

For cases where the control target y for the proportional feedback control in eq. (2.2) is unknown, Pyragas et al. present in [88, 89] a method similar to the washout filter-aided feedback control [1, 48, 62]. The method introduced by Pyragas combines the proportional control with a state observer $\alpha_2 \cdot (y - x)$ with $\alpha_2 \in \mathbb{R}\backslash\{0\}$ such that

$$\dot{x} = f(x, \mu) + \alpha_1 \cdot (y - x) \tag{2.3a}$$

$$\dot{y} = \alpha_2 \cdot (y - x)\,. \tag{2.3b}$$

In eq. (2.3b), the target is adapted proportionally to the distance between the system's state x and the actual target y. This allows finding the equilibrium point $\bar{x}$

for a fixed parameter value $\bar{\mu}$. The proportional control combined with the state observer (2.3) has also been applied successfully in laboratory experiments like, e. g. oscillatory electrodissolution of nickel [88] or a pedestrian evacuation scenario [80]. The stationary points of the original dynamical system (2.1) and the proportionally controlled system (2.3) are the same in the following sense: If $\bar{x}$ is a stationary point of eq. (2.1), it is $\dot{x} = 0 = f(\bar{x}, \bar{\mu})$. Furthermore, let the target $\bar{y}$ be identical to $\bar{x}$. Then, $\dot{y} = \alpha_2 \cdot 0$, and so $(\bar{x}, \bar{y})$ must be a stationary point of eq. (2.3). If reversely $(\bar{x}, \bar{y})$ is an equilibrium point of eq. (2.3), it holds $\dot{y} = 0$, and hence $(\bar{y} - \bar{x}) = 0$. Then $\dot{x} = 0 = f(\bar{x}, \bar{\mu}) + \alpha_1 \cdot 0 = f(\bar{x}, \bar{\mu})$, which is the sufficient condition for $\bar{x}$ to be an equilibrium of eq. (2.1). Since the control (2.3b) vanishes at an equilibrium point of eq. (2.1), the proportional control with the state observer is noninvasive.

2.1.1 *Controllability and observability of the proportional control with state observer*

Before stating the conditions for controllability of the dynamical system (2.1) with the proportional control with the state observer (2.3), we consider the linearization around the stationary point $(\bar{x}, \bar{y})$. We assume that the dynamics described by eq. (2.3) and written as

$$\dot{z} = h(z) = \frac{\mathrm{d}}{\mathrm{d}t} \begin{pmatrix} x \\ y \end{pmatrix} \quad \text{with z=(x,y)} \tag{2.4}$$

can be approximated sufficiently well by a linearization in each point of the neighborhood of $(\bar{x}, \bar{y})$. For this neighborhood, we introduce the notation

$$\delta z = z - \bar{z}\,,$$

which describes the vectors in the tangential space at the point $\bar{z} = (\bar{x}, \bar{y})$ and can be seen as a shift of the origin. The linearization of eq. (2.4) is then

$$(\dot{\delta z}) = Dh(\bar{z}) \cdot \delta z = \begin{pmatrix} \partial_x f(\bar{z}) - \alpha_1 & \alpha_1 \\ -\alpha_2 & \alpha_2 \end{pmatrix} \cdot \delta z, \tag{2.5}$$

where $\partial_x f$ is the partial derivative of f with respect to x, and $Dh\,(\bar{z}) \in \mathbb{R}^{2\times 2}$ is the Jacobian of h in the point $\bar{z} = (\bar{x}, \bar{y})$. Note that the value of the bifurcation parameter μ is constant during the whole control of one stationary point. The results from control theory for continuous so-called linear time-invariant systems (LTI) [104] can be applied to state controllability conditions of the controlled system (2.3). We have the 1-dimensional control $u := y - x$ for the system

$$\dot{v} = \mathsf{C}v(t) + \mathsf{D}u(t)\,,$$

with the state vector

$$v := \begin{pmatrix} x \\ y \end{pmatrix} \in \mathbb{R}^2\,,$$

the input matrix

$$\mathsf{D} := \begin{pmatrix} \alpha_1 \\ \alpha_2 \end{pmatrix} \in \mathbb{R}^2\,,$$

and the state matrix

$$C := \begin{pmatrix} \partial_x f & 0 \\ 0 & 0 \end{pmatrix} \in \mathbb{R}^{2\times 2}.$$

The resulting controllability matrix (see [104] and section 1.2) is

$$R = \left[\begin{array}{c|c} D & CD \end{array}\right] = \begin{pmatrix} \alpha_1 & \alpha_1 \cdot \partial_x f \\ \alpha_2 & 0 \end{pmatrix}. \tag{2.6}$$

Here, and throughout the whole chapter, the short form $\partial_x f$ of the partial derivative of f with respect to x will be used wherever the evaluation point is clear from the context. The results for LTI include that the system (2.3) is controllable if the controllability matrix (2.6) has full rank. This is fulfilled when $\alpha_1 \neq 0$, $\alpha_2 \neq 0$, and $\partial_x f \neq 0$. Hence, eq. (2.3) is controllable if for all $\bar{z}$ holds $\partial_x f(\bar{z}) \neq 0$, and if $\alpha_1 \neq 0$ and $\alpha_2 \neq 0$ can be found accordingly. Theoretically, the system (2.3) is controllable for all points $\bar{z}$ except for bifurcation points since $\partial_x f(\bar{z}) = 0$ is a necessary condition for a linear bifurcation. Due to physical limits, further restrictions on the values for the control parameters hold for laboratory experiments.
For the state feedback applied in eq. (2.3), the full state $v = (x, y)$ is assumed to be available, i. e., the full state can be constructed from the measurements or computed values of the output. Hence, the system (2.3) is considered to be fully observable.

2.1.2 *Stabilization of the proportional control with state observer*

In order to estimate the control gains α_1 and α_2 to guarantee stabilization of the controlled system (2.3), we consider the eigenvalues ν of the linearization matrix Dh in eq. (2.5). The characteristic polynomial of Dh is

$$p(\nu) = \nu^2 + (\alpha_1 - \alpha_2 - \partial_x f)\,\nu + \alpha_2 \cdot \partial_x f\,. \tag{2.7}$$

A necessary and sufficient condition for the negativity of the real parts of the eigenvalues ν of Dh is that the coefficients of eq. (2.7) are positive, i. e.

$$\alpha_1 - \alpha_2 - \partial_x f > 0\,, \quad \text{and} \tag{2.8a}$$
$$\alpha_2 \cdot \partial_x f > 0\,. \tag{2.8b}$$

From eq. (2.8b), we can deduce

$$\operatorname{sign}(\alpha_2) = \operatorname{sign}(\partial_x f)\,. \tag{2.9}$$

And from eq. (2.8a), we get

$$\alpha_1 > \alpha_2 + \partial_x f$$

which leads to the stronger condition

$$\alpha_1 > \alpha_2 + \sup_z \{\partial_x f(z)\} \tag{2.10}$$

for the case where $\partial_x f$ is bounded. Conditions (2.9) and (2.10) give sufficient conditions for stability, which can, except for bifurcation points, always be fulfilled for functions f whose partial derivative $\partial_x f$ is limited on the closed set of analyzed stationary points.
In condition (2.9), the sign of α_2 must be equal to the sign of $\partial_x f$. This condition is reminiscent of the *odd-number limitation* [74, 88] for time-delayed feedback control methods. Hence, the sign of α_2 depends on the original stability of the stationary point x. Additionally, bifurcation points are not stabilizable by eq. (2.3). So, no complete automatic continuation of stationary points over folds is possible with fixed values of the control parameters α_1 and α_2. When switching from a stable to an unstable branch or vice versa, the sign of α_2 needs to be changed.

2.2 EXTENDED PROPORTIONAL CONTROL

Once a dynamical system is stabilized by any control, the stationary points of the controlled system are asymptotically stable. Hence, direct analysis of the controlled system's dynamics cannot produce knowledge about the uncontrolled equilibria's stability. Therefore, an indirect method to analyze the original stability of the uncontrolled system (2.1) by using the information about the dynamics of the proportional control with state observer (2.3) is presented in the following section.
We use the fact that the dynamics of x are controlled by a proportional control with the control gain α_1. The motion of x consists of the original system $f(x, \mu)$ and a control part $\alpha_1 \cdot (y - x)$. We define the controlled dynamics eq. (2.3a) to be the function g and bring the controlled dynamics to predefined stability. So, another control eq. (2.11c) is applied on the already controlled system eq. (2.3). In control theory, this is also known as *pole placement* [68]. For simplicity, we aim for $\partial_x g = -1$. By this choice, the system is guaranteed to become stable since it holds for the eigenvalue $\partial_x g = -1 < 0$. This can be done by adapting α_1 continuously by the additional control $\dot{\alpha}_1 = \alpha_3 \cdot (\partial_x g + 1)$. This results in the extended control scheme

$$\dot{x} = f(x, \mu) + \alpha_1 \cdot (y - x) =: g\,(x, y, \alpha_1, \mu) \tag{2.11a}$$

$$\dot{y} = \alpha_2 \cdot (y - x) \tag{2.11b}$$

$$\dot{\alpha}_1 = \alpha_3 \cdot (\partial_x g + 1)\ , \tag{2.11c}$$

where $x \in \mathbb{R}$ is the state, $y \in \mathbb{R}$ is the adapted target, $\alpha_1 \in \mathbb{R}$ is the dynamic control parameter for x, $\alpha_2 \in \mathbb{R}$ is the control parameter for y, and $\alpha_3 > 0$ is a scaling factor for the adaption of α_1. Since it holds $\partial_x g = \partial_x f - \alpha_1$, we directly get the stability information $\partial_x f = \alpha_1 - 1$. Once the system has reached an equilibrium with a value of the control parameter α_1 such that $\partial_x g = -1$, the control vanishes. Hence, the control scheme is again noninvasive.
The idea of adapting the control parameter for a proportional feedback control dates back to the 1950s; see [126] for a summary and the references therein. The difference of the control in eq. (2.11) to existing adaptive proportional control techniques is the combination of control and stability information by the dynamic value of α_1. So, α_3 is a control gain for both control and original stability information.
The equilibrium points of the original system (2.1) are identical to the ones of the extended control scheme (2.11) in the following sense: If $(\bar{x}, \bar{y}, \bar{\alpha}_1)$ is a stationary

point of eq. (2.1) corresponding to $\bar{x}$, it is $\dot{x} = 0 = f(\bar{x}, \mu)$. Let $\bar{x}$ be identical to the control target, i. e., $(\bar{y} - \bar{x}) = 0$, and let $\bar{\alpha}_1 = \partial_x f + 1$ hold, which is always possible for bounded $\partial_x f$. Here $\partial_x f$ is a short form of $\partial_x f(\bar{x})$. Then, it holds $\dot{y} = \alpha_2 \cdot 0$ and $\dot{\alpha}_1 = \alpha_3 \cdot (\partial_x f - \bar{\alpha}_1 + 1) = 0$, and $(\bar{x}, \bar{y}, \bar{\alpha}_1)$ must be a stationary point of eq. (2.11). If reversely $(\bar{x}, \bar{y}, \bar{\alpha}_1)$ is an equilibrium point of eq. (2.11), it holds $\dot{y} = 0$ and hence $(\bar{y} - \bar{x}) = 0$. Additionally, it holds $\dot{x} = 0 = g(\bar{x}, \bar{y}, \bar{\alpha}_1, \mu)$. Then, $f(\bar{x}, \mu) = g(\bar{x}, \mu) - \bar{\alpha}_1 \cdot (\bar{y} - \bar{x}) = 0$, which is the sufficient condition for $\bar{x}$ to be an equilibrium of eq. (2.1). The control consisting of eqs. (2.11b) and (2.11c) disappears at an equilibrium point of eq. (2.1). This shows the noninvasiveness of the proposed extended control method.

2.2.1 *Controllability and observability of the extended state observer*

For controllability analysis, we follow again the results of the control theory for LTI [104] introduced in section 1.2. We can again assume that the dynamics of the controlled system (2.11) written as

$$\dot{z} = \check{h}(z) = \frac{\mathrm{d}}{\mathrm{d}t} \begin{pmatrix} x \\ y \\ \alpha_1 \end{pmatrix} \quad \text{with } z = (x, y, \alpha_1) \tag{2.12}$$

can be locally approximated by the linearization around each stationary point $\bar{z} = (\bar{x}, \bar{y}, \bar{\alpha}_1)$. Again, we use the notation

$$\delta z = z - \bar{z}$$

for the vector in the tangential space at the point $\bar{z}$. The linearization of eq. (2.12) is

$$\begin{aligned} (\dot{\delta z}) &= D\check{h}(\bar{z}) \cdot \delta z \\ &= \begin{pmatrix} \partial_x f(\bar{z}) - \bar{\alpha}_1 & \bar{\alpha}_1 & \bar{y} - \bar{x} \\ -\alpha_2 & \alpha_2 & 0 \\ \alpha_3 \cdot \partial_x(\partial_x g)(\bar{z}) & \alpha_3 \cdot \partial_x(\partial_y g)(\bar{z}) & \alpha_3 \cdot \partial_x(\partial_{\alpha_1} g)(\bar{z}) \end{pmatrix} \cdot \delta z \\ &= \begin{pmatrix} \partial_x f(\bar{z}) - \bar{\alpha}_1 & \bar{\alpha}_1 & \bar{y} - \bar{x} \\ -\alpha_2 & \alpha_2 & 0 \\ \alpha_3 \cdot \partial_x(\partial_x f)(\bar{z}) & 0 & -\alpha_3 \end{pmatrix} \cdot \delta z\,, \end{aligned} \tag{2.13}$$

where $D\check{h}(\bar{z})$ is the Jacobian of $\check{h}$ in the point $\bar{z} = (\bar{x}, \bar{y}, \bar{\alpha}_1)^T$. Again, the short form $\partial_x f$ for the partial derivative of f will be used wherever the context allows. Since the controllability of the system (2.11a) and (2.11b) is already shown in section 2.1.1, we only consider the additional control (2.11c), where the control vector is defined by $u := \dot{\alpha}_1 \in \mathbb{R}$. The dynamics of x, y, and α_1 are assumed to be coupled, but here, the original system and the control are distinguished sharply to keep the representation clear. The linearization (2.13) can be considered as the controlled system

$$\dot{v} = \mathsf{C}v(t) + \mathsf{D}u(t) \tag{2.14}$$

of the dynamics of the state vector

$$v := \begin{pmatrix} x \\ y \\ \alpha_1 \end{pmatrix} \in \mathbb{R}^3 ,$$

with the state matrix

$$\mathsf{C} := \left[\begin{array}{c|c} Dh & \begin{matrix} \partial_{\alpha_1} g \\ \partial_{\alpha_1} \dot{y} \end{matrix} \\ \hline 0 & 0 \end{array}\right] = \begin{pmatrix} \partial_x f - \alpha_1 & \alpha_1 & y - x \\ -\alpha_2 & \alpha_2 & 0 \\ 0 & 0 & 0 \end{pmatrix} \in \mathbb{R}^{3\times 3} ,$$

where Dh is the linearization matrix in eq. (2.5) of the proportional control with state observer (2.3). Even though the linearization matrix in eq. (2.5) is given in the stationary point $(\bar{x}, \bar{y}, \bar{\alpha}_1)^T$, we use here the general form for any point (x, y, α_1). This should make the text more readable. The input matrix for the system (2.14) is

$$\mathsf{D} := \begin{pmatrix} 0 \\ 0 \\ 1 \end{pmatrix} \in \mathbb{R}^3 .$$

The resulting controllability matrix is

$$\mathsf{R} = \left[\begin{array}{c|c|c} \mathsf{D} & \mathsf{CD} & \mathsf{C}^2\mathsf{D} \end{array}\right] = \begin{pmatrix} 0 & y - x & (\partial_x f - \alpha_1) \cdot (y - x) \\ 0 & 0 & -\alpha_2 \cdot (y - x) \\ 1 & 0 & 0 \end{pmatrix} .$$

Citing the results for the control theory on LTI [104] again, the system (2.14) is controllable if R has full rank, i. e. if $x \neq y$ and $\alpha_2 \neq 0$.
We already assumed x and y to be directly measurable for observability in section 2.1.1. If x is directly measurable with enough precision, either $\dot{x} = g(x, y, \alpha_1, \mu)$ is directly measurable or can be computed by a difference quotient of the time series for x. From these values of $\dot{x}$, the value of $\partial_x g$ can be approximated by the difference quotient

$$\partial_x g \approx \frac{\dot{x}(t_2) - \dot{x}(t_1)}{x(t_2) - x(t_1)} \tag{2.15}$$

consisting of the measurements at the times $t_1 < t_2$ if we assume that the changes in y and α_1 can be discarded. So, the state and the control of the extended proportional control (2.11) can be fully estimated only by output measurements. Hence, the system (2.11) is fully observable.
Applying a Newton method to achieve the derivative information $\partial_x g$ is an alternative for cases where initialization at different points is possible. The derivative information with respect to x, y, and α_1 could then be obtained by the time series with different initial values. Numerical results of the Newton method for the extended proportional control (2.11) applied on the normal form (1.7) will be presented in section 2.3.

Incidentally, in cases where numerical initialization is possible, a damped Newton method with

$$\dot{x} = -(\partial_x f(x, \bar{\mu}))^{-1} f(x, \bar{\mu})$$

locally guarantees convergence of x towards the equilibrium $(\bar{x}, \bar{\mu})$ of eq. (2.1), including the stability information $\partial_x f$. Since we assume to have no direct or numerically direct access to $\partial_x f$, this is ansatz is not further considered.

2.2.2 *Stabilization of the extended state observer*

As controllability, and hence stabilizability, of the extended state observer (2.11) is given for $x \neq y$ and $\alpha_2 \neq 0$, we only need find appropriate gains α_2 and α_3 to guarantee that the stationary points are asymptotically stable since $x = y$ must hold in these equilibrium points. As the considered points are stationary, i. e. the velocity is zero, it must hold $\alpha_1 = \partial_x f + 1$ in each stationary point of eq. (2.11). We use this knowledge to simplify the notion of the linearization matrix

$$D\check{h} = \begin{pmatrix} \partial_x f - \bar{\alpha}_1 & \bar{\alpha}_1 & \bar{y} - x \\ -\alpha_2 & \alpha_2 & 0 \\ -\alpha_3 \cdot \partial_x(\partial_x f) & 0 & -\alpha_3 \end{pmatrix} = \begin{pmatrix} -1 & \partial_x f + 1 & 0 \\ -\alpha_2 & \alpha_2 & 0 \\ \alpha_3 \cdot \partial_x(\partial_x f) & 0 & -\alpha_3 \end{pmatrix} \tag{2.16}$$

for the extended state observer (2.11), where the short form $\partial_x f$ is used again for legibility reasons. In order to guarantee that all real parts of the eigenvalues of the linearization matrix (2.16) are negative, we can consider the Routh-Hurwitz criterion [52, 95] (thm. 1.4). If the negative of the characteristic polynomial

$$p(\nu) = -\nu^3 + (\alpha_2 - \alpha_3 - 1) \cdot \nu^2 + (\alpha_2\alpha_3 - \alpha_2 \cdot \partial_x f - \alpha_3) \cdot \nu - \alpha_2\alpha_3 \cdot \partial_x f \tag{2.17}$$

of the Jacobian (2.16) is a Hurwitz polynomial, the system (2.11) is stable. The first condition is that all coefficients of eq. (2.17) are positive.
The coefficients of $-p(\nu)$ are the following:

$$a_3 = 1\,, \tag{2.18a}$$
$$a_2 = 1 + \alpha_3 - \alpha_2\,, \tag{2.18b}$$
$$a_1 = \alpha_2 \cdot \partial_x f + \alpha_3 - \alpha_2\alpha_3\,, \tag{2.18c}$$
$$a_0 = \alpha_2\alpha_3 \cdot \partial_x f\,. \tag{2.18d}$$

We can already see that $a_3 > 0$ is fulfilled. From $a_2 > 0$, we get the condition

$$\alpha_3 > \alpha_2 - 1\,. \tag{2.19}$$

And $a_0 > 0$ provides the conditions

$$\operatorname{sign}(\alpha_2) = \operatorname{sign}(\partial_x f)\,, \quad \text{and} \tag{2.20a}$$
$$\partial_x f \neq 0\,,\ \alpha_2 \neq 0\,,\ \alpha_3 \neq 0\,. \tag{2.20b}$$

Since $\alpha_3 > 0$ by assumption, the sign of a_0 depends only on the product $\alpha_2 \cdot \partial_x f$. Respecting condition (2.19), we choose

$$\alpha_3 := \alpha_2 - 1 + \epsilon > 0\,, \tag{2.21}$$

where $\epsilon > 0$. This leads to the following formulation of eq. (2.18c)> 0:

$$a_1 = -(\alpha_2)^2 + (2 + \partial_x f - \epsilon) \cdot \alpha_2 + \epsilon - 1 > 0\,.$$

With eqs. (2.19) and (2.21) it holds $\epsilon - 1 > \alpha_2$. So, if

$$-(\alpha_2)^2 + (\partial_x f - \epsilon + 1)\,\alpha_2 = \alpha_2 \cdot (-\alpha_2 + \partial_x f - \epsilon + 1) > 0$$

holds, then $a_1 > 0$ is fulfilled, too. This is true, if either

$$\{\alpha_2 > 0 \text{ and } \partial_x f - \alpha_2 - \epsilon + 1 > 0\} \quad \text{or} \tag{2.22a}$$
$$\{\alpha_2 < 0 \text{ and } \partial_x f - \alpha_2 - \epsilon + 1 < 0\}\,. \tag{2.22b}$$

Due to eqs. (2.20a) and (2.21) and $\alpha_3 > 0$, condition (2.22b) is fulfilled for the case of $\partial_x f < 0$. Condition (2.22a) leads to the choice

$$\alpha_2 + \epsilon < \partial_x f + 1 \Longrightarrow \alpha_3 < \partial_x f \quad \text{if } \partial_x f > 0.$$

The second condition for negativity of the eigenvalues' real parts of $D\check{h}$ is the positivity of the Hurwitz determinants and all its minors. The Hurwitz determinants give the following conditions.

$$H_1 = |a_2| > 0\,,$$

which is already fulfilled by eq. (2.19) and

$$H_2 = a_2 a_1 - a_3 a_0 = (1 + \alpha_3 - \alpha_2) \cdot (\alpha_2 \cdot \partial_x f + \alpha_3 - \alpha_2\alpha_3) - \alpha_2\alpha_3 \cdot \partial_x f > 0. \tag{2.23}$$

Inserting eq. (2.21) into eq. (2.23) leads to the following condition

$$\begin{aligned}&(-\partial_x f - \epsilon) \cdot \alpha_2^2 + \left(\partial_x f + 2\epsilon - \epsilon^2\right) \cdot \alpha_2 + \epsilon^2 - \epsilon \\ &= (1 - \alpha_2) \cdot (\alpha_2 \cdot \partial_x f + \epsilon \cdot (\alpha_2 + \epsilon - 1)) > 0\,.\end{aligned} \tag{2.24}$$

This is fulfilled, if

$$\alpha_2 < 1 \quad \text{and} \quad \alpha_2 \cdot \partial_x f + \epsilon \cdot (\alpha_2 + \epsilon - 1) = \alpha_2 \cdot \partial_x f + \epsilon\alpha_3 > 0\,. \tag{2.25}$$

The second condition in eq. (2.25) is always fulfilled by eq. (2.20a) and $\epsilon,\ \alpha_3 > 0$. Hence, the two factors in eq. (2.24) must be positive. Together with conditions (2.22), we get stabilization for

$$\epsilon > 0\,,\ \alpha_3 = \alpha_2 - 1 + \epsilon > 0\,, \text{ and } \begin{cases} \{\alpha_2 < 0\}\,, & \text{if } \partial_x f < 0 \\ \{0 < \alpha_2 < 1 \text{ and } 0 < \alpha_3 < \partial_x f\}\,, & \text{if } \partial_x f > 0\,. \end{cases}$$

Hence, the extended state observer (2.11) can be stabilized in every stationary point except for bifurcation points. To switch between the stable and the unstable branch, the control parameter α_2 needs to be adapted like for the proportional control with the state observer.
Since the sign of α_2 must change in the bifurcation point, one could think of an adaptive control law for α_2 in a kind as in eq. (2.11c) for α_1. Additionally, an alert to detect the neighborhood of a bifurcation could be implemented. Then the bifurcation point could be skipped, and the sign and size of the control parameter values be changed to continue on a branch with different stability.

2.3 NUMERICAL RESULTS ON THE EXTENDED PROPORTIONAL CONTROL

In the previous sections, the concepts of proportional control (2.3) and its extension (2.11) were introduced. This can be used to produce the bifurcation diagram, including the stability information of a dynamical system. In the following, the extended proportional control (2.11) was tested on the one-dimensional normal form

$$\dot{x} = \mu + x - x^3$$

for hysteresis. Once the k-th stationary point $\overline{x_k}$ is found and stabilized by eq. (2.11), the target $\tilde{y}_{k+1}$ for the next equilibrium point $(\overline{x_{k+1}}, \overline{\mu_k})$ is defined. It is the first component of a linear continuation $(\tilde{y}_k, \tilde{\mu}_k) := (\overline{x_k}, \overline{\mu_k}) + s \cdot \frac{(\overline{x_k}, \overline{\mu_k}) - (\overline{x_{k-1}}, \overline{\mu_{k-1}})}{\|(\overline{x_k}, \overline{\mu_k}) - (\overline{x_{k-1}}, \overline{\mu_{k-1}})\|}$ of stepsize s through the previous two equilibrium points $(\overline{x_{k-1}}, \overline{\mu_{k-1}})$ and $(\overline{x_k}, \overline{\mu_k})$. Let again $g(x, y, \alpha_1, \mu) = \mu + x - x^3 + \alpha_1 \cdot (y - x)$, and let

$$\check{h}(x, y, \alpha_1) = \begin{pmatrix} \dot{x} \\ \dot{y} \\ \dot{\alpha}_1 \end{pmatrix} = \begin{pmatrix} \mu + x - x^3 + \alpha_1 \cdot (y - x) \\ \alpha_2 \cdot (y - x) \\ \alpha_3 \cdot (\partial_x g + 1) \end{pmatrix} \tag{2.26}$$

describe the dynamics of the controlled system (2.11) in vector notation. Then, the Newton method with the l-th step

$$\begin{pmatrix} x_{k,l} \\ y_{k,l} \\ \alpha_{1k,l} \end{pmatrix} = \begin{pmatrix} x_{k,l-1} \\ y_{k,l-1} \\ \alpha_{1k,l-1} \end{pmatrix} - D\check{h}\left((x_{k,l-1}, y_{k,l-1}, \alpha_{1k,l-1})^T \right) \cdot \check{h}\left((x_{k,l-1}, y_{k,l-1}, \alpha_{1k,l-1})^T \right)$$

for the k-th equilibrium is applied to the controlled system (2.26) to find the stationary point, i. e., the point with velocity zero in each direction. Even though the analytical description of the derivative information for the Jacobian is available for the simulation model of the normal form (1.7), they were approximated by difference quotients like eq. (2.15) for $\partial_x g$. In order to obtain the partial derivatives $\check{h}_x$, $\check{h}_y$, and $\check{h}_{\alpha_1}$ for the Jacobian $D\check{h} \in \mathbb{R}^{3\times 3}$, the initial state is varied in each Newton step three times by $\Delta x = 0.001$, $\Delta y = 0.1$, and $\Delta\alpha_1 = 0.2$. The resulting Jacobian in the point $(\hat{x}, \hat{y}, \hat{\alpha}_1)$ is

$$\begin{aligned} &D\check{h}(\hat{x}, \hat{y}, \hat{\alpha}_1) \\ &\approx \begin{pmatrix} \frac{\check{h}_1(\hat{x}+\Delta x, \hat{y}, \hat{\alpha}_1) - \check{h}_1(\hat{x}, \hat{y}, \hat{\alpha}_1)}{\Delta x} & \frac{\check{h}_1(\hat{x}, \hat{y}+\Delta y, \hat{\alpha}_1) - \check{h}_1(\hat{x}, \hat{y}, \hat{\alpha}_1)}{\Delta y} & \frac{\check{h}_1(\hat{x}, \hat{y}, \hat{\alpha}_1+\Delta\alpha_1) - \check{h}_1(\hat{x}, \hat{y}, \hat{\alpha}_1)}{\Delta\alpha_1} \\ \frac{\check{h}_2(\hat{x}+\Delta x, \hat{y}, \hat{\alpha}_1) - \check{h}_2(\hat{x}, \hat{y}, \hat{\alpha}_1)}{\Delta x} & \frac{\check{h}_2(\hat{x}, \hat{y}+\Delta y, \hat{\alpha}_1) - \check{h}_2(\hat{x}, \hat{y}, \hat{\alpha}_1)}{\Delta y} & \frac{\check{h}_2(\hat{x}, \hat{y}, \hat{\alpha}_1+\Delta\alpha_1) - \check{h}_2(\hat{x}, \hat{y}, \hat{\alpha}_1)}{\Delta\alpha_1} \\ \frac{\check{h}_3(\hat{x}+\Delta x, \hat{y}, \hat{\alpha}_1) - \check{h}_3(\hat{x}, \hat{y}, \hat{\alpha}_1)}{\Delta x} & \frac{\check{h}_3(\hat{x}, \hat{y}+\Delta y, \hat{\alpha}_1) - \check{h}_3(\hat{x}, \hat{y}, \hat{\alpha}_1)}{\Delta y} & \frac{\check{h}_3(\hat{x}, \hat{y}, \hat{\alpha}_1+\Delta\alpha_1) - \check{h}_3(\hat{x}, \hat{y}, \hat{\alpha}_1)}{\Delta\alpha_1} \end{pmatrix}, \end{aligned}$$

where $\check{h}_j(\hat{z}) \approx \frac{\hat{z}_j(t_0+\Delta t) - \hat{z}_j(t_0)}{\Delta t}$ with $\Delta t = 0.02$.
As already stated in section 2.2, the continuation of stationary points must be done in three parts due to changes in the sign of the control parameter α_2 and limits for the control parameter α_3. See section 2.2.2 for further details on the control parameter choice. For the results of the continuation presented in fig. 2.1a,

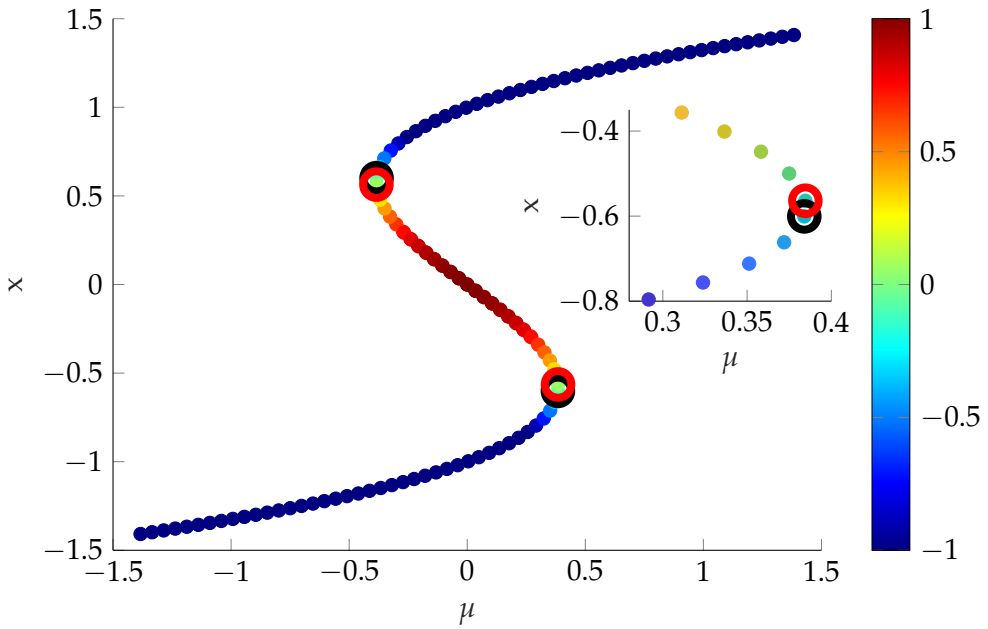

(a) Stability evaluation for the normal form controlled by the extended proportional control (2.11). Stability information is computed directly by control (2.11c). The black circles mark the end of the continuation on the stable branches, and the red ones indicate the simulation limits on the unstable branch. See the inset reduced to 10 significant points for details of the lower bifurcation point.

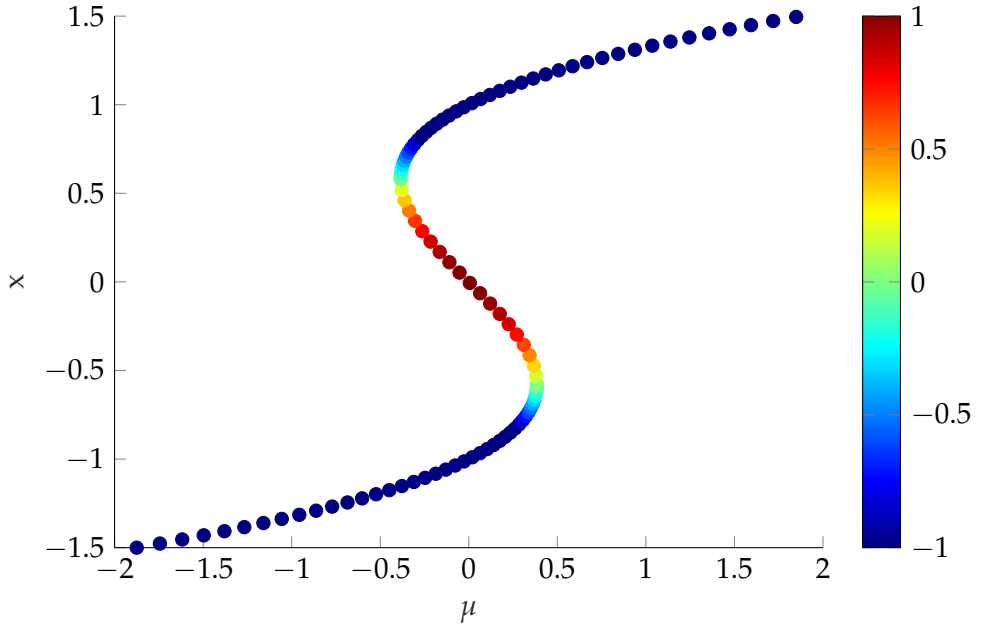

(b) Stability evaluation for the the normal form (1.7) by analytic computations.

Figure 2.1: Stability evaluation for the controlled the normal form (1.7). Stability information is given by color code. Blue indicates stability ($\partial_x f < 0$), and red indicates unstable stationary points ($\partial_x f > 0$). The bifurcation points are marked by green dots. The color scale is limited to the interval $[-1, 1]$ to emphasize the qualitative change in the neighborhood of the bifurcation points.

the choices mentioned above for the increments were made. The stable branches were produced with $\alpha_2 = -1$ and $\alpha_3 = 1$. The unstable branch was constructed under the control parameter values $\alpha_2 = 0.9$ and $\alpha_3 = 0.1$. Since the initialization in the neighborhood of a bifurcation point is hard to realize, the continuation for the unstable branch was initialized first at $(\mu_0, x_0) = (0.2731, -0.3)$ and then continued upwards. The second time, the continuation was initialized at $(\mu_0, x_0) = (-0.2731, 0.3)$ and then continued downwards. The complete branch was merged for fig. 2.1a. Note that the found parts of the branches do not intersect. The last found points are marked in fig. 2.1a by colored circles. For comparison, fig. 2.1b shows the analytically computed stability of the stationary points. Even for numerically computed derivatives, the stability information is accessible with the extended proportional control (2.11). For physical experiments, an initialization at different points is hard to realize. Indirect methods to estimate the derivative information, like the difference quotient (2.15), are an alternative to gaining the stability information and updating the control parameter α_3.

3

DATA-BASED STABILITY ANALYSIS BY PROPORTIONAL-DERIVATIVE (PD) CONTROL

In section 1.1, several approaches to stabilize stationary states were introduced. The present chapter aims to gain stability information about the originally uncontrolled dynamical system and construct the corresponding bifurcation diagram. Since explicit mathematical descriptions of the dynamics in physical systems are rarely available, the stability information cannot be computed analytically. The results herein are all published in the joint work [26], and the chapter's structure was adapted from this publication. Wherever a nontrivial formulation of a sentence or a paragraph was taken nearly literally from the original work, this is identified by "([26])".

3.1 CONTROL-BASED CONTINUATION

In [18, 19, 98], the authors introduce a PD control-based continuation scheme for experiments with forced nonlinear impact oscillators. The position of an equilibrium is predicted by a pseudo-arclength continuation [28, 29, 58, 59] (see also section 1.2) using the information about the previous two stationary points. The difference between the uncontrolled and the predicted state trajectories defines the PD control. Since periodic orbits appear in Fourier space as equilibrium points, the update for the pseudo-arclength continuation by the Newton step is done therein. When the control is switched off for a short time step, the trajectories of the actual state diverge from the controlled reference trajectories. This reveals the unstable branch which defines the separatrix. Estimating the corresponding Lyapunov exponents in the experiments in [18] allowed the authors to determine the original stability of the uncontrolled states.
A method to estimate the original stability of stabilized periodic orbits is presented by Barton in [6]. The stabilized orbit is perturbed slightly in its neighborhood in state space. The measured data is used for a least-squares fit to an autoregressive model with exogenous inputs. The Floquet exponents gained thereby serve to estimate the original stability information. By this method, the author produced a full bifurcation diagram, including stability information for a nonlinear tuned mass-damper system.
The two methods presented in [6, 18] allow for gaining stability information only from the measured data. However, the necessary robustness for the case of inactive control might not be given, and the intervention in the measurements for the case of perturbance might be hardly realizable.
The method presented in section 3.1.1 allows for obtaining a complete bifurcation diagram, including stability information, without further intrusions. Only the measured data of the controlled system serves as the basis for computing the stability information *a posteriori*.

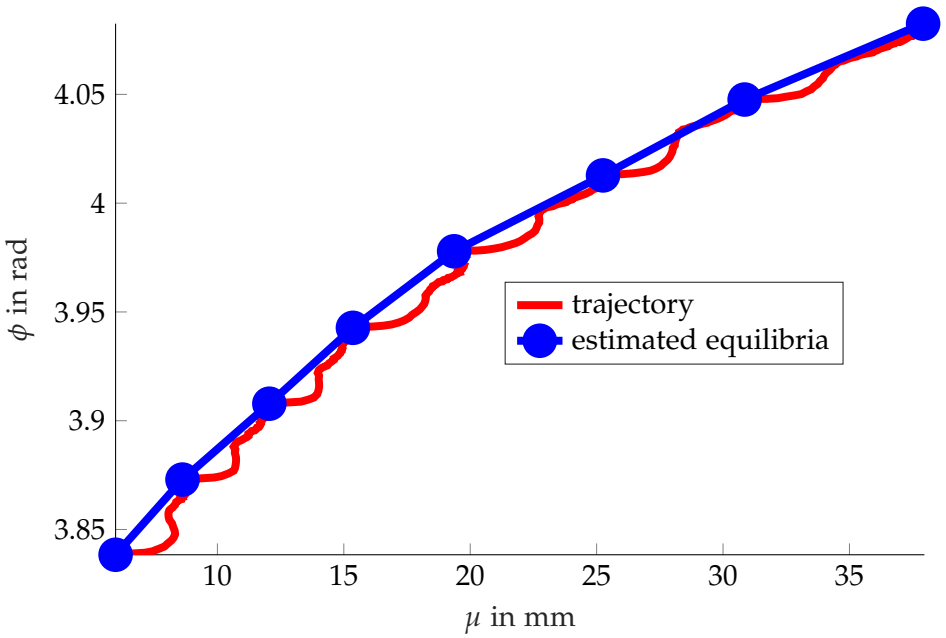

Figure 3.1: Magnified detail for the continuation of the curve of stationary points by control (3.2) for the resulting experimental system (3.10). The blue dots mark the estimated equilibria. The blue lines connecting the dots show the approximated equilibrium points in between the found ones. The red line segments represent the trajectory of the controlled system in phase space. Reproduced from [26] with kind permission from the Society for Industrial and Applied Mathematics (SIAM).

3.1.1 *PD control on the parameter*

The presented theory in this chapter is restricted to 2-dimensional dynamical systems for simplicity reasons with respect to data analysis, presentation, and comprehensibility. For the Zeeman catastrophe machine, which will be introduced in section 3.3 and serve as a test model throughout the next chapters and the present one, the limitation to 2 dimensions is sufficient. The machine's modeled state x consists of the state descriptions for a one-dimensional measured state ϕ and its derivative $\dot{\phi}$.
So, we will consider an autonomous dynamical system of the form

$$\dot{x} = f(x, \mu)\,, \tag{3.1}$$

where $x = (x_1,\ x_2) \in \mathbb{R}^2$ describes the state variable and $\mu \in \mathbb{R}$ is the bifurcation parameter. In the following, system (3.1) will be referred to as the *original system* since it is free of control.
In eq. (3.1), the dynamics of the state x are described as motion depending on μ. The usual or classical way is to see the resulting curve of stationary points locally as a function x depending on μ. For the proportional scheme (2.3), this description of the system's state is used, too. An unsolved problem for control (2.3) is to continue the curve of stationary points around folds. This is due to the singularity of x as a function of μ (see fig. 3.5 for an illustration) and does not

hinge on the control scheme. In numerical bifurcation analysis, the extension of system (3.1) by an additional dimension is often used to avoid these singularities. This approach is known as the *pseudo-arclength continuation* [28, 29, 58, 59]. A short description can be found in section 1.1, too. In the present chapter, we change to a different description of a similar problem and present a different control approach. To overcome the singularity problem, we extend the original system (3.1) by a differential equation expressing the motion of the one-dimensional bifurcation parameter μ as a function depending on x ([26]). The curve of stationary points is now seen as a function $\mu(x)$ in x. Following control theory [104], higher-dimensional systems can be controlled by lower-dimensional control. The control scheme works locally, starting in a previously found or known stationary point and driving the system to a defined target x^* in the neighborhood. The additional differential equation for the motion of μ describes the proposed additive feedback control. Adapting μ proportionally to the difference $(x - x^*)$ allows for reaching the new target x^*. The resulting extension of the system (3.1) with a local dynamic control scheme in μ has the following form

$$\dot{x} = f(x, \mu) \tag{3.2a}$$

$$\dot{\mu} = -K\,(x - x^*) = -K_P\,(x_1 - x_1^*) - K_D\,(x_2 - x_2^*) \tag{3.2b}$$

with the feedback gain $K = (K_P,\ K_D) \in \mathbb{R}^{1\times 2}$. The system (3.2) will be called the *controlled system* since the control (3.2b) is applied to the original system (3.1). In the literature, it is often referred eq. (3.2) to as the *PD control* because of the *proportional* part $K_P\,(x_1 - x_1^*)$ and the *differential* part $K_D\,(x_2 - x_2^*)$ since $x_2 = \dot{x}_1$ holds in our context. So, we define in advance of searching for an unknown equilibrium $(\bar{x}, \bar{\mu})$ the x-components of the controlled system (3.2) to be the target value x^* for the equilibrium of the original system (3.1). By changing the bifurcation parameter μ according to the distance between the actual state and the target x^*, we indirectly change the state x through the dynamics. Hence, only the x-components of the newly searched equilibrium of the system (3.2) are known. An illustration of the interplay between the first component of the state, x_1, and the bifurcation parameter μ is given in fig. 3.1.

The equilibrium points of the original system (3.1) are identical to the stationary points of the controlled system (3.2): If $\bar{x}$ is a stationary point for $\bar{\mu}$ of eq. (3.1), and if, in addition, the first component of the state, $\bar{x}_1$, is identical to the control target x_1^*, it is $\dot{x}_1 = x_2 = 0$, $\dot{x}_2 = 0$, and $(\bar{x}_1 - x^*) = 0$. Then $\dot{\mu} = 0$, and $(\bar{x}, \bar{\mu})$ is a stationary point of eq. (3.2). If reversely $(\bar{x}, \bar{\mu})$ is an equilibrium point of eq. (3.2), it holds $\dot{x} = f(\bar{x}, \bar{\mu}) = 0$ which is the sufficient condition for $\bar{x}$ to be a stationary point of eq. (3.1). Since the control (3.2b) disappears at an equilibrium point of eq. (3.1), the proposed method is noninvasive.

3.1.2 *Controllability and observability of PD-controlled systems*

In the following, the controllability conditions for a system of the form (3.1) controlled by (3.2b) are scrutinized and stated in a general way. The resulting system (3.2) can be written as

$$\dot{z} = \tilde{h}(z) = \frac{\mathrm{d}}{\mathrm{d}t}\begin{pmatrix} x_1 \\ x_2 \\ \mu \end{pmatrix} \quad \text{with } z = (x_1, x_2, \mu)\,. \tag{3.3}$$

Similar to eqs. (2.4) and (2.12), we assume that the dynamics described in eq. (3.3) can be locally approximated by a linearization around each stationary point $(\bar{x}_1, \bar{x}_2, \bar{\mu})$. Therefore, we again use the notation

$$\delta z = z - \bar{z}$$

for the vectors in the tangent space at the point $\bar{z} = (\bar{x}_1, \bar{x}_2, \bar{\mu})$. So, the linearization of eq. (3.2) is

$$(\dot{\delta z}) = D\tilde{h}(\bar{z}) \cdot \delta z = \left[\begin{array}{cc|c} & Df(\bar{z}) & f_\mu(\bar{z}) \\ -K_P & -K_D & 0 \end{array}\right] \cdot \delta z\,, \tag{3.4}$$

where $D\tilde{h}(\bar{z}) \in \mathbb{R}^{3\times 3}$ is the Jacobian of eq. (3.3) in the stationary point $\bar{z}$, which includes the linearization matrix Df of the uncontrolled system (3.1) and the gradient f_μ of f with respect to μ. This allows us to use results from control theory for continuous linear time-invariant (LTI) systems introduced in section 1.2. Even though the dynamics of x and μ in the controlled system (3.2) are assumed to be coupled, system and control are distinguished sharply in the following analysis to keep the representation clear and linear. Since the control (3.2b) is 1-dimensional, we use the control vector $u := \dot{\mu} \in \mathbb{R}$ and the state vector

$$v := \begin{pmatrix} x \\ \mu \end{pmatrix} \in \mathbb{R}^3$$

for the controlled system

$$\dot{v} = \mathsf{C}v(t) + \mathsf{D}u(t), \tag{3.5}$$

with the input matrix

$$\mathsf{D} := \begin{pmatrix} 0 \\ 0 \\ 1 \end{pmatrix} \in \mathbb{R}^3$$

and the state matrix

$$\mathsf{C} := \left[\begin{array}{cc|c} & Df & f_\mu \\ 0 & 0 & 0 \end{array}\right] \in \mathbb{R}^{3\times 3}\,,$$

where the short forms Df and f_μ are used due to reasons of legibility. This will again be the case throughout the whole chapter, wherever the context allows for it. So, we obtain the controllability matrix

$$\mathsf{R} = \left[\begin{array}{c|c|c} \mathsf{D} & \mathsf{CD} & \mathsf{C}^2\mathsf{D} \end{array}\right] = \left[\begin{array}{c|c|c} 0 & & \\ 0 & \mathsf{CD} & \mathsf{C}^2\mathsf{D} \\ 1 & & \end{array}\right] = \left[\begin{array}{c|c|c} 0 & f_\mu & Df \cdot f_\mu \\ 0 & & \\ \hline 1 & 0 & 0 \end{array}\right] \in \mathbb{R}^{3\times 3}.$$

Following the Kalman rank criterion [57] (thm. 1.5), i. e. the test if "$\operatorname{rank}([sI - \mathsf{CD}]) = n$ for all s" or "$\operatorname{rank}(\mathsf{R}) = n$", the original system (3.1) is controllable by eq. (3.2) if the controllability matrix R has full rank. This is fulfilled if $\left[f_\mu \mid Df \cdot f_\mu\right]$ has full rank, i. e., if $f_\mu \neq \mathbf{o} \in \mathbb{R}^{2\times 1}$ is not an eigenvector of $Df \neq \mathbf{o} \in \mathbb{R}^{2\times 2}$. Hence, the controllability depends only on the original system (3.1), namely Df and f_μ.
As stated at the beginning of section 3.1.1, bifurcation points of the original system (3.1) reveal singularities if the dynamics are considered as a function $x(\mu)$ ([26]). Since in the case of control (3.2a), μ is seen as a function of x, no singularities of the controlled system (3.2) occur at the fold bifurcation points of the original system (3.1).
The dual of controllability for a system is its observability, as stated in section 1.2. Therefore, observability is usually investigated together with controllability. Since for the presented case of the original system (3.1), it is assumed that the first component x_1 of the state is directly measurable and that the second component $x_2 = \dot{x}_1$ is either directly measurable or it can be approximated precisely enough by numerical methods like different quotient, no further investigation on the observability is needed. Only input and output measurements are needed to construct the full-state trajectory. The generalization of the following results requires further analysis to guarantee observability.

3.1.3 *Stabilization of PD-controlled systems*

In section 3.1.2, it is shown that the controllability by control (3.2b) of the original system (3.1) depends only on the system itself. We will now state sufficient conditions for the control parameter K that guarantee the linear stability of the controlled system (3.2), hence show by construction the existence of adequate control gains. For this purpose, eq. (3.2) is considered in the matrix-vector notation (3.4), i. e. a dynamical system describing the motion of a 3-dimensional state $(x, \mu)^T$. By linear stability theory and thm. 1.1, the original system (3.1) is linearly stabilized by eq. (3.2b), if the eigenvalues of the Jacobian $D\tilde{h}$ defined in eq. (3.2) have only negative real parts. Hence, K_P and K_D must be chosen accordingly to guarantee stability for all considered equilibria $(\bar{x}, \bar{\mu})^T$. In cases where no explicit model is given, experimental measurements could reveal information about the Jacobian Df of the original system.

3.2 DETECTION OF STABILITY AND BIFURCATION POINTS

One method to gain information about the original system's stability is to switch off the control and analyze the data from the uncontrolled behavior like it is presented,

e. g., in [18]. This approach is easily realizable, but involves the risk of harming the system and its physical structure. For the stability analysis presented in the following, the control can be kept permanently activated during the experiment ([26]). So, the closed-loop measurements with control (3.2b) allow for gaining stability information about the original dynamics. During the whole experiment, no further inventions or computations about the stability are needed. This approach is not restricted to the controlled system (3.2). It can be applied to every stability method where the system state's and the bifurcation parameter's behavior can be separated similarly. Since no exact mathematical description or model of the considered dynamical system is obtainable in many cases, neither the system's stability information nor bifurcation points must be found directly by detailed analytical detection. The presented method aims to find an approximation of the linearization for the original system (3.1) in the close neighborhood of each stabilized equilibrium point. The eigenvalues of the linearization matrix allow for determining the original stability. For simplicity, in sections 3.1.1 to 3.1.3, the system was assumed to be 2-dimensional. Even though this is not necessary for the following chapters, we weaken the assumption to an n-dimensional system of the general form $\dot{x} = f(x, \mu)$ with $f : \mathbb{R}^{n+1} \to \mathbb{R}^n$, which is controlled by a 1-dimensional control similar to eq. (3.2b) with parameter μ. The state of the controlled system will be denoted by $z := (x, \mu)^T \in \mathbb{R}^{n+1}$. As previously stated, the method aims to find an approximation of the linearization which can be done by Taylor expansion up to a linear term. Since, generally, the stationary point $\bar{z}$ is not the origin, the position of $\bar{z}$ defines the constant shift of the origin for the linearization. Hence, we need to find an affine linear map to approximate the original system's behavior. So, we search for a least-squares fit G, with $(G)_{ij} = g_{ij}$, of the measured data $\hat{z}$ to the general solution z of

$$\dot{z} = Gz - G\bar{z} = Gz - b\,. \tag{3.6}$$

The position of the equilibrium point $\bar{z}$, i. e. the shift of the origin, causes the constant term $G\bar{z}$ of the Taylor expansion. We apply a standard least-squares approach like in [10, 86] in order to find the closest or best-fitting solution of eq. (3.6) to the measured data $\hat{z} \in \mathbb{R}^{n+1}$. The data points are stored in matrices $\hat{Z}$, $\dot{\hat{Z}} \in \mathbb{R}^{(n+1)\times q}$, with each column describing the system's state or, respectively, its velocity. The collection of data points is denoted as

$$\hat{Z} := \left[\hat{z}(t_1)\ \hat{z}(t_2)\ \dots\ \hat{z}(t_q)\right] \quad \text{and} \quad \dot{\hat{Z}} := \left[\dot{\hat{z}}(t_1)\ \dot{\hat{z}}(t_2)\ \dots\ \dot{\hat{z}}(t_q)\right]\,.$$

This leads us to the affine linear ansatz with

$$\Gamma := \begin{bmatrix} 1 & 1 & \cdots & 1 \\ \hat{Z}_{1,1} & \hat{Z}_{1,2} & \cdots & \hat{Z}_{1,q} \\ \vdots & \vdots & \vdots & \vdots \\ \hat{Z}_{(n+1),1} & \hat{Z}_{(n+1),2} & \cdots & \hat{Z}_{(n+1),q} \end{bmatrix} \in \mathbb{R}^{(n+2)\times q}$$

for the least-square solution Ψ of

$$\dot{\hat{Z}} = G\hat{Z} - b \approx \Psi\Gamma\,. \tag{3.7}$$

This means the solution Ψ of eq. (3.7), is in the least-square sense, the solution of the minimization problem

$$\min_{\Gamma} \left\{ \left\| \Psi\Gamma - \dot{\hat{Z}} \right\|_F \right\},$$

with $\|H\|_F = \sqrt{\sum_{i=1}^{q}\sum_{j=1}^{r} |h_{ij}|^2}$ for $H \in \mathbb{R}^{q\times r}$ denoting the Frobenius norm. Classical results [83] state that the matrix

$$\Psi = \dot{\hat{Z}}\Gamma^{+} \in \mathbb{R}^{(n+1)\times(n+2)}$$

with $(\Psi)_{ij} = \psi_{ij}$, with $i = 1,\dots,n+1,\ j = 1,\dots,n+2$, and $(\Gamma)_{jk} = \gamma_{jk}$, with $j = 1,\dots,n+2,\ k = 1,\dots,q$ produces the minimum of the quadratic error $\|\Psi\Gamma - \dot{\hat{Z}}\|_F$ if Γ^{+} is the Moore-Penrose pseudoinverse of Γ. So, the least-squares solution of eq. (3.6) is given by

$$\begin{aligned}(\dot{\hat{Z}})_{ik} = \dot{\hat{z}}_{ik} &= \left(\sum_{j=1}^{n+2} g_{ij}\hat{z}_{jk}\right) - b_i\,, \quad \text{for } i = 1,\dots,n+1;\ k = 1,\dots,q \\ &= \psi_{i1}\gamma_{1k} + \sum_{j=2}^{n+2} \psi_{ij}\gamma_{jk}\,, \quad \text{with } \psi_{i1} = -b_i \text{ and } \gamma_{1k} = 1 \\ &= \sum_{j=1}^{n+2} \psi_{ij}\gamma_{jk} = (\Psi\Gamma)_{ik}\,.\end{aligned} \tag{3.8}$$

The information about the stationary point $\bar{z}$, i. e. the shifted center of the linearization, is defined as the first row of Ψ in eq. (3.8). This is motivated by the fact that the first column of G represents the dynamics of the equilibrium point. Hence, we approximate the Jacobian $D\tilde{h}$ of the controlled system (3.2) by the linearization matrix

$$G = (\Psi)_{1,\dots,n+1;2,\dots,n+2} \in \mathbb{R}^{(n+1)\times(n+1)}\,. \tag{3.9}$$

Following the partition of $D\tilde{h}$ defined in eq. (3.4), we assume

$$G \approx \left[\begin{array}{cc|c} & Df & f_\mu \\ \hline -K_P & -K_D & 0 \end{array}\right],$$

i. e., the linearization G approximates sufficiently precisely the Jacobian $D\tilde{h}$ of the controlled system (3.2), and that the upper left submatrix consisting of the first n rows and columns of G is the desired approximation for the Jacobian Df of the original system (3.1.) So, we can estimate the original stability in every equilibrium point by computing the entries of the linearization matrix of the underlying dynamical system ([26]). The real parts of the eigenvalues of Df reveal whether the stationary point is stable (all real parts are negative), unstable (there exists a positive real part), or a bifurcation point ("at least one real part is zero" is a necessary condition). See thm. 1.1 for details on stability information. Since no stability information is needed for the controlled continuation scheme, the computations for stability information

can be done in an *a posteriori* process ([26]).
An approach to approximate the right-hand side of eq. (3.6) by functions of even higher order could be realized by applying Sparse Identification of Nonlinear Dynamics (SINDy) introduced by Brunton, Proctor, and Kutz in [17]. The affine linear ansatz for the right-hand side in eq. (3.6) is replaced with a more general basis of nonlinear functions in Γ. Since the method proposed in this chapter aims to gain only information about the linear stability, we restrict ourselves to the affine linear ansatz and exclude higher-order terms.
From a pure simulator's perspective, the generated data's resolution can be as high as desired or at least necessary. From the experimenter's point of view, all measurements contain noise which one needs to bear in mind. By applying identification techniques naively to measurements of a controlled system, this noise is known to be biased (see, e. g. [103, Chapter 10]). The noise in the presented example of the Zeeman catastrophe machine was small with respect to the measured signal. This affected the control and the controlled system (3.2) only minimally; see fig. 3.1. In the present work, we restrict ourselves to the case of insignificantly small or absent noise since it has a minor relevance to the identification results. In order to avoid bias for noisy systems, one might incorporate more elaborate methods [103] than least-squares methods.

3.3 APPLICATION ON THE ZEEMAN CATASTROPHE MACHINE (ZCM)

The Zeeman catastrophe machine will serve as an example to demonstrate the proposed methods presented in chapters 3 and 4. Two stable branches clearly separated by an unstable branch form the bifurcation diagram. Each end of the unstable branch is connected to the end of one of the two stable branches by a saddle-node bifurcation point. The first intention for the introduction of the catastrophe machine by Zeeman [123] in 1972 was to give an example for the illustration of bistability and hysteresis [40, 85, 123–125]. The clear and simple construction, together with its well-described dynamics, made the machine a popular didactic tool to analyze dynamics in various aspects [72, 73, 124, 125]. Besides, the machine served as a toy model for testing and verifying methods to analyze and stabilize dynamical systems [21, 65, 82, 91], like in the present dissertation.
The names of the variables and quantities, including their values for the physical experiment and the numerical simulations described in section 3.4, can be found in table D.3 in appendix D.

3.3.1 *Setup of the ZCM*

The Zeeman catastrophe machine receives its nonlinearity from two identical springs with tensionless length L_0. Their spring constant is denoted by k. In the middle of the machine is a mass-carrying disk fixed at the origin $O = (0, 0)$, which is both the center of mass and the rotational center of the disk. Fig. 3.2 depicts the details of the experimental setup with a sketch in fig. 3.2a and a photo in fig. 3.2b. The technical details concerning the physical experimental setup can be found in appendix A. The first spring connects to the point P on the radius ρ of the disk and its fixed

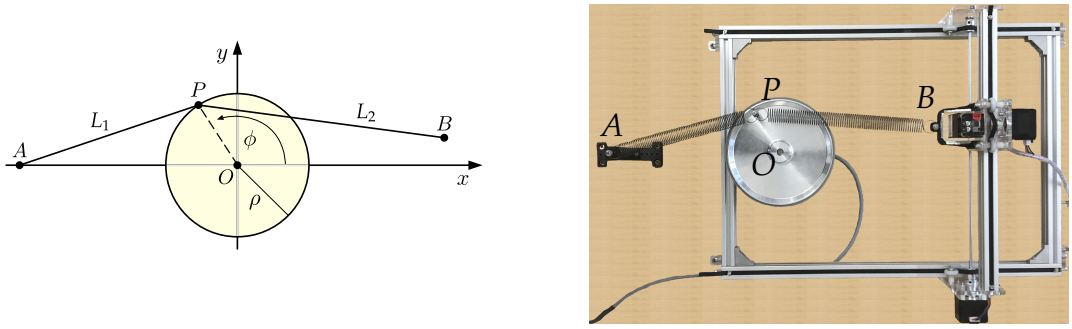

(a) Sketch (b) Photo

Figure 3.2: The Zeeman catastrophe machine illustrated as (a) sketch and (b) photo of the experiment. The point P on the disk with distance ρ to the origin O is connected with the fixed end $A = (-a, 0)$ via a spring. The second spring connects the point P with the movable point $B = (\lambda, \mu)$, whose y-coordinate is the bifurcation parameter in this chapter. A stepper motor moves the point B vertically to the line through A and O. For chapter 4, the x-coordinate is chosen as a second parameter, but for the experiments presented in chapter 3, it is kept constant. A movement in a horizontal direction is realized by a second stepper motor attached at one end of the rail for the first stepper motor. The angle ϕ of the point P is measured optically by a rotary encoder attached to the disk; see appendix A for technical details. Reproduced from [26] with kind permission from the Society for Industrial and Applied Mathematics (SIAM).

end at the point $A = (-a, 0)$ on the x-axis. The resulting length is L_1. The second spring is attached to the point P, too, and to the movable end $B = (\lambda, \mu)$. Due to the changes in μ in the y-direction, the second spring's length L_2 is variable and hence L_1, too. Note that λ, the first component of B, stays constant for the whole setup described in this chapter. The quantity of interest is the angle ϕ measured between the x-axis and the line connecting the origin with P and its velocity $\dot{\phi}$. Together, they define the state vector

$$x(t) = \begin{pmatrix} \phi(t) \\ \dot{\phi}(t) \end{pmatrix} \in \mathbb{R}^2$$

of the general dynamical system (3.1). The bifurcation parameter μ describes the y-component of the position B. In the experiment, the point B is moved by a stepper motor which is mounted on a rail that allows only movements in the vertical direction. The PD control described in section 3.1.1 is carried out by this dynamic change of the bifurcation parameter. The target angle ϕ^* is set close enough to the previous one. Since we aim for equilibrium points, the target angular velocity is set to be $\dot{\phi}^* = 0$. The difference between the actual state and the target $x^* = (\phi^*, \dot{\phi}^*)$ defines the velocity of μ by eq. (3.2b). Similar to eq. (3.2), the controlled system is

$$\begin{pmatrix} \dot{x}_1 \\ \dot{x}_2 \\ \dot{\mu} \end{pmatrix} = \frac{\mathrm{d}}{\mathrm{d}t} \begin{pmatrix} \phi \\ \dot{\phi} \\ \mu \end{pmatrix} = \begin{pmatrix} f_1(x, \mu) \\ f_2(x, \mu) \\ -K_P(\phi - \phi^*) - K_D(\dot{\phi} - (\dot{\phi})^*) \end{pmatrix} = \begin{pmatrix} f_1(\phi, \dot{\phi}, \mu) \\ f_2(\phi, \dot{\phi}, \mu) \\ -K_P(\phi - \phi^*) - K_D\dot{\phi} \end{pmatrix}, \tag{3.10}$$

where $f : \mathbb{R}^3 \to \mathbb{R}^2$ with $f = (f_1, f_2)^T$ describes the dynamics of ϕ and $\dot{\phi}$. The explicit description of the function f is unknown for the physical experiment.

3.3.2 *Controllability of the ZCM*

According to the general considerations in section 3.1.2, the machine's controlled system (3.10) can be linearized in the following matrix-vector form

$$\frac{\mathrm{d}}{\mathrm{d}t}\begin{pmatrix}\phi\\ \dot{\phi}\\ \mu\end{pmatrix} = \begin{pmatrix}0 & 1 & 0\\ \partial_\phi f_2 & \partial_{\dot{\phi}} f_2 & \partial_\mu f_2\\ -K_P & -K_D & 0\end{pmatrix}\begin{pmatrix}\phi\\ \dot{\phi}\\ \mu\end{pmatrix} = \begin{pmatrix}0 & 1 & 0\\ \partial_\phi f_2 & \partial_{\dot{\phi}} f_2 & \partial_\mu f_2\\ 0 & 0 & 0\end{pmatrix}\begin{pmatrix}\phi\\ \dot{\phi}\\ \mu\end{pmatrix} + \begin{pmatrix}0\\ 0\\ 1\end{pmatrix}\cdot\dot{\mu}\,. \tag{3.11}$$

Due to legibility reasons, the short form $\partial_x f$ for the partial derivatives is used wherever the evaluation point can be derived from the context. No assumptions about the function $f = (f_1, f_2)^T$ are made. Nevertheless, we know by the construction of the system of the Zeeman catastrophe machine that $\dot{x}_1 = x_2$ and hence $f_1(x, \mu) = \dot{\phi}$. Like in section 3.1.2, we follow from control theory [104] that eq. (3.11) can be interpreted as the time-invariant control system (3.5). With this interpretation, we get the one-dimensional control vector u, the state vector

$$v := \begin{pmatrix}\phi\\ \dot{\phi}\\ \mu\end{pmatrix}, \tag{3.12}$$

the state matrix

$$\mathsf{C} := \begin{pmatrix}0 & 1 & 0\\ \partial_\phi f_2 & \partial_{\dot{\phi}} f_2 & \partial_\mu f_2\\ 0 & 0 & 0\end{pmatrix},$$

and the input matrix

$$\mathsf{D} := \begin{pmatrix}0\\ 0\\ 1\end{pmatrix}. \tag{3.13}$$

So, the resulting controllability matrix is

$$\mathsf{R} = \left[\begin{array}{c|c|c} \mathsf{D} & \mathsf{CD} & \mathsf{C}^2\mathsf{D}\end{array}\right] = \begin{pmatrix}0 & c_{1,3} & c_{1,1}c_{1,3} + c_{1,2}c_{2,3}\\ 0 & c_{2,3} & c_{1,3}c_{2,1} + c_{2,2}c_{2,3}\\ 1 & 0 & 0\end{pmatrix} = \begin{pmatrix}0 & 0 & \partial_\mu f_2\\ 0 & \partial_\mu f_2 & \partial_{\dot{\phi}} f_2 \cdot \partial_\mu f_2\\ 1 & 0 & 0\end{pmatrix}.$$

Since generally no direct equations for the right-hand side of the original system (3.1) is obtainable, it is hardly possible to give a strict mathematical proof for the physical experiment to fulfill the controllability conditions found in section 3.1.2.

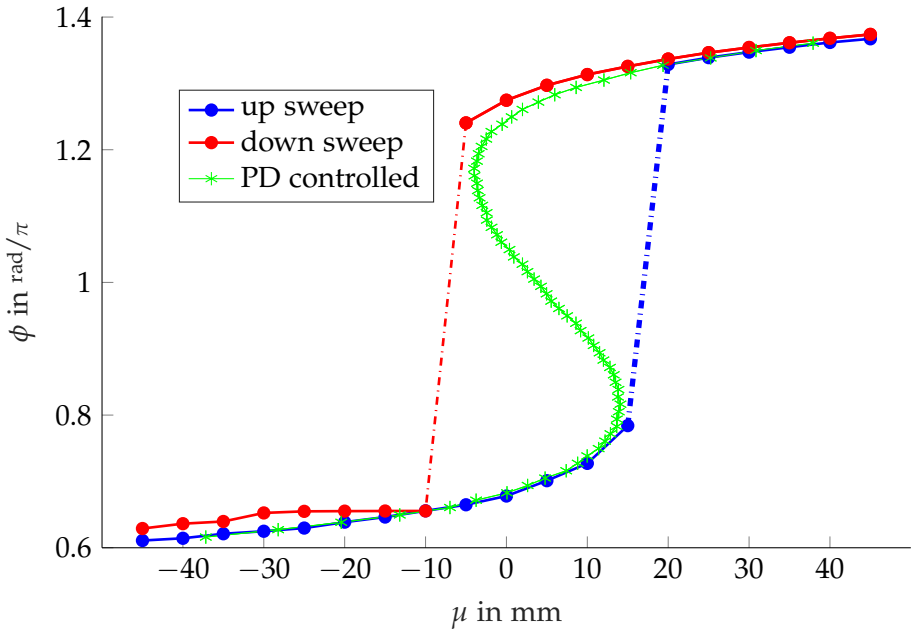

Figure 3.3: Parameter sweep for the physical Zeeman catastrophe machine with stable states compared to controlled stationary states. The measurements for the up and down sweep without control are depicted in blue and red, respectively. The dashed lines indicate the jumps, where no measurements are in between. The curve of green asterisks shows the stationary points' positions achieved by control (3.10) with control parameters $(K_P,\ K_D) = (-2\,\frac{\text{mm}}{^\circ},\ -3\,\frac{\text{mm}\cdot\text{s}}{^\circ})$. Reproduced from [26] with kind permission from the Society for Industrial and Applied Mathematics (SIAM).

Especially to give a rigorous proof for the rank of the controllability matrix R to be full is impossible. Nonetheless, after estimating the entries of the linearization matrices for the least-squares method from section 3.2, there is evidence of the controllability of the controlled system (3.10) of the Zeeman machine. First, the entries of the linearization matrix are computed by a simple difference quotient for the measured data. This is done assuming that the autonomous system (3.2a) is continuous in x and μ and locally monotone. In order to obtain robust values for the matrix entries, we apply the moving average over 10 neighboring stationary points. By these steps, we obtain $\partial_\mu f_2 < 0$ and that $\partial_{\dot\phi} f_2 < 0$ exists. These are the sufficient conditions for the controllability matrix R to have full rank. Therefore, we can conclude that the system of the physical experiment is controllable by the feedback control (3.2) in a neighborhood of all stationary points. This holds even for unstable equilibrium points.

3.3.3 *Stabilization of the controlled ZCM*

Similar to section 3.3.2 for controllability conditions, the conditions for stabilization by control (3.2b), found in section 3.1.3, will be examined in this section for the laboratory experiment of the Zeeman catastrophe machine. Hence, the eigenvalues

of the linearization matrix in eq. (3.11) must be investigated. The controlled system (3.10) is stable if all eigenvalues of its linearization matrix have negative real parts, see thm. 1.1. According to the Routh-Hurwitz criterion [52, 95] (thm. 1.4), this is fulfilled if the negative characteristic polynomial $p(\nu)$ of the linearization matrix, i. e. the normed polynomial with leading coefficient 1,

$$-p(\nu) = \nu^3 - \partial_{\dot{\phi}} f_2 \cdot \nu^2 + \left(K_D \cdot \partial_\mu f_2 - \partial_\phi f_2\right) \cdot \nu + K_P \cdot \partial_\mu f_2 \tag{3.14}$$

is a Hurwitz polynomial. This means all coefficients of eq. (3.14) must be positive. So, the first necessary conditions for stability are

$$\begin{aligned} K_D \cdot \partial_\mu f_2 > \partial_\phi f_2 \quad &\Longrightarrow \quad K_D \begin{cases} > \left(\frac{\partial_\phi f_2}{\partial_\mu f_2}\right) & \text{, if } \partial_\mu > 0 \\ < \left(\frac{\partial_\phi f_2}{\partial_\mu f_2}\right) & \text{, if } \partial_\mu f_2 < 0\,, \end{cases} \\ K_P \cdot \partial_\mu f_2 > 0 \quad &\Longrightarrow \quad \operatorname{sign}\left(K_P\right) = \operatorname{sign}\left(\partial_\mu f_2\right)\,. \end{aligned}$$

Secondly, the Hurwitz determinant and all its principle minors must be positive. For eq. (3.14), the Hurwitz determinant is

$$\begin{aligned} H_3 &= \begin{vmatrix} \partial_{\dot{\phi}} f_2 & K_P \cdot \partial_\mu f_2 & 0 \\ 1 & \left(\partial_\phi f_2 - K_D \cdot \partial_\mu f_2\right) & 0 \\ 0 & \partial_{\dot{\phi}} f_2 & K_P \cdot \partial_\mu f_2 \end{vmatrix} \\ &= K_P \cdot \partial_\mu f_2 \cdot \left(\partial_{\dot{\phi}} f_2 \cdot \left(\partial_\phi f_2 - K_D \cdot \partial_\mu f_2\right) - K_P \cdot \partial_\mu f_2\right) \end{aligned}$$

with its principal minors

$$H_1 = \left|\partial_{\dot{\phi}} f_2\right|$$

and

$$H_2 = \begin{vmatrix} \partial_{\dot{\phi}} f_2 & K_P \cdot \partial_\mu f_2 \\ 1 & \partial_\phi f_2 - K_D \cdot \partial_\mu f_2 \end{vmatrix} = \partial_{\dot{\phi}} f_2 \cdot \left(\partial_\phi f_2 - K_D \cdot \partial_\mu f_2\right) - K_P \cdot \partial_\mu f_2\,.$$

To fulfill $H_1 > 0$, we get the condition

$$\partial_{\dot{\phi}} f_2 \neq 0\,. \tag{3.15}$$

From $H_2 > 0$, we get the additional condition

$$\begin{aligned} &\partial_{\dot{\phi}} f_2 \cdot \left(\partial_\phi f_2 - K_D \cdot \partial_\mu f_2\right) - K_P \cdot \partial_\mu f_2 > 0 \\ \Longrightarrow\ &\partial_{\dot{\phi}} f_2 \cdot \left(\partial_\phi f_2 - K_D \cdot \partial_\mu f_2\right) > K_P \cdot \partial_\mu f_2 > 0 \\ \Longrightarrow\ &K_D \begin{cases} < \frac{\partial_\phi f_2}{\partial_\mu f_2} - \frac{K_P}{\partial_{\dot{\phi}} f_2} & \text{, if } \operatorname{sign}\left(\partial_\mu f_2\right) = \operatorname{sign}\left(\partial_{\dot{\phi}} f_2\right) \\ > \frac{\partial_\phi f_2}{\partial_\mu f_2} - \frac{K_P}{\partial_{\dot{\phi}} f_2} & \text{, if } \operatorname{sign}\left(\partial_\mu f_2\right) \neq \operatorname{sign}\left(\partial_{\dot{\phi}} f_2\right)\,. \end{cases} \end{aligned} \tag{3.16}$$

The last condition $H_3 > 0$ leads to

$$\begin{aligned} &K_P \cdot \partial_\mu f_2 > 0 \\ \Longrightarrow\ &\operatorname{sign}\left(K_P\right) = \operatorname{sign}\left(\partial_\mu f_2\right)\,. \end{aligned} \tag{3.17}$$

So, the signs and values of the partial derivatives of f_2 determine the conditions for the choice of values for the control parameter $K = (K_P, K_D)$. From section 3.3.2, it is already known that $\partial_\phi f_2 < 0$, which is a stronger statement than (3.15). Additionally, in section 3.3.2, it is also stated that $\partial_\mu f_2 < 0$. According to condition (3.17), the control parameter K_P must be negative. In order to obtain robust results for the values of $\partial_\phi f_2$, it is again computed by the difference quotient out of the measured data and by the moving average over 10 neighboring equilibrium points. We can derive from the values of the partial derivatives that $\partial_\phi f_2 / \partial_\mu f_2 > -1.8 \frac{\text{mm·s}}{^\circ}$ applies for all stationary points in the region of interest. Keeping to (3.16), we get the condition $K_D < -1.8 \frac{\text{mm·s}}{^\circ} - \frac{K_P}{\partial_\phi f_2}$ for the second control parameter. Considering the small noise in the experiment and some inaccuracies concerning the model, it was chosen to take $K_P = -2 \frac{\text{mm}}{^\circ}$ and $K_D = -3 \frac{\text{mm·s}}{^\circ}$. Even though no rigorous proof could be given under the assumption of having no acurate model available, the successful stabilization of unstable states in the experiment (see fig. 3.3) substantiates the stability of the controlled system (3.10). The numerical results for the analytical model (3.19) presented in section 3.4 support the assumption.

3.3.4 *Detection of stability and bifurcation points in the experiment*

The search for the asymptotically stable stationary points can be done in the uncontrolled experiment. They are the ω-limit sets found in a quasi-stationary sweep. The branch of stationary points can be found by starting at one of the edges of the rail for the motor as point B. The first position of B defines the value for μ of the first equilibrium point. Once the point B has reached the position $\bar{\mu}$, we let the system evolve until its measured absolute value of the velocity of ϕ and hence of the stationary angle $\bar{\phi}$ is below a tolerance of $0.00122 \frac{\text{rad}}{\text{s}}$ $\left(= \frac{0.001^\circ}{0.0143\,\text{s}}\right)$. This determines the position of the stationary point $(\bar{\phi}, 0, \bar{\mu})$. For the laboratory and the numerical model it is clear that the target $\dot{\phi}^*$ must be zero. For other systems fulfilling the general form eq. (3.2), the target value for the second coordinate x_2 may not be that obvious. Then, the value of $\bar{\mu}$ is increased by 5 mm in the up sweep. This procedure is repeated until B reaches the other edge of the rail. The observed quasi-stationary behavior is due to the slow change of parameters. In order to find the second stable branch, a down sweep starts at the second edge of the rail. The stationary points are again found by letting the system evolve until nearly no movement is detected. Instead of increasing, the position $\bar{\mu}$ is decreased by 5 mm for a down sweep. As already stated in the introduction to section 3.3, the resulting stable branches of stationary points are clearly interrupted by an unstable one. This bistable behavior, particularly the hysteresis, is visualized in fig. 3.3.

In order to localize the bifurcation points and the branch of unstable equilibria, we apply the feedback control (3.2b). The sweep starts again for the position of B at one edge of the rail, preferably on a stable branch outside the bistable regime. From the up or down sweep, the coordinates $(\bar{\phi}, 0, \bar{\mu})$ of the equilibrium of that starting position are known. The angle $\bar{\phi}$ is set to be the first target ϕ^* for the controlled system. With the choice $K_P = -2 \frac{\text{mm}}{^\circ}$ and $K_D = -3 \frac{\text{mm·s}}{^\circ}$ motivated in section 3.3.3 to guarantee the stability of the controlled system, the curve of the bifurcation diagram is obtained. The controlled system (3.10) is evolved until it

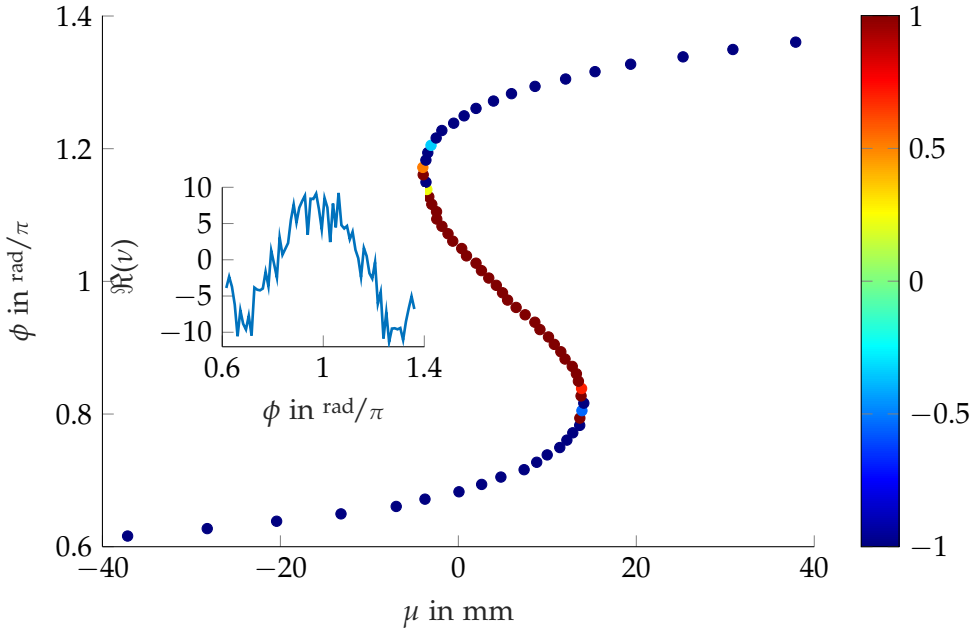

(a) Stability information evaluated in each stationary point taking the trajectory data in the neighborhood of each stationary point. The slight estimation inaccuracies are mostly due to nonoptimal lengths of the trajectories and noise.

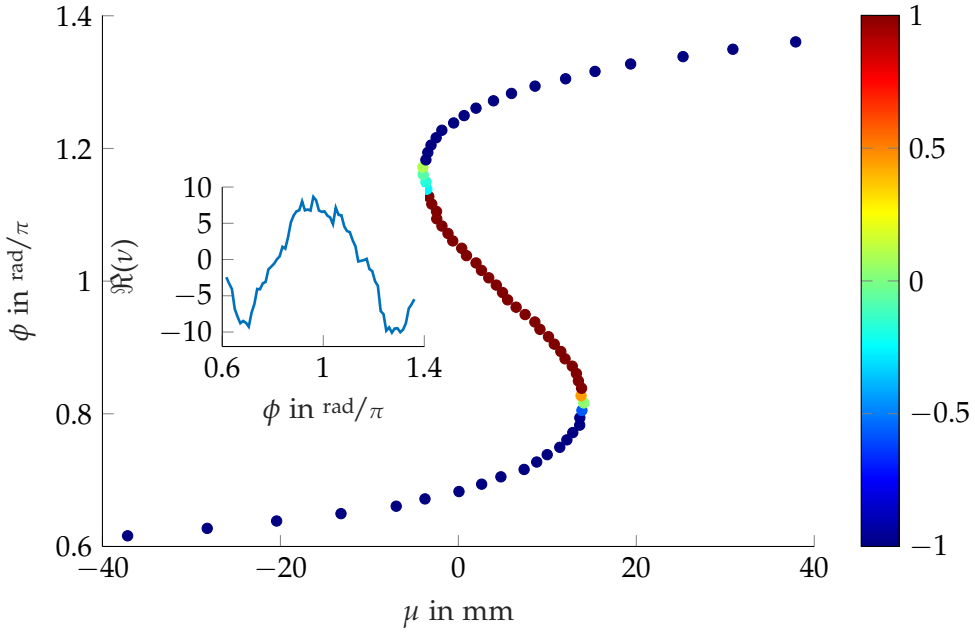

(b) Stability information evaluated as a moving average, including the 2 neighboring points of the stationary points depicted in (a). The average is then taken of 3 points in the interval $[\phi^* - \Delta\phi, \phi^* + \Delta\phi]$ with $\Delta\phi = 0.0349\,\text{rad}(= 2°)$.

Figure 3.4: Stability evaluated for the controlled physical experiment by approximating G for $\dot{\hat{Z}} = G\hat{Z}$ with the least-squares approach from section 3.2. The color code indicates the largest real part of the eigenvalues of G in eq. (3.9) and hence the estimated stability of each stationary point. The color scale is limited to the interval $[-1, 1]$ for stressing out the behavior in the neighborhood of the bifurcation points. The insets plot the maxima of the eigenvalues' real parts against ϕ. Reproduced from [26] with kind permission from the Society for Industrial and Applied Mathematics (SIAM).

reaches an equilibrium. Contrary to the previously described sweeps for finding stable branches, the parameter μ is dynamic, and its motions are defined by the control law (3.2b). The dynamics of μ is an extension of the original system and brings it to the whole branch of stationary points. As already proven in section 3.1.1, the sets of stationary points traceable by eq. (3.10) and the original system are the same. Hence, the motor moves the position of B following the discretized version of the scheme for the feedback control (3.2b):

$$\mu_{k+1,l} = \mu_{k,l} - K_P\,(\phi_{k,l} - \phi_l^*) - K_D\,\left(\frac{\phi_{k+1,l} - \phi_{k,l}}{\Delta t}\right). \tag{3.18}$$

Here, k is the index for the number of stabilizing updates for the l-th found equilibrium with $\bar{\phi} = \phi_l^*$. For simplicity reasons, the time-difference quotient for the change $\left(-K_P\,(\phi_{k,l} - \phi_l^*) - K_D\,\left(\frac{\phi_{k+1,l}-\phi_{k,l}}{\Delta t}\right)\right)$ is set to 1. The system is considered to have reached an equilibrium when only velocities below certain tolerances for $(\phi, \dot{\phi}, \mu)$ are reached. Then, the target ϕ^* is increased by 0.0349 rad $(= 2°)$ before the system evolves again and settles at the next stationary point. Following this procedure, the curve of stationary points contains two stable branches and its originally unstable connection. The result compared to the ones of the quasi-stationary up-and-down sweeps is presented in fig. 3.3. The slight mismatch between the curve of only-stable equilibria and the one including the bifurcation and unstable stationary points is most likely caused by some inaccuracies concerning the experimental setup. The timing belt mechanism or missed transitions from the rotary encoder could cause imprecisions ([26]).

The stationary points shown in fig. 3.3 can be directly determined to be asymptotically stable because the controlled system (3.10) reaches them by direct evolution. Since we are interested in the stability information of the stationary points of the underlying originally uncontrolled system, we apply the method proposed in section 3.2 to the data generated by the controlled system following the curve of stationary points. Fig. 3.4 shows the result. Even though some values of partial derivatives and hence the individual entries of approximation (3.9) for the linearization matrix are not exactly determined, the eigenvalue information is fairly robust. In the bistable regime and even in an area around it, the largest real part of the eigenvalues determining the stability is depicted as blue for negative, red for positive, and green for values close to zero, i. e. numerically seen as quasi-zero. The insets in fig. 3.4 visualize the same facts but directly overview the value of the largest eigenvalue over the angle ϕ. To gain reliable stability information, the method of section 3.2 needs sufficiently different data points apart from low-noise measurements. In order to avoid measuring only noise in the ω-limit set, the target value ϕ^* should not be too close to the initial point. In the experimental setup, avoidable measurement noise and slackness in the experimental data can be obviated by tightening up the timing belt ([26]).

As mentioned above, the measurement data should not be taken from the ω-limit set. If the system is already close to the asymptotically stable equilibrium point, the overall-existing noise is large compared to the quasi-vanishing velocity. To circumvent this problem, only the first 40 time steps with $\Delta t = 1/70\,\mathrm{s}$ (or even less if the system settles earlier) in the neighborhood of each stationary point are

taken for the stability analysis. In order to get more robust and hence even more reliable estimates, the stability information for each stationary point (ϕ_k, μ_k) in fig. 3.4b is computed as the moving average, including the two neighboring states (ϕ_{k-1}, μ_{k-1}) and (ϕ_{k+1}, μ_{k+1}) of the values used to produce fig. 3.4a. The positions of the equilibrium points are the same in both figures.

Besides the question about the choice of data for the analysis, the physical setup of the experiment has some limitations which may not be respected in the pure mathematical notation of the differential equation system (3.10) describing approximately the main dynamical processes. In the specific case of the Zeeman machine presented in section 3.3.1 and appendix A, the usage of the rotary encoder implies two restrictions, namely an upper limit for the resolution due to the discretization of angles and bounded speed of signal tranmissions ([26]). No effect on the angle measurements could be identified, whereas the detection rate for the signal transmission is crucial. In case of missing such a transmission, the measurements for the angle variable ϕ are offset, i. .e., the originally desired control target ϕ^* is then identified as another value and will not be reached in that step of the sweep. For cases with different setups, particularly those that allow faster dynamics (e. g., lower mass or stronger springs), the hardware must perform the signal readout faster for the angular position. As already mentioned, in the case of a sufficiently tightened timing belt, almost no measurement noise could be detected by using the digital metering of the angle. Therefore, no further considerations will be made on the effect of noise on the specific system of the Zeeman machine. For systems with relevant noise due to different dynamics or sensor devices, more elaborate methods [103] are noteworthy for identifying the signal.

The static friction, which lets the system stop before reaching the target state, creates additional difficulty for the experimental performance. In particular, for the sweep with only originally stable points, i. e. disabled control, the friction caused imprecisions in the determination of the angular positions for stationary points. In this case, the motor controlling the position of the point B is first moved twice the step size forward and then one step back in order to increase the angular velocity in the neighborhood of the equilibrium point.

Apart from the physical limitations, choosing the values for the control parameters is challenging since the system reaches its final state only after several oscillatory periods around the equilibrium ([26]). On the one hand, one aim is to keep the number of periods as small as possible because with the choice $K = (K_P,\ K_D) = (-2\,\frac{\text{mm}}{^\circ},\ -3\,\frac{\text{mm}\cdot\text{s}}{^\circ})$ motivated in section 3.3.3 tracing the entire bifurcation diagram (figs. 3.3 and 3.4) last 15 minutes, whereas a simple up or down sweep takes only 3 minutes. Faster convergence to the ω-limit sets and hence faster realization of the experiment can be achieved by increasing the absolute values of the control parameters K_P and K_D. In section 3.3.3, we have shown that only lower bounds exist for their absolute values to guarantee stability. On the other hand, physical experiments entail some limits due to the technical realizations (e. g. motors, belts, or measurement hardware). This restricts the choice of the values of K since too large values would make it impossible to follow the control output. For mechanically more sensitive, "real-world" systems, it may be impractical to have such a slow convergence towards the ω-limit sets because of e. g. changes in

environmental parameters like the temperature ([26]). If these circumstances continuously modify the system's characteristics, more sensitive measurement hardware could enable the choice of larger absolute values of the control parameter for higher convergence speed. This is a minor question for simple systems such as the Zeeman machine.

3.4 RESULTS FOR THE MATHEMATICAL MODEL

When applying the technique to determine the original stability presented in section 3.2, generally, no explicit mathematical description is obtainable for the system under investigation. Only data can give useful information. In the case of the Zeeman machine presented in section 3.3, a good mathematical model for the dynamics exists and will be taken to compare analytical and data-based results. So, this section gives evidence for the analysis and results from physical experiments and especially for the obtained data in section 3.3.

3.4.1 *Mathematical model for the ZCM*

The model for the motion of the angle ϕ and its velocity $\dot{\phi}$ can be derived by classical mechanics under the usage of the Lagrange formalism, e. g. in [72]. Even though the trajectories differ depending on the disk's geometry and mass distribution, the position of the stationary points stays constant under such alterations ([26]). We assume a pointlike mass m at the point P for a simple approximation of the disk's behavior. The term $-d\dot{\phi}$ summarizes all relevant friction of the joints at points A, B, and P and in the rotational axis. The model is given as the two first-order ordinary differential equations

$$\frac{\mathrm{d}\phi}{\mathrm{d}t} = \dot{\phi} \tag{3.19a}$$

$$\frac{\mathrm{d}\dot{\phi}}{\mathrm{d}t} = \frac{k}{m\rho}\left(\frac{L_1(\phi) - L_0}{L_1(\phi)} \cdot a \cdot \sin\phi + \frac{L_2(\phi) - L_0}{L_2(\phi)} \cdot (\mu \cdot \cos\phi - \lambda \cdot \sin\phi)\right) - d \cdot \dot{\phi} \tag{3.19b}$$

with the spring lengths

$$L_1(\phi) = \sqrt{(\rho \cdot \cos\phi + a)^2 + (\rho \cdot \sin\phi)^2} \qquad \text{and}$$

$$L_2(\phi) = \sqrt{(\lambda - \rho \cdot \cos\phi)^2 + (\mu - \rho \cdot \sin\phi)^2}\,.$$

The system is again stabilized by the one-dimensional control

$$u = \dot{\mu} = -K_P(\phi - \phi^*) - K_D\,\dot{\phi}\,. \tag{3.20}$$

like in section 3.3. To keep the control law well-defined, we assume $\phi, \phi^* \in (\pi, 2\pi)$. The aim of section 3.4 is to obtain a good comparison between the data from the experiment and the simulation. Therefore, the following values for the simulation are chosen similar to the experimental setup: spring constant $k = 5\,\mathrm{N/m}$, mass $m = 0.3\,\mathrm{kg}$, distance $\rho = 65\,\mathrm{mm}$ from the origin to the point P on the disk, length

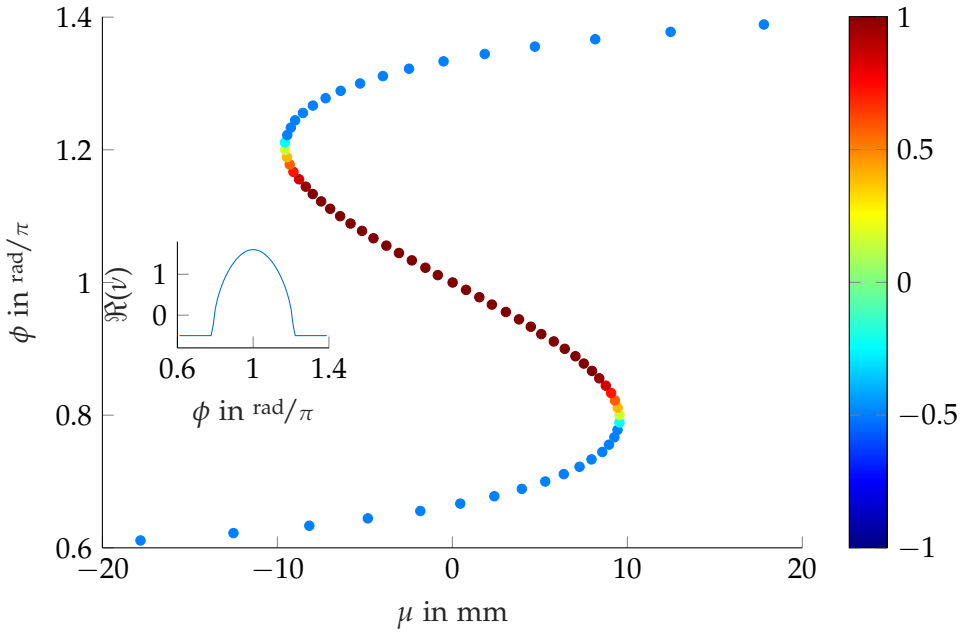

(a) Stability computed by the largest real part of eigenvalues of the Jacobian for the analytical model (3.19).

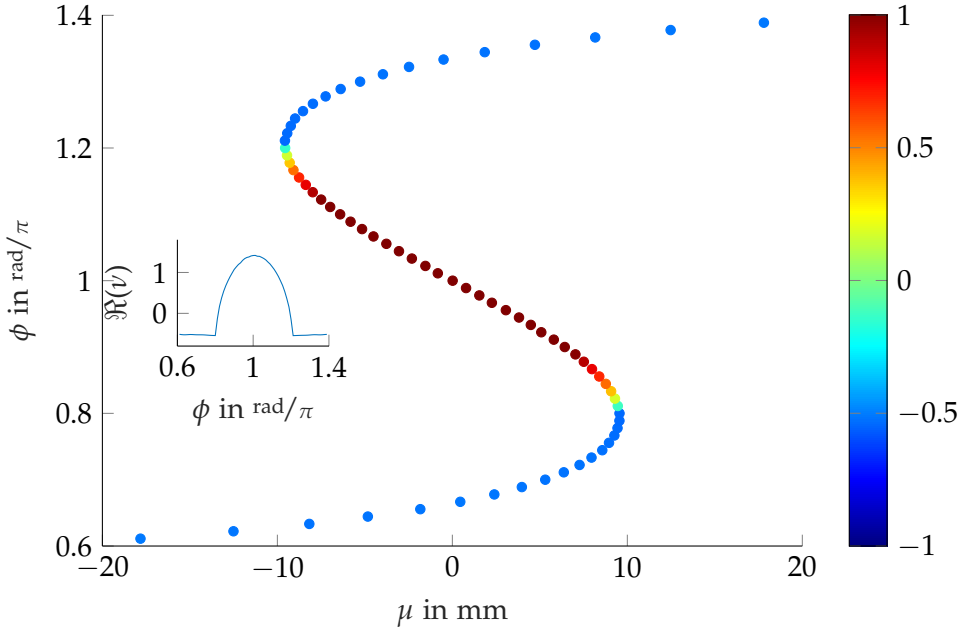

(b) Stability computed by largest real part of the eigenvalues of G for the least-squares approach $\dot{\hat{Z}} = G\hat{Z}$ in section 3.2 with trajectory data in the neighborhood of each stationary point. The data points must be at a distance large enough to the stationary point to reveal information on the dynamic behavior.

Figure 3.5: Stability evaluation for the original simulation model (3.19) with data from the system controlled by eq. (3.20). The color code indicates the largest real part of the eigenvalues of G in eq. (3.9) and hence the estimated stability of each stationary point. The color scale is limited to the interval $[-1, 1]$ for stressing out the behavior in the neighborhood of the bifurcation points. The insets plot the maxima of the eigenvalues' real parts against ϕ. Reproduced from [26] with kind permission from the Society for Industrial and Applied Mathematics (SIAM).

$L_0 = 55\,\text{mm}$ of the springs without tension, distance $|a| = 244\,\text{mm}$ from the origin to the fixed end A, and distance $\lambda = 230\,\text{mm}$ from the origin O to the movable end B. Since no direct measurements are available, we assume $d = 1\,\text{s}^{-1}$ for the damping constant $\delta = d \cdot m$.

3.4.2 *Controllability of the ZCM model*

Like in section 3.3.2, the model of the controlled system (3.19) with eq. (3.20) can be written in a matrix-vector form. Compared to eq. (3.10), for $f : \mathbb{R}^3 \to \mathbb{R}^2$, $(\phi, \dot{\phi})^T \to (\dot{\phi}, \ddot{\phi}, \mu)^T$ describing the dynamics, we can give the explicit analytic partial differentials

$$\begin{aligned}\partial_\phi f_2 =& \frac{k}{m\rho} \cdot \Bigg(- \frac{L_0 \cdot \rho \cdot (a \cdot \sin\phi)^2}{(L_1(\phi))^3} + \frac{L_1(\phi) - L_0}{L_1(\phi)} \cdot a \cdot \cos\phi \\ & - \frac{L_0 \cdot \rho \cdot (\lambda \cdot \sin\phi - \mu \cdot \cos\phi)^2}{(L_2(\phi))^3} - \frac{L_2(\phi) - L_0}{L_2(\phi)} \cdot (\mu \cdot \sin\phi + \lambda \cdot \cos\phi) \Bigg),\end{aligned} \tag{3.21}$$

$\partial_{\dot{\phi}} f_2 = -d$, and

$$\begin{aligned}\partial_\mu f_2 =& \frac{k}{m\rho} \Bigg(\frac{\partial}{\partial\mu} \left(\frac{L_2(\phi) - L_0}{L_2(\phi)} \right) \cdot (\mu \cdot \cos\phi - \lambda \cdot \sin\phi) \\ & + \frac{L_2(\phi) - L_0}{L_2(\phi)} \cdot \frac{\partial}{\partial\mu} (\mu \cdot \cos\phi - \lambda \cdot \sin\phi) \Bigg) \\ =& \frac{k}{m\rho} \Bigg(\frac{L_0}{L_2(\phi)^{5/2}} \cdot (\mu^2 \cdot \cos\phi - \lambda \cdot \mu \cdot \sin\phi - \mu \cdot \rho \cdot \cos\phi \cdot \sin\phi \\ & + \lambda \cdot \rho \cdot \sin^2\phi) + \frac{L_2(\phi) - L_0}{L_2(\phi)} \cdot \cos\phi \Bigg).\end{aligned} \tag{3.22}$$

This results in the linearization

$$\frac{\mathrm{d}}{\mathrm{d}t} \begin{pmatrix} \phi \\ \dot{\phi} \\ \mu \end{pmatrix} = \begin{pmatrix} 0 & 1 & 0 \\ \partial_\phi f_2 & -d & \partial_\mu f_2 \\ -K_P & -K_D & 0 \end{pmatrix} \begin{pmatrix} \phi \\ \dot{\phi} \\ \mu \end{pmatrix} = \begin{pmatrix} 0 & 1 & 0 \\ \partial_\phi f_2 & -d & \partial_\mu f_2 \\ 0 & 0 & 0 \end{pmatrix} \begin{pmatrix} \phi \\ \dot{\phi} \\ \mu \end{pmatrix} + \begin{pmatrix} 0 \\ 0 \\ 1 \end{pmatrix} \cdot \dot{\mu},$$

which can be interpreted as the system (3.5) with the one-dimensional control $u := \mu$, the state vector (3.12), the input matrix (3.13), and the state matrix

$$\mathsf{C} = \begin{pmatrix} 0 & 1 & 0 \\ \partial_\phi f_2 & -d & \partial_\mu f_2 \\ 0 & 0 & 0 \end{pmatrix}.$$

The resulting controllability matrix is

$$\mathsf{R} = \left[\begin{array}{c|c|c} \mathsf{D} & \mathsf{CD} & \mathsf{C}^2\mathsf{D} \end{array} \right] = \begin{pmatrix} 0 & c_{1,3} & c_{1,1}c_{1,3} + c_{1,2}c_{2,3} \\ 0 & c_{2,3} & c_{1,3}c_{2,1} + c_{2,2}c_{2,3} \\ 1 & 0 & 0 \end{pmatrix} = \begin{pmatrix} 0 & 0 & \partial_\mu f_2 \\ 0 & \partial_\mu f_2 & -d \cdot \partial_\mu feq : df2dm_2 \\ 1 & 0 & 0 \end{pmatrix}.$$

Since the numerical model eqs. (3.19) and (3.20) only served for comparison, an analytical determination of the limits for $\partial_\mu f_2$ in eq. (3.22) was eschewed.
A numerical evaluation of the partial derivative given in eq. (3.22) with realistic values given in section 3.4.1 indicates that $-15 < \partial_\mu f_2 < 0$ for $(\mu, \phi) \in [-0.15, 0.15] \times [1.8, 4.4]$. Hence, $\mathrm{rank}(\mathsf{R}) = 3$ holds for the considered bistable area. In section 3.1.2, it was discussed that this is a sufficient condition for the controllability of the system in stationary points. Simulations for larger parameter intervals of ϕ and μ reveal the controllability of even larger areas.

3.4.3 *Stabilization of the ZCM model*

In order to find the criteria for the choice of values for the control parameter K, we can analyze the linearization matrix $D\tilde{h}$ of the model (3.19) together with its control (3.20), which is given as

$$D\tilde{h} = \begin{pmatrix} 0 & 1 & 0 \\ \partial_\phi f_2 & -d & \partial_\mu f_2 \\ -K_P & -K_D & 0 \end{pmatrix} . \tag{3.23}$$

Similar to section 3.3.3, we consider the Routh-Hurwitz criterion [52, 95] (thm. 1.4) for the sign of the eigenvalues' real parts of $D\tilde{h}$. Inserting $\partial_\phi f_2 = -d$ into eq. (3.14), the negative of the characteristic polynomial of $D\tilde{h}$ can be written as

$$-p(\nu) = \nu^3 + d\nu^2 + \left(K_D \cdot \partial_\mu f_2 - \partial_\phi f_2\right) \nu + K_P \cdot \partial_\mu f_2 \, .$$

The generally given conditions (3.15,3.17) together with $\partial_\phi f_2 = -d < 0$ lead to the following conditions for the model (3.19) and (3.20):

$$d > 0 \, , \tag{3.24a}$$

$$\Longrightarrow K_D \begin{cases} < \frac{\partial_\phi f_2}{\partial_\mu f_2} + \frac{K_P}{d} & , \text{ if } \partial_\mu < 0 \\ > \frac{\partial_\phi f_2}{\partial_\mu f_2} + \frac{K_P}{d} & , \text{ if } \partial_\mu > 0 \end{cases} , \quad \text{and} \tag{3.24b}$$

$$\mathrm{sign}\left(K_P\right) = \mathrm{sign}\left(\partial_\mu f_2\right) \, . \tag{3.24c}$$

The condition (3.24a) is fulfilled because it holds $d > 0$ for the damping factor by definition. According to section 3.4.2, it is known from numerical evaluations that $\partial_\mu f_2 < 0$ holds for $(\mu, \phi) \in [-0.15, 0.15] \times [1.8, 4.4]$ and realistic values given in section 3.4.1. Hence, it must be $K_P < 0$ for guaranteed stability. The same numerical evaluations also show that $\partial_\phi f_2$ is bounded, and a value

$$K_D < \min_{(\mu,\phi)} \left\{ \frac{\partial_\phi f_2}{\partial_\mu f_2} \right\} + \frac{K_P}{d} \tag{3.25}$$

always exists for the control parameter, thus. For the given realistic values in the model (3.19), it holds $\frac{\partial_\phi f_2}{\partial_\mu f_2} > -0.7 \, \frac{\mathrm{mm \cdot s}}{^\circ}$. So, $K_D < (K_P - 1)\,\mathrm{s}$ is a safe choice for the control. Hence, with the right choice for the control parameters K_P and K_D satisfying conditions (3.24c) and (3.25), each stationary point of the model system (3.19) can be stabilized by control (3.20).

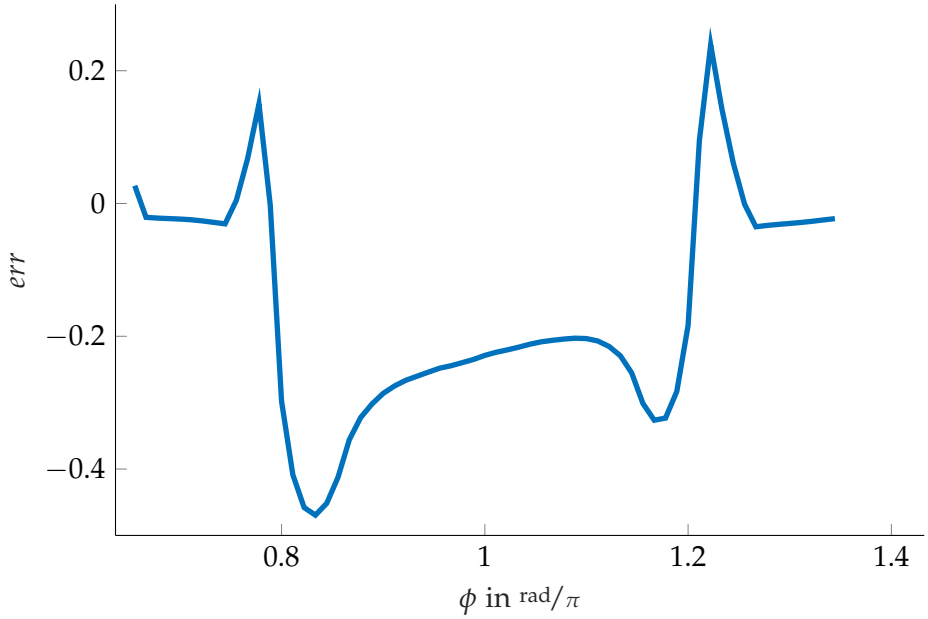

Figure 3.6: Comparison of the distance $err = r_a - r_e$ between stability results r_a for the analytical model (3.19) of the ZCM and r_e for the largest real part of the eigenvalues of the least-squares solution G in $\hat{\dot{Z}} = G\hat{Z}$ in section 3.2. The corresponding values are shown in color code in fig. 3.5a and fig. 3.5b respectively.

3.4.4 *Detecting stability and bifurcation points of the ZCM model*

In order to compare the results of the simulation for the model (3.19,3.20) with the ones for the experiment presented in section 3.3, we chose the control parameters $K_P = -2\,\frac{\text{mm}}{\circ}$ and $K_D = -3\,\frac{\text{mm}\cdot\text{s}}{\circ}$ to be similar to the experiment. According to the conditions (3.24c) and (3.25) and the numerically evaluated partial derivatives of f_2, stability of the stationary points can be guaranteed.
The detection of stability information on the underlying uncontrolled system (3.19) follows the same steps as in the experiment presented in section 3.3.4. First, the whole curve of stationary points is found by simulation of the model system (3.19) controlled by (3.20). The procedure has the same rules for the detection of stationarity as the one for the experiment presented in section 3.3.4. The angular position and velocity, together with the value for the parameter μ in each time step, are stored. Then, the optimal approximation in the least-squares sense for the linearization matrix (3.23) is derived by the routine of section 3.2 applied to the motion data. One motivation for choosing the Zeeman machine as an example was its easily accessible model. The analytically derived partial derivatives given in eqs. (3.21) and (3.22) and by $\partial_\phi f_2 = -d$ allow for constructing the whole linearization $D\tilde{h}$. Its largest real parts of the eigenvalues are compared to the least-squares approximation in each stationary point that the simulation finds. The results are presented in fig. 3.5. The analytically obtained stability information is shown in fig. 3.5a. They are set into comparison to the least-squares solution (3.9) for the numerically generated data, which is presented in fig. 3.5b. A quantitative comparison between the analytical results and the least-squares solution approach is presented in fig. 3.6. It can be seen

that the stability information of the originally stable stationary points is almost met by the least-squares approach. The values of the largest real part of the eigenvalues of the linearization matrix in originally unstable stationary points are overestimated by the least-squares approach, whereas the eigenvalue information in the bifurcation points (peaks in fig. 3.6) is underestimated. The number of time steps taken for the estimation of the least-squares solution G in $\dot{\hat{Z}} = G\hat{Z}$ introduced in section 3.2 is not varied for the whole bifurcation diagram. The different systematic errors concerning the sign of the errors in the neighborhood of bifurcation points and the originally unstable equilibria could be caused by this mismatch in the time-series length. The asymmetry of the graph in fig. 3.6 is mostly due to the direction of changes of the target ϕ^*. Here, ϕ^* is changed by the positive increment $\Delta\phi = 2^\circ$ for each next equilibrium.

Even though the model (3.19) and (3.20) simplifies the mechanical processes, the great similarity of fig. 3.5 and fig. 3.4 give evidence for a good approximation of the mechanical behavior of the physical experiment.

In addition, the already-known values of the control parameter $K = (K_P,\ K_D) = (-2\,\frac{\mathrm{mm}}{^\circ}, -3\,\frac{\mathrm{mm\cdot s}}{^\circ})$ can be directly derived from the last line of the linearization matrix (3.9) with a relative error of less than 2%. This is possible because no noise was present in the numerical model.

4

CONTINUATION OF BIFURCATION POINTS

In chapters 2 and 3, the investigated systems $\dot{x} = f(x, \mu)$ were assumed to rely only on a one-dimensional parameter $\mu \in \mathbb{R}$. In the present chapter, we extend the system by an additional variable parameter $\lambda \in \mathbb{R}$. The aim is then to continue the curve of bifurcation points of the extended system $\dot{x} = f(x, \mu, \lambda)$ depending on μ and λ instead of following the curve of stationary points for a fixed λ.
For explicitly given models, a bifurcation point can be detected by investigating points at which the Jacobian has a singularity. A change of sign for the prediction step in a secant method might be an indication of the neighborhood of a bifurcation point, see, e. g. [28, 29]. The type of this bifurcation can be explored by test functions like in, e. g., [61, Chapter 10]. This already leads to the idea of detecting bifurcation points in experimental setups but requires information about the derivatives or the possibility of initializing the system several times at the same point. Since this is generally not given and hardly obtainable from laboratory experiments, the theory must be adapted to a data-oriented approach.
Other model-oriented methods extend the pseudo-arclength method introduced in chapter 3 by an additional condition for the equilibrium to be a bifurcation point. A good overview and an extension to a higher-dimensional system can be found in, e. g. [75]. These methods need numerical derivative information for Newton-like methods that are in experimental setups hardly or not available. Hence, their application on data-oriented problems or even direct measuring in bifurcation points is not robust.
Data-oriented approaches to track the curve of limit-point bifurcations or backbone curves like, e. g., [7, 93, 94] analyze directly bifurcation diagrams which depend on the first bifurcation parameter μ and are constructed for a set of fixed values of the second bifurcation parameter λ. The curve of bifurcation points depending on μ and λ can be reconstructed in an *a posteriori* process.
Another data-oriented approach is introduced in [93]. The authors propose to use the control-based continuation (CBC) first introduced in [101] to track limit-point bifurcations and backbone curves. Similar to the previously presented approaches, they keep the additional parameter λ fixed for finding one bifurcation point. With an estimated target position for the new bifurcation point, predefined by a linear prediction from the two previously found bifurcation points, several experimental repetitions with varied target positions around the estimated one are run with CBC. The gained data is then used for polynomial regression of the bifurcation point's position. The fact that the bifurcation point is an extremum in the bifurcation parameter μ is used for the position's estimation [61, Chapter 3]. With this method, even for a laboratory experiment on a mechanical single-degree-of-freedom oscillator, the curve of bifurcation points could be constructed except for cusp bifurcations. This is a general problem in higher-order singularities; see [98] and the results presented in sections 4.2 and 4.3 for further details.

4.1 CONTINUATION OF BIFURCATION POINTS IN PD-CONTROLLED SYSTEMS

In the following, a data-based continuation method is presented that needs simply one prediction for a bifurcation point as the initialization. For all subsequent bifurcation points, starting in a previously found bifurcation point and searching with any target in a coarse neighborhood is sufficient. In chapters 2 and 3, we considered a dynamical system of the type

$$\dot{x} = f(x, \mu) \tag{4.1}$$

with $\mu \in \mathbb{R}$. So, the dynamics of the state x depend on a one-dimensional bifurcation parameter. In the following, we will aim to find bifurcation points of eq. (4.1) that are dependent on the additional parameter $\lambda \in \mathbb{R}$, which was, e. g. in chapter 3, a fixed value for the model (3.19) of the Zeeman catastrophe machine. Therefore, we assume that the function f depends on the state $x \in \mathbb{R}^2$ and the bifurcation parameter $(\mu, \lambda)^T \in \mathbb{R}^2$. This leads to the dynamical system

$$\dot{x} = f(x, \mu, \lambda)\,, \tag{4.2}$$

which will be referred to as the *original system* throughout the present chapter. The idea of the following control method is to bring the original system (4.2) to a stabilized bifurcation point with the predefined target x^* for the state x of the underlying uncontrolled system (4.1) for a fixed λ. The control mechanism (3.2b) for the bifurcation parameter μ from section 3.1 can be kept unchanged. This ensures a stable stationary point. But we include an additional condition, namely the point to be a bifurcation point of the original system. One necessity for the point to be a bifurcation point is that one eigenvalue of the Jacobian Df of f for the linearization of eq. (4.2) has a zero real part. We use this fact for the control applied the bifurcation parameter λ.
Since we approach the bifurcation point usually from the branch of stable equilibria, it is sufficient to consider the largest real part of the eigenvalues. Further bifurcation points could exist on the branch of unstable stationary states that are not detected by this method because the largest eigenvalue is $\nu > 0$. So, only bifurcations in which at least one stable stationary point collides are traceable. For the herein studied cases, this limitation is sufficient.
Let ν be the real part of the largest eigenvalue of Df. It is estimated by the stability detection method presented in section 3.2. Here, the Jacobian Df is estimated by the first n rows and columns of G in eq. (3.9). The parameter is adapted proportionally in the opposite direction of ν to force the system to a bifurcation point of the originally uncontrolled system (4.2), i. e., controlled with a control target $\nu^* = 0$. This results in the following control scheme

$$\dot{x}_1 = x_2 \tag{4.3a}$$
$$\dot{x}_2 = f_2(x_1, x_2, \mu, \lambda) \tag{4.3b}$$
$$\dot{\mu} = -K_P(x_1 - x_1^*) - K_D x_2 \tag{4.3c}$$
$$\dot{\lambda} = -K_B \cdot \nu \tag{4.3d}$$

with the control parameter $K = (K_P, K_D, K_B) \in \mathbb{R}^3$. So, the control parameter K consists of the proportional part K_P and the differential part K_D to stabilize

the stationary points and the part K_B to guarantee an original bifurcation point. Therefore, the difference $(\nu - \nu^*)$ is simply ν. The control (4.3d) vanishes at a bifurcation point of the original system, and the method is hence again noninvasive. The bifurcations points of the original system (4.1) for fixed λ are identical to the stationary points of the bifurcation-point continuation (4.3): If $(\overline{\overline{x}}, \overline{\overline{\mu}})$ is a bifurcation point for $\overline{\overline{\lambda}}$ of eq. (4.1) corresponding to the point $(\overline{\overline{x}}, \overline{\overline{\mu}}, \overline{\overline{\lambda}})$, and if, in addition, the state $\overline{\overline{x}}$ is identical to the control target x^*, it is $\dot{x} = 0$, $(\overline{\overline{x}} - x^*) = 0$, and it holds $\nu = 0$ for the largest real part ν of the eigenvalues of the linearization matrix. Then $\dot{\mu} = 0$ and $\dot{\lambda} = 0$, and $(\overline{\overline{x}}, \overline{\overline{\mu}}, \overline{\overline{\lambda}})$ must be a stationary point of eq. (4.3). If reversely $(\overline{\overline{x}}, \overline{\overline{\mu}}, \overline{\overline{\lambda}})$ is an equilibrium point of eq. (4.3), it holds $\dot{x} = 0$, $\dot{\lambda} = 0$, and $\nu = 0$, which means that $(\overline{\overline{x}}, \overline{\overline{\mu}})$ is a bifurcation point of eq. (4.1). Since the control (4.3c) and (4.3d) vanishes at a bifurcation point of eq. (4.1), the proposed control method is noninvasive.

4.1.1 *Controllability and observability of the bifurcation-point continuation*

To show the controllability of the bifurcation-point continuation (4.3), we assume again that the dynamics are similar to the linearization around each stationary point $(\bar{x}_1, \bar{x}_2, \bar{\mu}, \bar{\lambda})$ in the region of interest, particularly each bifurcation point. Analogously to eqs. (2.4), (2.12) and (3.3), the controlled system (4.3) can be written as

$$\dot{z} = \check{h}(z) = \frac{\mathrm{d}}{\mathrm{d}t} \begin{pmatrix} x_1 \\ x_2 \\ \mu \\ \lambda \end{pmatrix} \quad \text{with } z = (x_1, x_2, \mu, \lambda)\,. \tag{4.4}$$

Since the linearization is a local approximation, we again use the notation

$$\delta z = z - \bar{z}$$

for the vectors in the tangent space at the stationary point $\bar{z} = (\bar{x}_1, \bar{x}_2, \bar{\mu}, \bar{\lambda})$. So, the right-hand side of the linearization of eq. (4.4) defined on the neighborhood of the point $\bar{z}$ can now be written as

$$(\dot{\delta z}) = D\check{h}(\bar{z}) \cdot \delta z = \begin{pmatrix} 0 & 1 & 0 & 0 \\ \partial_{x_1} f_2 & \partial_{x_2} f_2 & \partial_\mu f_2 & \partial_\lambda f_2 \\ -K_P & -K_D & 0 & 0 \\ -K_B \cdot \partial_{x_1}\nu & -K_B \cdot \partial_{x_2}\nu & -K_B \cdot \partial_\mu \nu & -K_B \cdot \partial_\lambda \nu \end{pmatrix} \cdot \delta z\,, \tag{4.5}$$

where ν is the largest real part of the eigenvalues of the Jacobian Df of the uncontrolled system (4.1). Again, we use the short form $\partial_x f$ for the partial derivatives of f with respect to x and omit the evaluation point for legibility reasons. The linearized form (4.5) allows for applying the results from control theory for linear time-invariant (LTI) systems introduced in section 1.2; see also [104]. The dynamics of x, μ, and λ in the bifurcation-point continuation system (4.3) are assumed to be

coupled. Nevertheless, we distinguish sharply in the following analysis for a clear and linear representation. The control consisting of eqs. (4.3c) and (4.3d) is applied to μ and λ. Hence, the control vector is

$$u := \begin{pmatrix} \mu \\ \lambda \end{pmatrix} \in \mathbb{R}^{2\times 1}$$

for the controlled system

$$\dot{v} = \mathsf{C}v(t) + \mathsf{D}u(t)\,,$$

with the state vector

$$v := \begin{pmatrix} x_1 \\ x_2 \\ \mu \\ \lambda \end{pmatrix} \in \mathbb{R}^{4\times 1}\,,$$

the input matrix

$$\mathsf{D} := \begin{pmatrix} 0 & 0 \\ 0 & 0 \\ 1 & 0 \\ 0 & 1 \end{pmatrix} \in \mathbb{R}^{4\times 2}\,,$$

and the state matrix

$$\mathsf{C} := \left[\begin{array}{cc|cc} & Df & f_\mu & f_\lambda \\ \hline 0 & 0 & 0 & 0 \end{array}\right] = \begin{pmatrix} 0 & 1 & 0 & 0 \\ \partial_{x_1} f_2 & \partial_{x_2} f_2 & \partial_\mu f_2 & \partial_\lambda f_2 \\ 0 & 0 & 0 & 0 \\ 0 & 0 & 0 & 0 \end{pmatrix} \in \mathbb{R}^{4\times 4}\,,$$

with the linearization matrix Df of the original system (4.1), and the gradients $f_\mu\,,\ f_\lambda \in \mathbb{R}^{2\times 1}$ of f with respect to μ and λ. Similar to the previous chapters, for reasons of legibility, the short forms $\partial_x f$ are used wherever no specific evaluation point is meant. The resulting controllability matrix is

$$\mathsf{R} = \left[\begin{array}{c|c|c|c} \mathsf{D} & \mathsf{CD} & \mathsf{C}^2\mathsf{D} & \mathsf{C}^3\mathsf{D} \end{array}\right] = \left[\begin{array}{cc|c|c|c} 0 & 0 & & & \\ 0 & 0 & \mathsf{CD} & \mathsf{C}^2\mathsf{D} & \mathsf{C}^3\mathsf{D} \\ 1 & 0 & & & \\ 0 & 1 & & & \end{array}\right]$$

$$= \left[\begin{array}{cc|c|c|c} 0 & 0 & f_\mu \mid f_\lambda & Df\cdot f_\mu \mid Df\cdot f_\lambda & (Df)^2\cdot f_\mu \mid (Df)^2\cdot f_\lambda \\ 0 & 0 & & & \\ \hline 1 & 0 & & & \\ 0 & 1 & \mathbf{o} & \mathbf{o} & \mathbf{o} \end{array}\right],$$

with $\mathbf{o}$ denoting a matrix containing only zero-entries and

$$\left[\; Df \cdot f_\mu \;\middle|\; Df \cdot f_\lambda \;\right] = \begin{pmatrix} \partial_\mu f_2 & \partial_\lambda f_2 \\ \partial_{x_2} f_2 \cdot \partial_\mu f_2 & \partial_{x_2} f_2 \cdot \partial_\lambda f_2 \end{pmatrix},$$

$$(Df)^2 \cdot f_\mu = \begin{pmatrix} \partial_{x_2} f_2 \cdot \partial_\mu f_2 \\ \partial_{x_1} f_2 \cdot \partial_\mu f_2 + \partial_{x_2} f_2 \cdot \left(\partial_\mu f_2\right)^2 \end{pmatrix}, \quad \text{and}$$

$$(Df)^2 \cdot f_\lambda = \begin{pmatrix} \partial_{x_2} f_2 \cdot \partial_\lambda f_2 \\ \partial_{x_1} f_2 \cdot \partial_\lambda f_2 + \left(\partial_{x_2} f_2\right)^2 \cdot \partial_\lambda f_2 \end{pmatrix}.$$

The controllability matrix R has full rank if and only if $f_\mu \neq \mathbf{o} \in \mathbb{R}^{2\times 1}$ is not an eigenvector of $Df \neq \mathbf{o} \in \mathbb{R}^{2\times 2}$. Since f_μ and f_λ are parallel, $[f_\mu | f_\lambda]$ does not have full rank. So, it must hold $\partial_\mu f_2 \neq 0$ or $\partial_\lambda f_2 \neq 0$, and $\partial_{x_2} f_2 \neq 0$. Since we are interested in the stationary, particularly bifurcation points, i. e., $\partial_{x_2} f_2 = 0$, it must be $\partial_{x_1} f_2 \neq 0$ for a full rank of R in the bifurcation points. According to the Kalman rank criterion [57] (thm. 1.5), the bifurcation-point continuation method (4.3) is controllable if $\partial_{x_1} f_2 \neq 0$ and $\partial_\mu f_2 \neq 0$ hold.
For the observability of the system (4.3) holds the same argument as in sections 2.1.1, 2.2.1 and 3.1.2. Since the full state trajectory is only constructed from input and output measurements, i. e. x_1 and x_2, the controlled system (4.3) is fully observable for the case $\dot{x}_1 = x_2$ and low noise. To avoid bias in the case of noisy system measurements, one might consider more elaborate methods [103] than the least-squares method for estimating the eigenvalues' largest real part, as already stated in section 3.2. Generalizing the results presented in chapter 4 requires further analysis to guarantee observability.

4.1.2 *Stabilization of the bifurcation-point continuation*

In order to guarantee stability of the found bifurcation points $(\overline{\overline{x}}, \overline{\overline{\mu}}, \overline{\overline{\lambda}})$ by the bifurcation-point continuation (4.3), the values of the control parameter K must be chosen such that the Jacobian $D\check{h}((\overline{\overline{x}}, \overline{\overline{\mu}}, \overline{\overline{\lambda}}))$ defined eq. (4.5) has only eigenvalues with negative real parts. General conditions depending on the Jacobian $D\check{h}$ cannot be given like in sections 2.1.2, 2.2.2 and 3.1.3 because the Jacobian of the controlled system (4.3) is 4-dimensional. This does not allow for giving just a handful of conditions on the parameter values. Hence, the conditions for the negativity of all real eigenvalue parts must be checked for each individual case.
A numerical analysis of the eigenvalues of $D\check{h}$ for the model (3.19) of the Zeeman catastrophe machine in section 4.3 shows that finding the right values for the control parameter is generally possible. See appendix B for a detailed analysis of the bifurcation-point continuation for the model (3.19) of the Zeeman catastrophe machine. Furthermore, the laboratory experiment results presented in section 4.2 prove the general stabilizability.

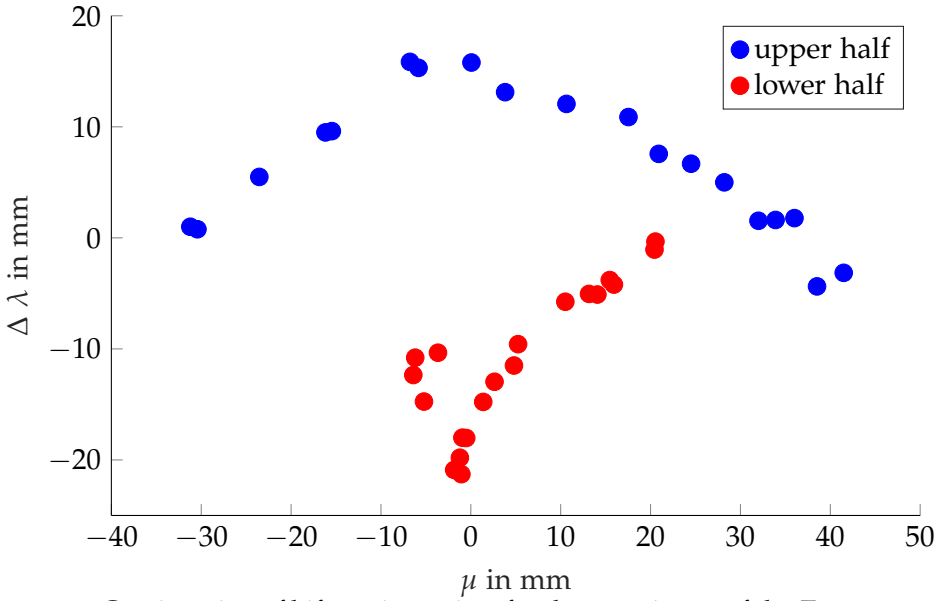

Figure 4.1: Continuation of bifurcation points for the experiment of the Zeeman catastrophe machine. The blue dots show the measurements for a starting point with λ larger than the value for the cusp ($\Delta\lambda = 0$ at $\lambda = 242.5\,\text{mm}$). The red dots show the results for the lower branch. The asymmetry of the measurements comes from the asymmetry of the experimental setup. Continuation over the cusps with respect to μ was possible due to the large step size of the prediction.

4.2 EXPERIMENTAL RESULTS FOR LABORATORY EXPERIMENTS OF THE ZCM

The experimental setup of the bifurcation-point continuation (4.3) for the Zeeman catastrophe machine is similar to the continuation of stationary points described in section 3.3.1. The system is initialized in a small neighborhood around a bifurcation point $\left(\overline{\overline{\phi}}, 0, \overline{\overline{\mu}}, \overline{\overline{\lambda}}\right)$ found either by the controlled system (3.10) for a fixed value of λ and the stability determination presented in section 3.2 or by a sweep without control for a fixed value of λ. Here, it is again $x_1 = \phi$ and $x_2 = \dot{x}_1 = \dot{\phi}$, as in chapter 3. The first coordinate, i. e., the value of ϕ of the estimated point, is taken as the first target ϕ^*. The same values as in section 3.3.4 are taken for the absolute values of the control parameters K_P and K_D, whose sign depends on λ with respect to the cusp bifurcation. The additional parameter for the control on bifurcation points is set to $|K_B| = 0.063\,\text{mm}$, where the sign depends again on λ. For the sake of completeness, the control parameters are with units $|K_P| = 3\frac{\text{mm}}{^\circ}$ $\left(\approx 0.05236\,\frac{\text{mm}}{\text{rad}}\right)$, $|K_D| = 2\frac{\text{mm}\cdot 1/70\,\text{s}}{^\circ}$ $\left(\approx 2.4435\,\frac{\text{mm}\cdot\text{s}}{\text{rad}}\right)$, and $|K_B| = 0.063\,\text{mm}$. Then the system under control (4.3c) and (4.3d) is run until the distances are below the thresholds $|\phi - \phi^*| < 0.0087\,\text{rad} (\approx 0.5^\circ)$ and $|\dot{\phi}| < 0.00122\,\frac{\text{rad}}{\text{s}}$ $\left(\approx \frac{0.001^\circ}{0.0143\,\text{s}}\right)$. Then, the largest real part ν of the linearization matrix' eigenvalues is computed out of at least 20 and at most 40 time steps of size $1/70\,\text{s}$ since the last update of λ. This value is used to update λ according to the discrete update scheme of eq. (4.3d):

$$\lambda_{k+1,l} = \lambda_{k,l} - K_B \cdot \nu_k\,, \tag{4.6}$$

where k is the index for the number of stabilizing updates for the l-th found bifurcation point with $\overline{\overline{\phi}}_l = \phi^*$. For reasons of simplicity, the time difference between $\lambda_{k,l}$ and $\lambda_{k+1,l}$ for the change $(-K_B \cdot \nu_k)$ is set to 1, like in eq. (3.18) for the continuation of stationary points. The position of λ is changed by a stepper motor similar to the one for μ described in section 3.3.1; see appendix A for details. When the newly computed value $|\nu|$ is < 0.5, the system is considered to have reached a stable equilibrium point of the controlled system (4.3) which is a bifurcation point of the original system (4.1). When the system has settled at a bifurcation point, the target is increased or decreased by $\Delta\phi^* = 5^\circ (\approx 0.087\,\text{rad})$ depending on the direction with respect to the singularities. The continuation has to stop in the neighborhood of a cusp bifurcation which is a singularity with respect to the bifurcation parameters. In a cusp, both real parts of the eigenvalues reach zero. Hence, it is called a *codimension-two bifurcation*. So, the routine needs to be initialized at least 2 times. So far, no other data-based bifurcation-point continuation method for the controlled systems that could circumvent this problem is known to the author; see also [93]. Additionally, the sign of the control parameters needs to be changed at the cusp due to geometrical reasons. At this cusp, it is $\overline{\overline{\lambda}} \approx 242.5\,\text{mm}$. The experimental results are shown in fig. 4.1.

Due to the step size $\Delta\phi^* = 5^\circ$, continuation over the quasi-singularities in $\overline{\overline{\mu}} = 0$ is possible. For smaller step sizes of the target ϕ^*, the estimating the eigenvalues' largest real part ν is unreliable. The initialization would be too close to the ω-limit set, and the noise would be large compared to the motion. Besides, the limitation of the measurement solution mentioned in section 3.3 might be a limitation for the results here, too. The asymmetry between the upper ($\overline{\overline{\lambda}} > 242.5\,\text{mm}$) and the lower ($\overline{\overline{\lambda}} < 242.5\,\text{mm}$) half in parameter space is caused by the slight asymmetry of the experimental setup. When the point P on the disk is closer to the point B and hence to the stepper motor, the measured trajectories of the angle ϕ and its velocity $\dot{\phi}$ provide more reliable information. This might be due to the static friction at the suspensions for the springs varied by the angle ϕ. Eventually, an adaptive number of considered time steps could lead to better stability estimations for the lower part. Additionally, the tension of the timing belt causes an asymmetry between the left ($\mu < 0$) and right ($\mu > 0$) half in parameter space. This is clearly visible for the bifurcation-point curve with $\overline{\overline{\lambda}} < 242.5\,\text{mm}$. So, diagrams with a higher resolution of the curve might be realizable with a finer machine setup or an adapted routine. Compared to the PD control of chapter 3, the stability determination introduced in section 3.2 from the generated data needs an on-time update. Here, the eigenvalue ν_k is computed from the data with the least-squares method described in section 3.2 after 20 to 40 time steps. Hence, the time resolution must be fine enough, and the hardware must be fast enough for a good estimate. Additionally, the stability information must be reliable. Since this is only the case if the initial point of the time series is not too close to the ω-limit set, the target distance must be large enough. For details of the resolution limits in the laboratory experiment, see section 3.3.4. Hence, a finer diagram seems to be only possible with a different hardware setup.

4.3 RESULTS OF THE SIMULATION FOR COMPARISON

For the comparison with the results of the laboratory experiment presented in section 4.2, we take the model (3.19) of the Zeeman catastrophe machine again as the original system (4.1). To gain faster smooth bifurcation-point curves, we take the same parameter values as in section 3.4.1 except for the spring constant $k = 1\,\mathrm{N/m}$. As stated in section 4.2 for the laboratory experiment, the sign of the control parameter values must be changed depending on the direction towards the cusps for $\lambda \approx 242.5\,\mathrm{mm}$. So, we chose for $\lambda < 242.5\,\mathrm{mm}$ the values $K_P = -1\,\frac{\mathrm{mm}}{\circ}$, $K_D = -1.5\,\frac{\mathrm{mm\cdot s}}{\circ}$, and $K_B = 0.002\,\mathrm{mm}$. For $\lambda > 242.5\,\mathrm{mm}$, the following results are taken under control (4.3) with parameter values $K_P = 1\,\frac{\mathrm{mm}}{\circ}$, $K_D = 1.5\,\frac{\mathrm{mm\cdot s}}{\circ}$, and $K_B = -0.002\,\mathrm{mm}$. Hence, the continuation must be initialized at least two times, once for the branch with $\lambda > 242.5\,\mathrm{mm}$, and once for $\lambda < 242.5\,\mathrm{mm}$. Note that the values for the control gains K_P, K_D, and K_B differ from the ones used for the physical laboratory experiment presented in section 4.2 due to different time steps Δt and different target steps for ϕ^*.
In principle, the numerical simulation follows the procedure for the laboratory experiment described in section 4.2. The continuation starts at a point close to a bifurcation point found by the direct simulation of eq. (3.19) for a fixed value of λ. Then the target ϕ^* is increased or respectively decreased by $\Delta\phi = 0.05\,\mathrm{rad}$. The numerical simulation of the controlled system (4.3) is run with a maximal time step size $\Delta t = 0.002\,\mathrm{s}$. For larger Δt, the target step size $\Delta\phi$ must be increased for reliable results. This could explain why experiments with a much coarser time resolution cannot be continued with such small target steps. The positions of the bifurcation points projected into the (μ, λ)-plane are shown together with their stability information in fig. 4.2b. Their positions in the set of all stationary points, including the coordinates of the angle ϕ is depicted in fig. 4.2a and with shifted axes in fig. 4.3 for comparison.
In section 3.4.1, we assumed $\phi \in (\pi, 2\pi)$ for $\lambda = 230\,\mathrm{mm}$. This is still assumed for $\lambda < 242.5\,\mathrm{mm}$. For $\lambda > 242.5\,\mathrm{mm}$, we assume $\phi \in (0, \pi)$ to keep the control law still well-defined.

4.3.1 *Controllability for the machine's model by the bifurcation-point continuation*

In section 4.1.1, the general conditions for controllability of a system (4.1) controlled by eqs. (4.3c) and (4.3d) are $\partial_\phi f_2 \neq 0$, and $\partial_\mu f_2 \neq 0$ or $\partial_\lambda f_2 \neq 0$. Since we have four singularities in the parameter range where bifurcation occurs, we cannot continue the branch within one approach. As seen in fig. 4.1 for the experimental realization, for coarse steps for the target ϕ^*, a continuation is possible for the singularity with $\overline{\overline{\mu}} = 0$. For the fine simulations, this is not the case. But we can estimate the position of these singularities and investigate the controllability conditions for the parameter range except for a small neighborhood around the singularities. Due to the system's symmetry with respect to $\mu = 0\,\mathrm{m}$ and $\lambda \approx 242.5\,\mathrm{mm}$, the controllable parameter range can be split into four parts. Even though the cusp in fig. 4.2 looks rotationally symmetric, the machine is only axially symmetric to the y-axes and the line parallel to the x-axes with $\lambda \approx 242.5\,\mathrm{mm}$. This is due to the different origins of the singu-

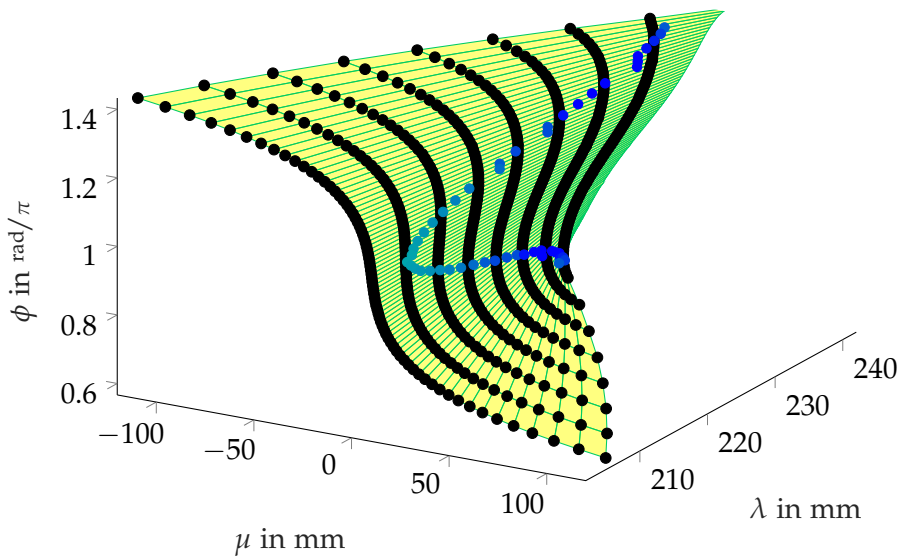

(a) Bifurcation points inside the set of the Zeeman catastrophe machine's model (3.19) controlled by eq. (4.3). Colored dots (blue and green) are the found bifurcation points of the lower half ($\lambda \in [210, 240]$ mm) with the same color as in fig. 4.2b. Black dots are stationary points achieved by the PD-controlled system (3.10) for different values of λ. The yellow surface is the interpolation of stationary points between the simulated sweeps.

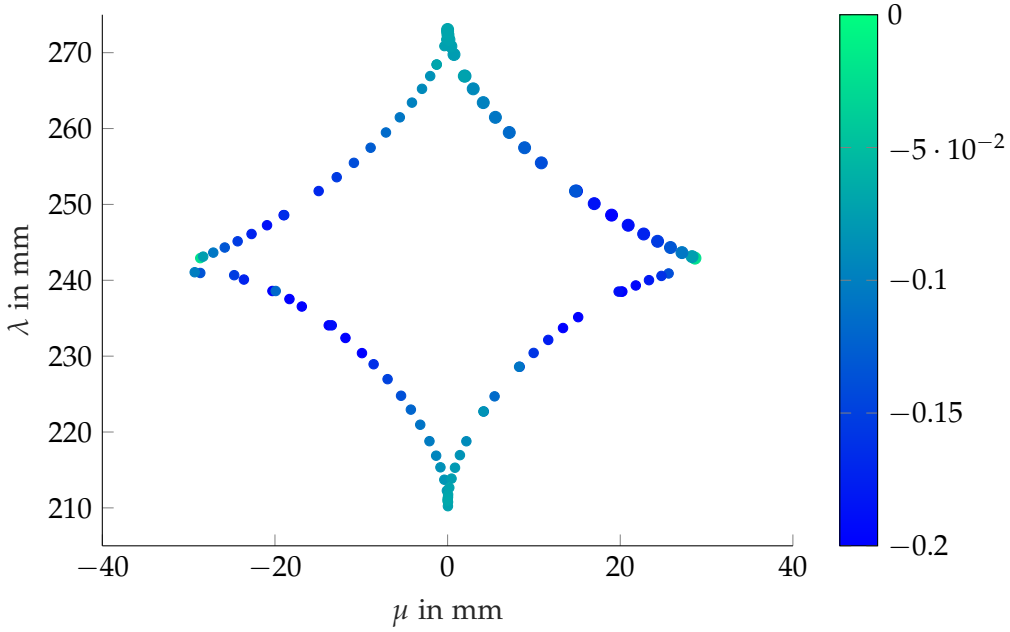

(b) Projection into the (μ, λ)-plane of the bifurcation points. The colors indicate the stability of the points estimated by the largest real part of the linearization matrix $D\check{h}$'s eigenvalues defined in eq. (4.5). Stability computations are made for the control parameter values $|K_P| = 0.5$, $|K_D| = 1.2$, and $|K_B| = 0.0005$. The sign of the control parameters depends on the value of λ. See the explanation in section 4.3.

Figure 4.2: Bifurcation points of the ZCM found by the controlled bifurcation-point continuation (4.3). The points (a) in the (μ, λ, ϕ)-space are the same as the ones (b) in the (μ, λ)-plane. The colors of the bifurcation points indicate their stability computed by the largest eigenvalue of $D\check{h}$ in eq. (4.5).

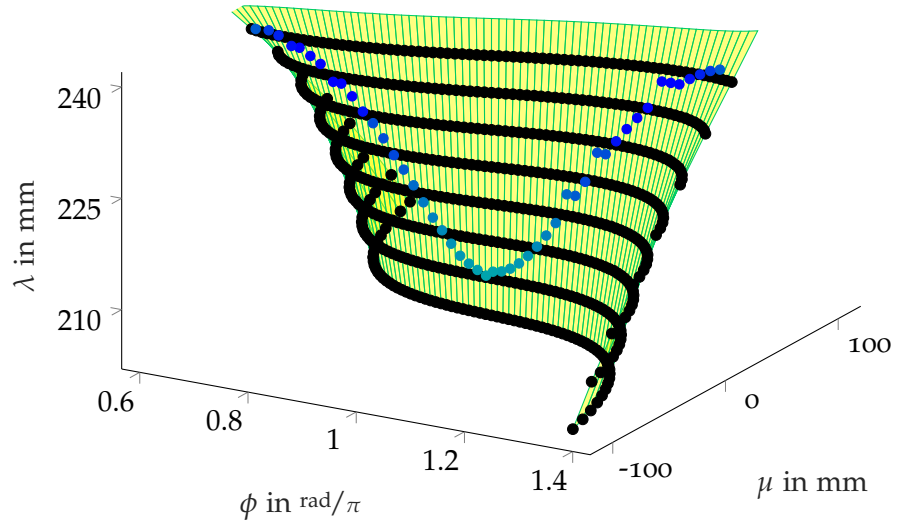

Figure 4.3: Bifurcation points corresponding to the angle ϕ inside the set of the Zeeman catastrophe machine's model (3.19) controlled by eq. (4.3). Data similar to fig. 4.2. Different view to fig. 4.2a with shifted axes. Here, the shape of the curve in fig. 4.2b is clearly visible.

larities. So, for the singularities in $\mu = 0$, a continuation is possible, whereas the singularities in $\lambda = 242.5\,\mathrm{mm}$ cannot be overcome by the bifurcation-point continuation (4.3). Hence, we consider the parameter range $(\phi, \mu, \lambda) \in M_1 \cup M_2$ consisting of the upper half $M_1 = \{\{[-1.5, 1.5]\,\mathrm{rad}\} \times \{[-25.5, 25.5]\,\mathrm{mm}\} \times \{[243, 280]\,\mathrm{mm}\}\}$ and lower half $M_2 = \{\{[1.6, 4.7]\,\mathrm{rad}\} \times \{[-25.5, 25.5]\,\mathrm{mm}\} \times \{[210, 242]\,\mathrm{mm}\}\}$ of the parameter range where bifurcations occur. For this range, the numerical calculations show $\left|\partial_\phi f_2\right| > 1.1 \cdot 10^{-6}$ and $\left|\partial_\mu f_2\right| > 1.7$. In the neighborhood of the bifurcation points, it is $\left|\partial_\phi f_2\right| > 2.4 \cdot 10^{-4}$. If the points close to the singularities are excluded, the absolute value of $\partial_\mu f_2$ is even large, which allows for assuming it is nonvanishing in the realistically considered regime. For the analytical derivatives of f_2, see eqs. (3.21), (3.22) and (B.1). So, the system is controllable with this method. The small absolute values of $\partial_\phi f_2$ are due to the small distance to the singularities and to points far from the curve of bifurcation points within the considered cubes in the parameter space.

4.3.2 *Stabilization of the machine's model by the bifurcation-point continuation*

Linear stability of the controlled bifurcation points is guaranteed if all real parts of the eigenvalues of the linearization matrix $D\check{h}$ are negative. As already stated in section 4.1.2, due to $D\check{h}$ being a (4×4)-matrix, a small number of conditions for the original system (4.1) and the control parameter values $K = (K_P, K_D, K_B)$ cannot be computed analytically. Since we use the explicitly given model (3.19) for the simulation, we can compute the entries of $D\check{h}$ analytically. For details, see appendix B. A numerical evaluation for $(\phi, \mu, \lambda) \in M_1 \cup M_2$ showed that the bifurcation points found by the numerical bifurcation-point continuation presented in fig. 4.2 lie in the area where all eigenvalues have negative real parts. The results are shown in fig. 4.2. The sets M_1 and M_2 are the same as in section 4.3.1. For better

visual comprehension, the points (ϕ, μ, λ) are projected onto the (μ, λ)-plane. Their largest real part ν of the eigenvalues is shown by color code. It can be seen that the two branches of bifurcation points lie in the stable regime. Hence, the points found by bifurcation-point continuation (4.3) are stabilizable, particularly for the Zeeman catastrophe machine's model.
In addition to the stability of the stabilized bifurcation points, it is visible in fig. 4.2a that the stability, namely the absolute value of the largest real part of the linearization matrix' $D\check{h}$ eigenvalues, is decreasing in the direction towards the cusps. For the case of singularities at $\lambda \approx 242.5\,\mathrm{mm}$, the largest eigenvalue tends to zero. This coincides with the results in [93], where no continuation based on linear prediction was possible.

5

CONTROL-BASED CONTINUATION OF PERIODIC ORBITS

In chapters 2 to 4, the control-based continuation of stationary points and bifurcation points has been discussed. The present chapter focuses on periodically driven dynamical systems where periodic orbits appear. These periodic orbits are equilibrium points in Fourier space.

As pointed out in section 1.1, classical noninvasive feedback control methods require knowledge about either explicit formulations of the underlying differential equations or the periodic orbit's time profile. When stabilizing physical systems, often, none of this information is available. The following paragraphs are intended as a summary of the already-existing methods to stabilize periodic orbits. Further details can be found in chapter 1.

The washout filter-aided feedback control methods introduced by Abed et al. in [1, 48, 62] work rather like PI control to stabilize unstable periodic orbits or stationary points. Their structures are similar to the proportional control combined with a state observer (2.3) introduced in [88, 89]. As mentioned in chapter 2, periodic orbits or stationary states can only be tracked around fold bifurcations when the sign of the parameter α_2 in eq. (2.3b) is changed. Another widely used feedback control method to stabilize unstable periodic orbits, the OGY method [78] introduced by Ott, Grebogi, and Yorke, is similar to the washout filter-aided feedback control. The periodic orbits are stabilized by giving them a kick in the desired direction.

The so-called *Pyragas control* [87] uses a time-delayed feedback control signal to stabilize the periodic orbits of dynamical systems. It was the inspiration for a different time-delayed feedback control proposed in [101]. The method does not require further knowledge about the dynamics for the continuation of the branches of periodic orbits. The continuation for direct tracking, even around fold bifurcation points, can be realized by pseudo-arclength control.

Another approach to track branches of periodic orbits by pseudo-arclength continuation for experiments is proposed in [18, 19, 98]. The authors propose to apply a local PD control based on the difference between the trajectories of the uncontrolled state and the predicted state in Fourier space. The necessary Newton step for the pseudo-arclength continuation is realized in Fourier space since periodic orbits emerge as equilibrium points in Fourier space. The transition to the Fourier space was also used in the application [100] of [101].

In [7], the authors propose to make use of a secant prediction for the estimation of the next periodic orbit. By running the system under a proportional feedback controller in Fourier space, the system is assumed to have reached an ω-limit point.

The hereafter presented PD control-based continuation of periodic orbits could be seen as a combination of ideas presented in [7] and chapter 3. Also, the periodic orbits are expressed here as equilibria in Fourier space. Instead of estimating the new equilibrium's position, the state's target is defined as in eq. (3.2) by the user step by step. This way, the whole region of interest is scanned to obtain the bifurca-

tion diagram. Analogously, the orbit is stabilized by a PD control applied to the bifurcation parameter.

5.1 EXAMPLE OF THE ATOMIC FORCE MICROSCOPE (AFM)

The Atomic Force Microscope (AFM) is a powerful tool to measure the topographical landscape of surfaces on an atomic scale. Its mechanism is based on classical mechanics like Hooke's law for springs and quantum mechanics like London dispersion forces [30, 66, 67] between atoms. An introduction to Atomic Force Microscopy can be found, e. g. in [49] and [113]. The latter served as a basis for sections 5.1.1 to 5.1.3.

5.1.1 *Scanning Probe Microscopes*

Atomic Force Microscopy is one of the techniques summarized by the term *Scanning Probe Microscopy*. These methods all have in common that they measure the interaction between the sample surface and the probe and that they work with atomic resolution. The instruments have a size of about $10\,\mathrm{cm} = 10^{-1}\,\mathrm{m}$ and a resolution of $1\,\text{Å} = 10^{-10}\,\mathrm{m}$, i. e. 10^{-9} times their size. Voigtländer illustrates this with the words: *"Scaling this precision of* 10^{-9} *up to macrosize dimensions would correspond to using a pencil* $1,000\,km$ *in length to write letters from Cologne (Germany) in a notebook in Rome (Italy) with* $1\,mm$ *resolution!"* [113, p. 3]
The first Scanning Probe Microscope (SPM) was the *Scanning Tunneling Microscope* (STM) based on its forerunner, the so-called *Topografiner*, introduced by Young, Ward, and Scire in 1972 [122]. In 1981/1982, Binning, Rohrer, and coworkers [12–14] invented the STM, for which they received the Nobel Prize in 1986 [76]. The mode of operation for the scanning is measuring the tunneling current of conducting samples.

5.1.2 *Foundations of the AFM*

As mentioned in section 5.1.1, the STM allows for measuring reliably on a nanoscale for the first time. Since the tunneling current is measured for quantifying the electron density, the STM can only be applied to conducting samples. Measuring by an AFM allows for investigating insulating samples, too. Therefore it has an even broader range of applications. The AFM was invented by Binnig, Quate, and Gerber in 1985 [11]. It is also known as *Scanning Force Microscope* (SFM) since the force between the tip and the sample is the measured quantity. Generally, three different tips-sample distance regimes are considered [113]. If the distance between the tip and the surface is large, the force between them is insignificant. For smaller distances, an attractive, i. e. negative, force between the tip and the sample is measurable. In the case of very small tip-sample distances, a repulsive, i. e. positive, interaction force exists. The *static mode* is one option for measuring the force between the tip and the sample. The deflection of a cuboid-shaped flat spring,

the so-called *cantilever*, serves to measure the force. According to Newton's second law, the equation of motion is

$$ma = m\frac{\mathrm{d}^2 z}{\mathrm{d}t^2} = m\ddot{z} = F \tag{5.1}$$

for the second derivative a of z, the pointlike mass m, and for the force F on the cantilever. Since the cantilever is a linear spring in good approximation, Hooke's law

$$F_{sp} = -k(z - z_0) \tag{5.2}$$

can be used, where k is the spring constant and $(z - z_0)$ the distance of the cantilever's actual position z to its equilibrium position z_0 without the vicinity of the sample. The deflection of the spring is measured by photodiodes using the deviation of a laser beam's reflection, see fig. 5.1. To gain comparable measurements of the position, the force between tip and sample is kept constant by a feedback loop for the z-position. The measurement's result is an image of the sample's topography [113]. In the regime of a repulsive force, the tip touches the sample surface. This contact mode is a problem for e. g. polymers or biological samples since they would be manipulated or destroyed by direct contact with the tip. One option to avoid this problem is the so-called *non-contact mode* or *dynamic mode*. A dizer piezo with a frequency ω_{ex} close to its free resonance frequency bring the cantilever to oscillations, resulting in a periodically-driven nonlinear oscillator. Close to or on the sample surface, the force between the tip and the sample changes the cantilever's frequency. This force is similar to a second spring's influence on the cantilever spring's dynamics [113]. The change in the resonance frequency corresponds to a change in the cantilever amplitude indirectly measured by the laser beam's reflection. For analyzing a sample surface, this amplitude change serves as a feedback signal in order to keep the interaction force or force gradient constant between the tip and the sample. The position adjustment is often realized by a PI control. For the hereafter presented continuation of periodic orbits, the change of amplitude and the phase between driving and resonance frequency are the considered quantities of the bifurcation analysis.

5.1.3 *The mathematical model for the AFM*

As introduced in section 5.1.2, the AFM indirectly measures the cantilever's deflection. Since we do not consider the technical realization of the signal processing, only the motion of the cantilever tip is an object of the following model. The acceleration a of the tip is proportional to the forces working on it in accordance with Newton's second law. To approximate the real system, we focus on the relevant forces working on the cantilever on the nanoscale. In section 5.1.2, the force F_{sp} due to the spring-like behavior of the cantilever is motivated by Hooke's law (5.2). The dynamic mode of the AFM uses the excitation force

$$F_{ex}(t) = A_{ex} \cdot \sin(\omega_{ex} t)\,, \tag{5.3}$$

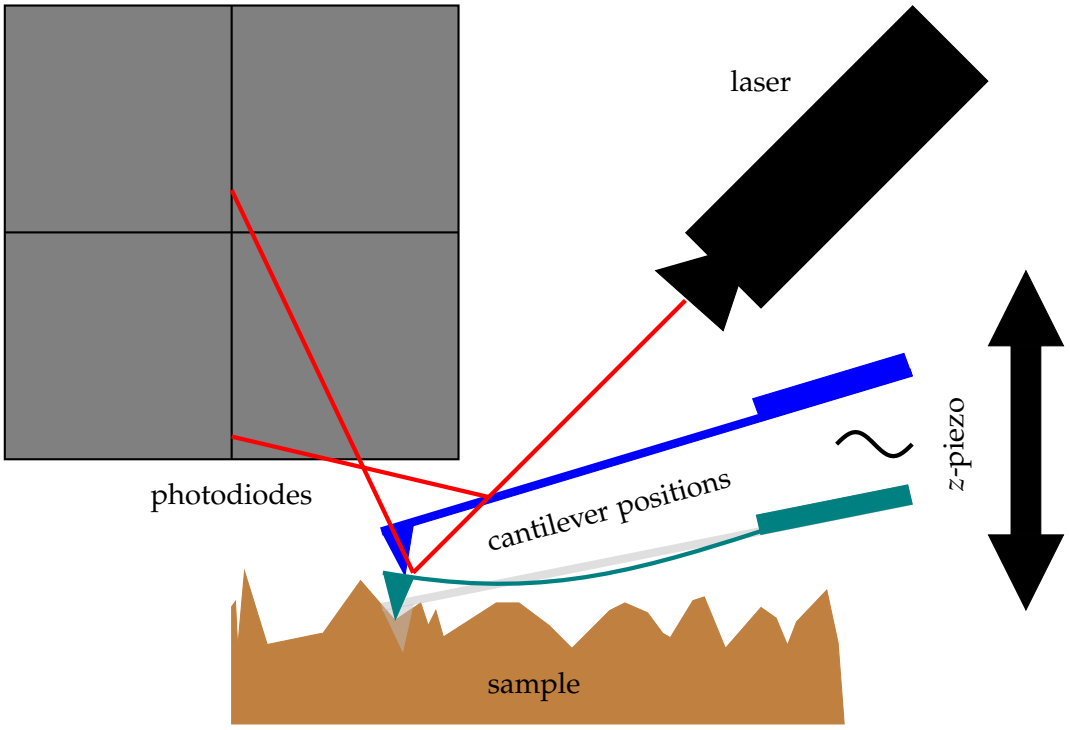

Figure 5.1: Sketch of an AFM. The cantilever is periodically driven in the z-direction by a piezo. Different colors indicate the different possible positions. The greenish cantilever is bent by the forces of the sample. Its position without a sample is depicted in gray. This bending is detected by the laser beam's reflection measured by the photodiodes.

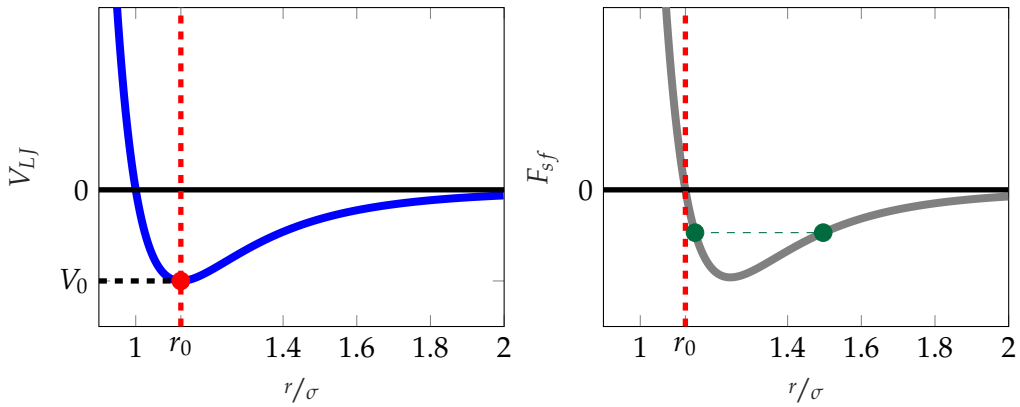

(a) Lennard-Jones potential.

(b) Surface force.

Figure 5.2: Lennard-Jones potential and the resulting surface force depending on the distance r between the atoms. (a) Sketch of the Lennard-Jones potential V_{LJ} of eq. (5.5) in blue. The dashed red line indicates the border between the repulsive ($r < \sigma$) and the attractive ($r > \sigma$) regime. The potential is minimized by r_0 at V_0, marked by the dashed black and red lines. (b) Surface force (5.6) induced by V_{LJ}. Inside the attractive regime ($F_{sf} < 0$), one value of the surface force belongs to two different distances.

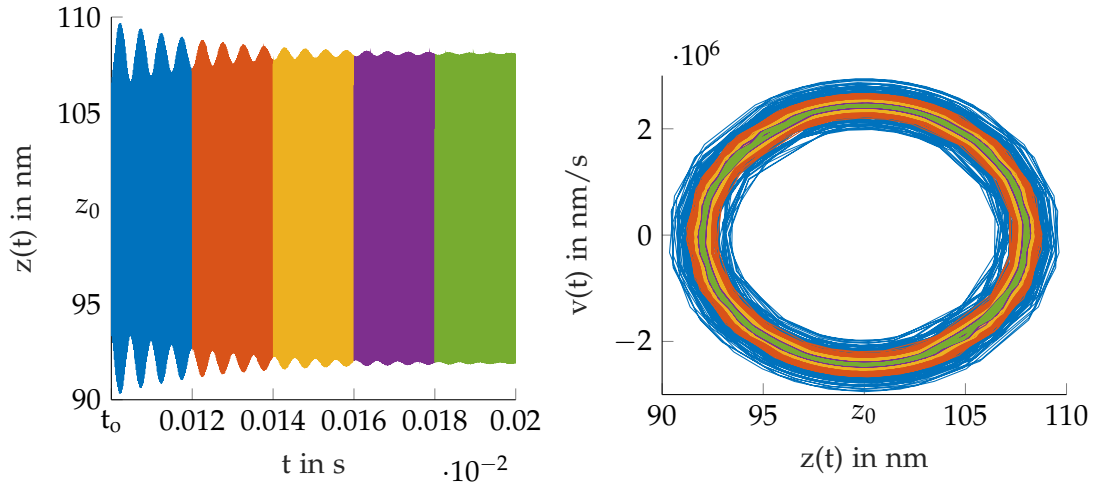

(a) Time-position diagram

(b) Phase portrait

Figure 5.3: Dynamics of the AFM model (5.8) with excitation frequency $\omega_{ex} = 48.0321\,\text{kHz}$ in (a) the position z of the cantilever over time and (b) the corresponding phase portrait. The same colors indicate the same time intervals and show convergence towards the periodic orbit. The discontinuous line segments are due to the resolution limits of the picture.

which drives the cantilever periodically, similar to the driving force for a harmonic oscillator with the driving frequency ω_{ex} and the driving amplitude A_{ex}. It holds for the driving amplitude

$$A_{ex} = \frac{k \cdot A_0}{Q},$$

where A_0 is the free amplitude and Q is the quality factor of the cantilever in free oscillation mode. The quality factor Q is dimensionless and describes the underdamping of the oscillator and is defined by

$$Q = 2\pi \cdot \frac{\text{stored initial energy}}{\text{lost energy per cycle}}, \tag{5.4}$$

which means that oscillators with a high Q are lowly damped and oscillate longer than those with a low quality factor [37, 113].
In section 5.1.2, the tip-sample difference is subdivided into different regimes [113]. The interaction between two neutral atoms in the probe tip and the sample surface can be approximately described by the Lennard-Jones potential. The potential is an approximative description of the theoretical potential between atoms of a noble gas proposed by Lennard-Jones in [54, 55, 63]. The attraction is described by the van der Waals forces [114] approximated by the London dispersion forces [30, 66, 67], which consist of a term decaying with the sixth power of the distance r between the atoms. The repulsive part is motivated by the Pauli repulsion [81], which is assumed to decay with the twelfth power of r. This results in the Lennard-Jones model potential

$$V_{LJ}(r) = 4V_0 \cdot \left[\left(\frac{\sigma}{r}\right)^{12} - \left(\frac{\sigma}{r}\right)^{6}\right] = V_0 \cdot \left[\left(\frac{r_0}{r}\right)^{12} - 2 \cdot \left(\frac{r_0}{r}\right)^{6}\right], \tag{5.5}$$

where V_0 is the depth of the potential well and $\sigma = 2^{-1/6} \cdot r_0$ is the distance for which the Lennard-Jones potential is zero, i. e., $V_{LJ}(\sigma) = 0$, and r_0 as the minimizer of the Lennard-Jones potential, see fig. 5.2 for illustration. The resulting surface force with $z = r$ distance to the surface is

$$\begin{aligned} F_{sf}(z) &= -\partial_r V_{LJ}(z) = \frac{12V_0}{z} \cdot \left[\left(\frac{r_0}{z}\right)^{12} - \left(\frac{r_0}{z}\right)^{6} \right] \\ &= \frac{12V_0}{z} \cdot \left[\left(\frac{r_0^2}{z^2}\right)^{6} - \left(\frac{r_0^2}{z^2}\right)^{3} \right] . \end{aligned} \tag{5.6}$$

Its relation to the Lennard-Jones potential is illustrated in fig. 5.2. Note that F_{sf} is not an injective map, i. e., two different distances map to one surface force inside the attractive regime with $F_{sf} < 0$. For the numerical model, singularities in the neighborhood of $z = 0$ must be avoided. Therefore, we approximate $z \approx \sqrt{z^2 + (\Delta z)^2}$ for $\Delta z \ll r_0$. The surface force is approximated accordingly by

$$F_{sf}(z) \approx \frac{12V_0}{\sqrt{z^2 + (\Delta z)^2}} \cdot \left[\left(\frac{r_0^2}{z^2 + (\Delta z)^2}\right)^{6} - \left(\frac{r_0^2}{z^2 + (\Delta z)^2}\right) \right] .$$

The system is damped by the oscillation damping force

$$F_{od}(z(t)) = -\frac{k}{Q\omega_0} \cdot v(t) ,$$

which is proportional to the position's velocity v with the quality factor Q of the cantilever and its free resonance frequency ω_0. The damping is additionally caused by the sample with the sample damping force

$$F_{sd}(z, v) = -s \cdot \frac{v}{z^3} ,$$

where s is the damping factor.
Summing up all relevant forces, the total force acting on the cantilever is

$$F_{tot} = F_{sp} + F_{sf} + F_{ex} + F_{od} + F_{sd} . \tag{5.7}$$

Since we are interested in equations of motion for the position z of the cantilever's tip, we deduce from eqs. (5.1) and (5.7) the system

$$\dot{z} = v \tag{5.8a}$$

$$\begin{aligned} \dot{v} = a &= \frac{F_{tot}(z(t), t)}{m} \\ &= \omega_0^2 \cdot \left(-(z - z_0) + \frac{1}{k} \cdot \left(F_{sf}(z) + A_{ex} \cdot \sin(\omega_{ex} t) - \frac{s \cdot v}{z^3} \right) \right) - \frac{\omega_0}{Q} \cdot v , \end{aligned} \tag{5.8b}$$

since it holds for the eigenfrequency $\omega_0 = \sqrt{\frac{k}{m}}$.
In the case of a physical experiment, the signal usually needs to be processed by hardware and software tools like e. g., a lock-in amplifier or a low-pass filter due to noise. Additionally, the thermodynamic drift during a measurement series is not negligible since the experiments are realized on an atomic scale [113, Chapter 17].

For reasons of simplicity and realizability, the model does not include these details. The question of more precise models for nanoscale forces in experiments is addressed in, e. g. [22]. The authors propose a data-driven analysis by SINDy [17]. Nevertheless, the numerical results for the model and its control are shown in fig. 5.5 show a similar behavior to the experimental measurements depicted in fig. 5.4.
All names of variables and symbols used for the AFM are summarized in table D.4 in appendix D.

5.2 BISTABILITY FOR THE VIBRATING TIP OF AN AFM'S CANTILEVER

One physical example where the bistability of periodic orbits occurs is the dynamic mode in AFMs. Theoretical models [107, 116, 119] and physical measurements [36, 90, 105] have shown the bistability of the cantilever's amplitude and the phase shift for variations of the driving frequency ω_{ex}. For experimental measurements, see fig. 5.4, too. Since dissipation, i. e., energy transmission from the macroscopic system to higher harmonics [97], is optimal on the branch of unstable periodic orbits in between the two stable ones, access to the unstable branch may allow for a higher quality factor (5.4). In addition, the fluctuations on the unstable branch influence the direction towards which stable state the system is converging. Hence, the unstable states may reveal information on the forces that cause the dissipation [24, 109] or, more generally, the surface energy and its dependent quantities [106]. Generally, accurate measurements in this bistable regime could help to characterize 2-dimensional materials with respect to e. g. pre-tension or elasticity, which can be measured contactless [25, 46, 112].
The mathematical model (5.8) of the AFM describes the motion of the cantilever tip. If all parameters are kept constant, the system (5.8) reaches a periodic orbit for large times, i. e. it holds $z(t_0) = z(t_0 + T)$ for all t_0 and $T = 2\pi/\omega_{ex}$. The connection between constant amplitude and periodic orbit is visualized in fig. 5.3. In fig. 5.3a, the cantilever's position z is plotted over time for a fixed value of ω_{ex}. The corresponding so-called *phase portrait* in fig. 5.3b shows the velocity v over z with the same colors in figs. 5.3a and 5.3b for the same time segment. In fig. 5.3b, it is clearly visible that the trajectory converges towards an orbit corresponding to the final amplitude, whereas the signal's amplitude in fig. 5.3a converges towards a limit. Since the position z is not fixed, z is rather unsuitable to describe the periodic orbit. For the scope of physical realization, the quantities z, A, and φ can be regarded in the sense of time-scale separation. Here, the position z can be seen as acting on the fast time scale, whereas amplitude A and phase φ correspond to the slow time scale, i. e., changing in the rate of the period length T. Applying control only on the slow time scale is easier to realize than full real-time control for many systems, particularly the herein presented AFM. We will now focus on cases where this is sufficient to control unstable periodic orbits. Therefore, a different variable is taken to define the periodic orbits. One intuitive choice for the measured quantity is the amplitude A during one period. It describes the maximal magnitude of the oscillations around the equilibrium position z_0. Since the period's length T is defined by the driving frequency ω_{ex}, each periodic orbit has a unique amplitude. In sections 5.3 and 5.4,

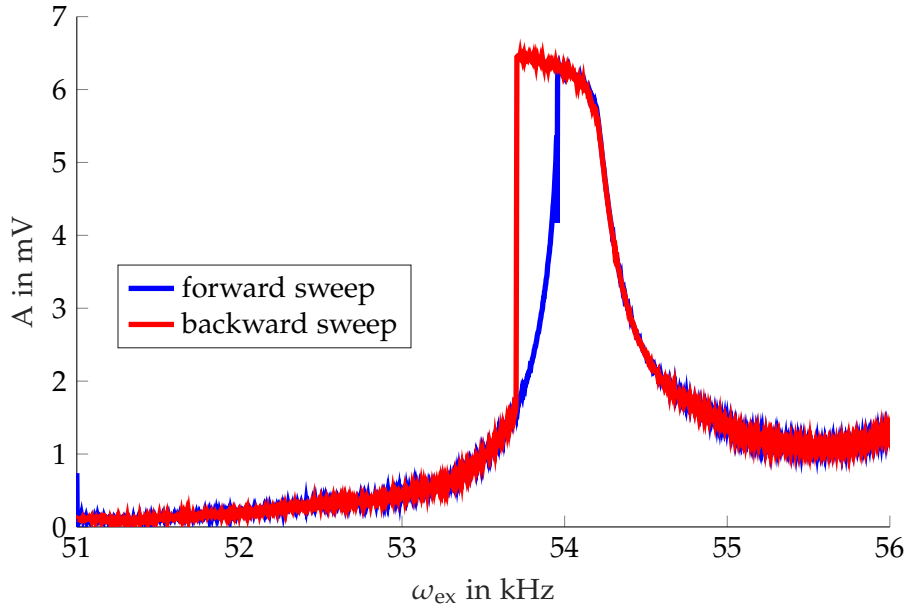

(a) Amplitude

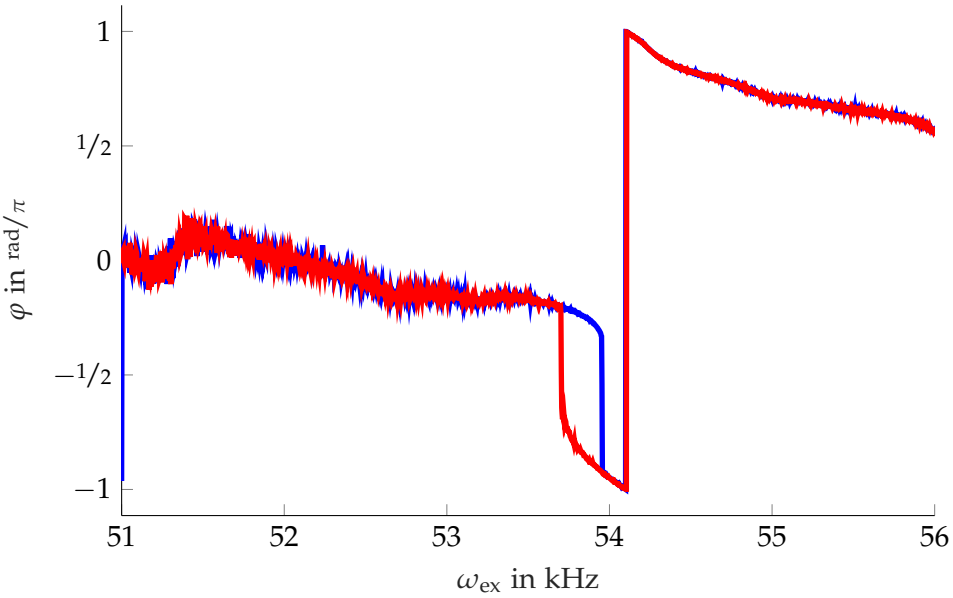

(b) Phase

Figure 5.4: Dynamics of the AFM experiment without control for (a) amplitude and (b) phase shift over the excitation frequency ω_{ex}. Note that the amplitudes are measured indirectly by the electric current of the photodiode activated by the laser beam. It can be linearly calibrated into the value of the amplitude in metric entities. The blue line is achieved by a forward sweep, and the red line by a backward sweep. The jump in (b) is presumably caused by a modulo operation to restrict the signal to $[-\pi, \pi)$. Measurements in the vicinity of a Si surface. Cantilever of length 225 μm has a silicon tip with a radius < 10 nm and a height of $50 - 60\,\mu$m (model SD-PXL-FM by NANOSENSORS™[71]). Measurements were done by Lukas Böttcher and can be found in the joint work [27].

it is discussed that the amplitude A does not serve well to find unstable periodic orbits because the branches of stable and unstable periodic orbits have very small distances for many parameter settings; see also fig. 5.5a for illustration. Another choice for the measured quantity is the *phase shift* φ between cantilever oscillation and driving signal. During one period, the system's position $x = (z, v)^T$ passes through a quasi-circle in case of scaling, see fig. 5.3b, where the phase ϕ describes the angle between the actual position and the horizontal axis. The phase is linearly connected to the angular frequency ω by the relation $\phi(t) = \omega t + \phi_0$ and $\omega = \frac{2\pi}{T}$. Hence, it is accessible from the position's signal. The phase shift, now called simply *phase* $\varphi := \phi_{ex} - \phi_z$, describes the difference between the phase ϕ_{ex} of the driving signal and the phase ϕ_z of the tip. It can be detected by the difference between the maxima or the zero crossings of the signals. Alternatively, φ can be obtained by, e. g., Fast Fourier Transformation (FFT), where the periodic orbits of the cantilever's position become stationary points.

As indicated above, the driving frequency ω_{ex} is an obvious choice for the bifurcation parameter. Laboratory experimental results and simulations [36] showed bistable behavior of both the amplitude and the phase for varying ω_{ex}. In principle, the simulation's and the experiment's procedure are similar to the sweep of the Zeeman catastrophe machine introduced in section 3.3. The forward sweep is initialized with a driving frequency $\omega_{ex} < \omega_0$ smaller than the free resonance frequency. Then, the system is run until it reaches a periodic orbit. The system is said to have reached a periodic orbit if the amplitude's difference after one period T is smaller than a predefined tolerance. When the system has reached a periodic orbit, the phase ϕ is approximated by the first harmonic and computed by the difference between the maxima of driving and oscillation signal during the last period. In the case of directly determining the phase by e. g. FFT, it is also possible to observe directly if the phase velocity reaches the tolerance. For reasons of simplicity, only the first harmonic is considered. Simulations and test measurements for this specific case of the AFM have shown that the whole phase signal is sufficiently precisely approximated by the first harmonic. In principle, the method works similarly for several harmonics. Then the value of ω_{ex} is increased, and the system is run again until it reaches a periodic orbit. After the forward sweep, the backward sweep can start with the final value of ω_{ex} from the forward sweep. Then the value of ω_{ex} is decreased in every step, and the system is run until it reaches the periodic orbit. The backward sweep is finished when ω_{ex} reaches the initial value of the forward sweep. The resulting stable branches of periodic orbits are clearly separated by an unstable one both for phase and amplitude. In fig. 5.5, the bistable behavior, particularly the hysteresis, is visualized.

The bistable behavior has its origin in the nonlinear surface force F_{sf} in eq. (5.6) and the attractive and repulsive regime depending on the tip-sample distance illustrated in fig. 5.2b. A good explanation and illustration are given in [116], which serves as a model for the following two paragraphs and fig. 5.5. When the cantilever is driven with a frequency much smaller than ω_0, the system is in a periodic orbit corresponding to a point on the graph in fig. 5.5b left of the point I. The system is in free vibration, which is visualized by the green color of the graph. When the driving frequency ω_{ex} of the cantilever's amplitude increases, the minimum of

the tip-sample distance decreases. When the driving frequency reaches the value corresponding to the point I, the cantilever tip's lowest position is so close to the surface that the attractive forces are large enough to let the system jump to the periodic orbit corresponding to the point I'. This point I' corresponds to the tip-sample distance of $r = r_0$ where the Lennard-Jones potential (5.5) is minimal, and F_{sf} is zero. If the driving frequency is further increased, the surface force becomes repulsive, which is illustrated by the dark red color of the graph in fig. 5.5. Hence, the resonance frequency is increased. This repulsion inhibits the decrease of the amplitude and phase until ω_{ex} reaches the value corresponding to the point II, and the repulsive forces become large enough to bring the system to a smaller periodic orbit with an amplitude corresponding to the point II'. Then, the system is in free vibration again. The inhibition of the decrease in amplitude leads to a larger effective spring constant k. This behavior is called *hardening* since the cantilever acts like an effectively harder spring. As a result, the tip of the resonance curve is shifted to the right.
When the driving frequency is larger and an amplitude smaller than the ones in point III, the system is in free vibration. When ω_{ex} is decreased, the tip-sample distance r leaves the repulsive regime at III, and the surface force becomes attractive. This attraction induces a lower resonance frequency, resulting in a smaller increase in amplitude and phase. The points corresponding to periodic orbits with attractive force are illustrated in lilac. At the point III', the attractive force becomes large enough to let the system jump to a periodic orbit with a larger amplitude and phase corresponding to point III''. The points II and III' are connected by a branch of unstable periodic orbits visualized as blue and red dots. At the point III'', the repulsive forces dominate until the system reaches point I'. When the driving frequency ω_{ex} is then decreased, the attractive forces slow down the resonance frequency enlarging the amplitude. So, the cantilever acts effectively like a spring with a smaller spring constant k. This behavior is called *softening* in analogy to hardening. The result is a shift of the resonance curve's tip to the left. When the driving frequency reaches a value corresponding to the one of point IV, the tip-sample distance becomes large, and the system jumps to point IV'. Then, it is in free vibration again. Due to the cubic-like shape of F_{sf}, the points I and IV must be connected by a second branch of unstable periodic orbits, too. The points I,IV,II, and III' can be identified as bifurcation points.

5.3 PD CONTROL ON PERIODIC ORBITS

A driving frequency ω_{ex} close to the free resonance frequency ω_0 allows for a higher sensitivity of measurements in the dynamic mode [23]. Since these frequencies lie in the bistable regime, perturbations, especially in the vicinity of the sample surface, could push the oscillations to the other stable periodic orbit corresponding to the same driving frequency. In order to gain more reliable measurements within this bistable regime, control methods , e. g. [2–4, 110, 120], for models of an AFM often focus on time-delayed feedback control to stabilize originally stable orbits further and avoid irregular or even chaotic behavior for improving the scanning rate. Considering the phase instead of the cantilever amplitude's change as the detection

quantity increases additionally the sensitivity due to faster recognition [117]. The first experimental time-delayed feedback control was realized on a sample of a polyimide film scanned by a magnetically coated cantilever [121]. Besides the classical time-delayed feedback control, other control techniques like, e. g. state-dependent Riccati equation control [5, 77] or Poincaré maps for entropy minimization [96] have also been developed for orbit stabilization for the AFM's dynamic mode. The approach of eliminating virtually the instabilities by an additional nanowire in the model's construction is followed in [23].
The above-presented works focus on avoiding irregular behavior, whereas accessing the unstable periodic orbits in between the stable branches is the aim of chapter 5. In order to explore the originally unstable branch of periodic orbits, in [92, 99], feedback control is applied to a theoretical AFM model. Since the already mentioned OGY method requires only very little knowledge about the system and its dynamics, it is a good choice for stabilizing periodic orbits in a physical system. This was realized in theory on an AFM model in [70] and allowed for tracking the originally unstable periodic orbits. These works give great insight into the dynamics but need derivative information or at least reliable approximations. Since the measurement signal for the physical experiments in an AFM is noisy, these methods can hardly be implemented in a laboratory experiment.
At the beginning of chapter 5, techniques to generally stabilize and continue branches of periodic orbits are presented. As already mentioned, some of them require further knowledge about the underlying system or are hard to implement in laboratory experiments. In the following, a control method to continue the branch of unstable periodic orbits is presented that does not require further knowledge about the underlying dynamics. It can be understood as a continuation of the control presented in chapter 3 onto periodic orbits. The method is explained and demonstrated in the example of the AFM model, but there is no limitation to this specific case. In general, the same conditions presented in section 3.1 concerning controllability and stabilizability must hold for the macroscopic function with respect to a suitable variable, e. g., phase or amplitude and the bifurcation parameter.
The main idea of the following is to implement a control that needs as little information as possible about the dynamics. When considering the periodic orbits of the cantilever tip z as stationary points of the phase φ, the PD control (3.2) for the continuation of stationary points presented in section 3.1.1 can be used similarly. The continuation starts in a small neighborhood around an already-known periodic orbit. The corresponding phase is set as the first target φ_1^* for the algorithm. Then the system is run for a predefined, not necessarily integer, number of periods T. The actual phase φ is estimated by the measurements or values of the simulation. Its derivative $\dot{\varphi}$ can be approximated by numerical methods like, e. g. difference quotient or more elaborate ones in the case where it is needed and possible. After the predefined time step $\Delta t = qT$, a multiple of the period length, for one update of the phase and its derivative, one control step is done. Similar to eq. (3.18), the driving frequency is updated by the discretized scheme

$$(\omega_{ex})_{k+1,l} = (\omega_{ex})_{k,l} - K_P(\varphi_{k,l} - \varphi_l^*) - K_D \left(\frac{\varphi_{k+1,l} - \varphi_{k,l}}{\Delta t} \right)$$

of the PD control, where k is the index for the number of stabilizing updates for the l-th found equilibrium with $\bar{\varphi} = \varphi_l^*$. Again, we set the time-difference quotient for the change $\left(-K_P(\varphi_{k,l} - \varphi_l^*) - K_D\left(\frac{\varphi_{k+1,l}-\varphi_{k,l}}{\Delta t}\right)\right)$ to 1. In the case of direct access to the phase, a PD control is possible with

$$\frac{\mathrm{d}}{\mathrm{d}t}\begin{pmatrix}\varphi\\ \dot{\varphi}\\ \omega_{ex}\end{pmatrix} = \begin{pmatrix}\dot{\varphi}\\ f_2(\varphi,\dot{\varphi},\omega_{ex})\\ -K_P(\varphi-\varphi^*) - K_D\dot{\varphi}\end{pmatrix}. \tag{5.9}$$

When the distance $|\varphi_{k,l} - \varphi_l^*|$ is smaller than a predefined tolerance and the absolute value of the derivative $\dot{\varphi}_{k,l}$ is below another predefined tolerance, the system is considered to have reached the desired periodic orbit. Then, the target is increased by $\Delta\varphi$, and the control procedure is iterated until the system reaches the periodic orbit.
The formulation of controllability and stabilizability conditions for periodic orbits similar to the ones in section 3.1.1 become technically more involved, particularly since we cannot resort no longer to a simple linearized control system. The matter would become simpler if we resorted to Poincaré maps, an approach we will return to in section 5.5.

5.4 RESULTS FOR THE MATHEMATICAL MODEL OF THE AFM

As a first example to test the proposed PD-control scheme (5.9) for the continuation of periodic orbits, it was applied to the AFM model (5.8) derived in section 5.1.3. In order to gain results approximating the dynamics of the physical AFM, the values of the parameters were chosen as follows: the spring constant $k = 0.7\,\mathrm{N/m}$, the cantilever equilibrium position $z_0 = 100\,\mathrm{nm}$, free amplitude $A_0 = 250\,\mathrm{nm}$, the quality factor $Q = 400$, the depth $V_0 = 4.2\,\mathrm{aJ}\,(= 4.2 \cdot 10^{-18}\,\mathrm{J})$ of the Lennard-Jones potential well, its minimizer $r_0 = 2.8\,\mathrm{nm}$, and hence a distance $\sigma \approx 2.5\,\mathrm{nm}$, and $\Delta z = 0.5\,\mathrm{nm}$ to avoid singularities in the surface force, the free resonance frequency $\omega_0 = 50\,\mathrm{kHz}$, and the damping factor $s = 7 \cdot 10^{-4}\,\mathrm{nN \cdot nm^2 \cdot s}$. For values of the driving frequency ω_{ex} between 48 kHz and 52 kHz, bistable behavior for forward and backward sweeps can be observed for a step size of $\Delta\omega \approx 81.6\,\mathrm{Hz}$, see fig. 5.5. Both diagrams are achieved by the same simulations. In fig. 5.5a, the bistable behavior with respect to the amplitude is clearly visible. Nevertheless, the bifurcation point on the stable branch with respect to the backward sweep is not recognizable by a first view. A PD-controlled continuation of starting on this branch would be harder to implement than for the phase, see fig. 5.5b, where the branches are clearly separated from each other.
Even though the continuation with the PD-control scheme (5.9) looks familiar from the previous chapters, it is much harder to implement. This is due to several reasons. For the Zeeman catastrophe machine model (3.19), an analytic description of the angle ϕ's movement is given, and the motions are recognizable by human eyes. For the AFM model, no explicit equations of motion of the phase φ or amplitude A are available, and the system's motion is only indirectly detectable. The availability of an analytical description simplifies the search for the right control parameters

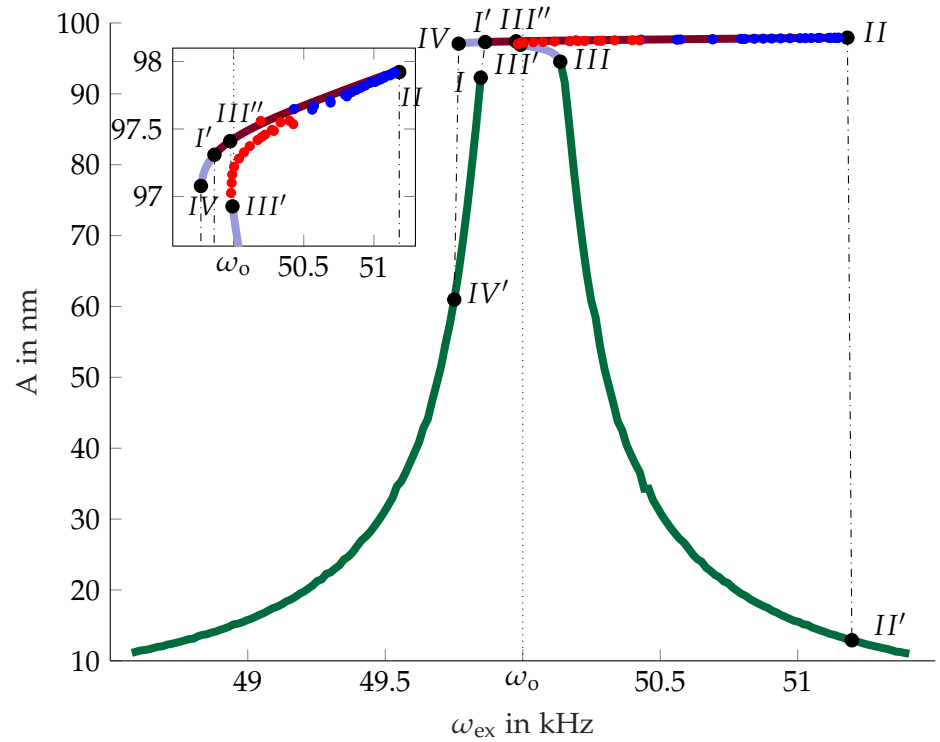

(a) Amplitude. Inset: zoom on the unstable branch. The small distance between the unstable and the upper stable branch complicates the continuation of unstable periodic orbits.

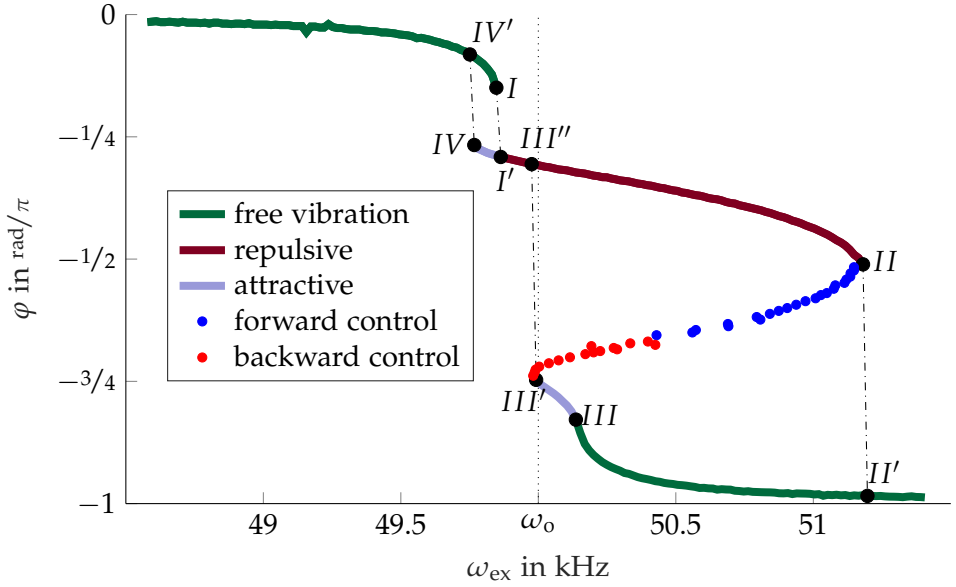

(b) Phase

Figure 5.5: Parameter sweep for the AFM model (5.8) with originally stable states compared to controlled stationary states. The continuous lines are achieved by direct simulation without control. The colors indicate whether free vibration (green), repulsive surface forces (dark red), or attractive surface forces (lilac) dominate. The dotted lines are produced by the controlled system (5.9), where the blue points are achieved by a start on the upper branch and the red ones by starting on the lower branch. The black dots visualize the bifurcation points where jumps (dashed lines) occur for the uncontrolled system. These lines are not perpendicular to the x-axis since they connect two successive points of the sweep.

since the conditions for controllability and stabilizability can be computed or numerically approximated. The Zeeman machine and its model are independent of time, whereas the oscillation mainly caused by the modeled excitation force F_{ex} is time-dependent, see eq. (5.3). So, implementation of the AFM model (5.8) must be initialized at the right time. Additionally, the Zeeman machine was introduced as a didactic tool and hence has a manageable nonlinearity, whereas the AFM's nonlinearity comes from several origins on atomic nanoscales, including repulsion or attraction. As a result of these challenges, it is possible to stabilize the unstable periodic orbits, but so far, only with specifically chosen different values of the control parameters for segments of the branches. These values for the control parameters to stabilize the periodic orbits with the PD control (5.9) can be found in tables C.1 and C.2. Additionally, the branch of unstable periodic orbits was found by composing two parts: one party by starting on the forward branch and the other one by starting on the backward branch. Around the value $\omega_{ex} = 50.4\,\mathrm{kHz}$, no continuation could be found. Therefore, the two parts are shown in different colors in fig. 5.5. This could indicate a singularity within the controlled system. Remarkably, the unstable branch lies very close to the forward branch in fig. 5.5a. This shows again the difficulties when choosing the amplitude as the macroscopic variable. Besides the missing analytical description, it is also likely that the regions of attraction around the PD-controlled periodic orbits are rather small. This also impedes the search for periodic orbits and could be an object of future investigations. In addition to the small distance between the stable and the unstable branch of the amplitude, the difference in the magnitude between phase φ and excitation frequency ω_{ex} is challenging for the control algorithm. In the prediction step, a scaling factor for the prediction of the initial value $\omega_{k,0}$ for ω for the k-th stationary point $(\bar{\varphi}_k, \bar{\omega}_k)$ was used to weigh the influence of the directions according to the scheme

$$\omega_{k,0} = \bar{\omega}_{k-1} + \frac{\varphi_k^* - \bar{\varphi}_{k-1}}{\bar{\varphi}_{k-1} - \bar{\varphi}_{k-2}} \cdot (\bar{\omega}_{k-1} - \bar{\omega}_{k-2})\,.$$

Here, $(\bar{\varphi}_{k-1}, \bar{\omega}_{k-1})$ and $(\bar{\varphi}_{k-2}, \bar{\omega}_{k-2})$ are the two previously found stationary points, and φ_k^* is the target for the phase of the k-th stationary point. The initial value for ϕ is $\phi_k^0 = \phi_k^*$.

Other difficulties in tracking the branch of unstable stationary orbits could result from signal processing. So far, the derivative $\dot{\varphi}$ is approximated by a simple difference quotient of the computed phase because the data for φ is coarse due to the period dependency. Additionally, the phase φ and its derivative $\dot{\varphi}$ are taken as the average over the computed phases of the last six periods of length $1/\omega_{ex}$. So, they are measured only discretely.

In the case of direct estimation of φ, more elaborate methods to estimate $\dot{\varphi}$ might be possible and could improve the result. As mentioned in section 5.3, direct and continuous access to φ could decrease the control delay, which is, in the described case, only working at discrete time steps. Similarly, the phase φ is just an approximation of the first harmonic in the described procedure for reasons of simplicity. Even though the higher harmonics are of minor importance for the measured signal, their contribution to the phase is included in the value of φ. In contrast, the PD control (5.9) only considers the difference between φ and the desired first harmonic φ^*; see

[23]. Generally, the PD control (5.9) could be extended to any number n of harmonics. The control parameters K_P and K_D must then be n-dimensional matrices.
Overall, several possibilities exist to optimize the presented PD control on the AFM model. In particular, the presented method allows no or only negligibly small noise. More elaborate methods with further requirements concerning knowledge about the dynamical behavior or signal processing might lead to more robustness.

5.5 STROBOSCOPIC MAP

In the previous sections, a PD-control-based method to continue the branch of periodic solutions of dynamical systems was presented. The online adjustment of the frequency hampered a detailed theoretical analysis of the previous control scheme. This turns stability considerations into Floquet problems, which are hard to tackle by analytic means. If we move to a simplified scheme, where we adjust the control input only at the beginning of each period and keep the value constant through a whole period of the orbit, we may turn the problem again into a study of plain fixed points, which is then amenable to an analytic approach. Hence, the following method aims for the same target and is inspired by the afore-presented approach. Similarly, no explicit mathematical description of the system is assumed to be given. But the periodicity is directly used by introducing the *stroboscopic map* that works discretely in time only at integer multiples of the period length. The ideas date back to the OGY method [78]. In contrast to OGY or typical control methods on discrete maps like e. g. [64], the stroboscopic control keeps the control parameter value constant over the length of whole periods. The following section is based on the structure and recent results in the joint work [27]. Nontrivial formulations of sentences and paragraphs that are taken nearly literally from the original work are marked by "([27])". The table D.5 of all symbols and variables introduced for the stroboscopic control can be found in appendix D.
For the following, a T-periodic time-dependent nonautonomous dynamical system is given that can be described by the differential equations

$$\dot{x} = f(x, \mu; t)\,, \quad f(x, \mu; t) = f(x, \mu; t + T)\,, \tag{5.10}$$

where $x \in \mathbb{R}^2$ is the state, $\mu \in \mathbb{R}$ is the parameter on which the system is dependent, and $f : \mathbb{R}^4 \to \mathbb{R}^2$ is the system's right-hand side. We restrict ourselves again for reasons of simplicity on the 2-dimensional case for the state x, but a generalization for the n-dimensional case is possible. As already stated at the beginning of section 5.5, eq. (5.10)'s description is not assumed to be known explicitly. Still, the measured or simulated signal must be free from any significant noise in order to guarantee access to the later required derivative information. Let

$$\zeta(t; x_0, \mu) \coloneqq x(t)$$

denote the solution of eq. (5.10) with initial condition $x(0) = x_0$. The system (5.10) can then be written as

$$\dot{\zeta}(t; x_0, \mu) = f(\zeta(t; x_0, \mu), \mu; t)\,, \quad \zeta(t; x_0, \mu) = x_0\,. \tag{5.11}$$

Since we are interested in periodic orbits and hence in changes of the state after integer multiples of the period length T, we can introduce the *stroboscopic map*

$$x_{k+1} = F(x_k, \mu) := \zeta(T; x_k, \mu) \tag{5.12}$$

of the dynamical system (5.10). Here $x_k = x(T_k)$ is the solution at times T_k, where $T_k = kT$ are discrete time points with a distance of one-period length T of the driving field. This could be, e. g. , the end of the k-th period. A T-periodic solution of eq. (5.10) corresponds to a fixed point x_* of the stroboscopic map (5.12). This means

$$x_* = F(x_*, \mu)\,, \tag{5.13}$$

with $x(t) = \zeta(t; x_*, \mu) = \zeta(t + T; x_*, \mu)$, is the periodic state of eq. (5.10) dependent on time. With $x_k = x_* + \delta x_k$, the variational equation (5.13) of the stroboscopic map reads

$$\delta x_{k+1} = DF(x_*, \mu) \cdot \delta x_k\,, \tag{5.14}$$

with $DF(z)$ denoting the Jacobian of F in the point z. Following the Jury criterion [56] (thm. 1.7) for the stability of fixed points, the eigenvalues of $DF(x_*, \mu)$ determine the stability of x_*. Only if both eigenvalues lie inside the unit circle the fixed point is stable. See section 1.2 for further details.
Since the method's aim is to stabilize and follow the branch of time-period solutions of eq. (5.10) for an explicit description of the right-hand side f, only the measured or simulated time series $x(t)$ with $x(kT) = x_k$ can be used for the parameter μ's update within the control. It is assumed that the following analytically computed derivatives could be estimated numerically by fitting the generated data. Hence, the data must be noise-free, and data points must be dense enough. For physical experiments, this is hard to accomplish. In addition, even for numerically simulated data, if $x(t)$ reaches a fixed point, only a limited number of different data points is accessible. So, data quality is one of the main challenges for the following control method.
Similar to the PD control (5.9), the following control relies on feedback for the k-th update step

$$\mu_k = \mu_R + \xi^T \cdot (x_k - x_R) \tag{5.15}$$

of the parameter μ, where $\xi^T = (\xi_1, \xi_2)$ is the control gain, μ_R and x_R are reference values. The closed-loop dynamics (5.13) become

$$x_{k+1} = F(x_k, \mu_k)\,. \tag{5.16}$$

The fixed point of eq. (5.16) combined with eq. (5.15) is then

$$x_* = F(x_*, \mu_*) \tag{5.17a}$$
$$\mu_* = \mu_R + \xi^T \cdot (x_* - x_R)\,. \tag{5.17b}$$

Thus, the intersection of the fixed point manifold given in eq. (5.13) with a hyperplane defined by the reference value of (x_R, μ_R) defines the fixed point $(x_*, \mu*)$ of

the controlled system (5.17) [27]. Similar to eq. (5.14), the variational equation of eq. (5.16) can be denoted by

$$\delta x_{k+1} = DF(x_*, \mu_*)\delta x_k + \partial_\mu F(x_*, \mu_*)\left(\xi^T \cdot \delta x_k\right) = \Xi \cdot \delta x_k \,. \tag{5.18}$$

Here, Ξ is the square matrix given by

$$\Xi = DF_* + \partial F_* \otimes \xi^T \,, \tag{5.19}$$

with the shorthand notation

$$DF_* = DF(x_*, \mu_*) \,, \quad \partial F_* = \partial_\mu F(x_*, \mu_*)$$

for the expressions inside a fixed point. Here, $\partial F_* \otimes \xi^T$ denotes the dyadic product.

5.5.1 *Controllability and stabilization by the stroboscopic control*

As already mentioned above, the Jury criterion for fixed points states the condition for stability of the fixed points (x_*, μ_*) of the variational equation (5.18). Both eigenvalues of Ξ must be inside the unit circle. Hence, for the 2-dimensional case, the Jury criterion simplifies to the following two conditions

$$\det(\Xi) < 1 \,, \tag{5.20a}$$
$$|\mathrm{tr}(\Xi)| < 1 + \det(\Xi) \,. \tag{5.20b}$$

Thus, the trace and the determinant of Ξ must be considered in detail for a stability and controllability analysis. From the variational equation (5.18), it can be derived

$$\mathrm{tr}(\Xi) = \mathrm{tr}\,(DF_*) + \xi^T \cdot \partial F_* \,, \tag{5.21a}$$
$$\det(\Xi) = \det(DF_*) + \xi^T \cdot \mathrm{adj}(DF_*) \cdot \partial F_* \,, \tag{5.21b}$$

where $\mathrm{adj}(DF_*)$ denotes the adjugate matrix of DF_*; see [16, 108]. In comparison to the inverse of a matrix, the adjugate matrix $\mathrm{adj}(M)$ is still well-defined even if the matrix M is not regular. It holds for the matrix product $M \cdot \mathrm{adj}(M) = \det(M)$. A simplex inside the space of all possible control value sets is spanned by the set of parameter values for the control gains ξ that satisfy the conditions (5.20) for eq. (5.21). As already stated in section 1.2, controllability implies stability. So, the set of parameter values that guarantee controllability lies inside the above-defined stability region. If the two vectors ∂F_* and $\mathrm{adj}(DF_*) \cdot \partial F_*$ span a nonempty triangle, i. e., if they are linearly independent, the Kalman rank criterion [57] (thm. 1.5) is fulfilled. This is equivalent to the linear independence of the set $\{\partial F_*, DF_* \cdot \partial F_*\}$. For a non-singular matrix DF_* the equivalence is obvious. Under certain circumstances, it can be shown for singular matrices, too. See [27] for further details. If the Kalman rank criterion is violated, i. e. if ∂F_* is an eigenvector of DF_*, there are cases where the control (5.15) is still successfully applicable, similar to the previously cited OGY method [78].

5.5.2 *Optimal control gains*

Following the linear stability perspective, the control gains are optimal if the fixed points are superstable, which means that the transients are as short as possible. See, e. g., [109] for details. This is achieved if both eigenvalues of Ξ in eq. (5.19) are zero. The solution of eq. (5.15) for $\mathrm{tr}(\Xi) = \det(\Xi) = 0$ is

$$\zeta^T = -\frac{u^\perp \det(DF_*) + v^\perp \mathrm{tr}(DF_*)}{v^\perp \cdot \partial F_*}\,, \tag{5.22}$$

with the vectors

$$u^\perp = ((\partial F_*)_2\,,\, -(\partial F_*)_1) \quad \text{and} \tag{5.23a}$$

$$v^\perp = (-(\mathrm{adj}(DF_*) \cdot \partial F_*)_2\,,\, (\mathrm{adj}(DF_*) \cdot \partial F_*)_1) \tag{5.23b}$$

orthogonal to the set $\{\partial F_*, \mathrm{adj}(DF_*) \cdot \partial F_*\}$. The computation of the control gains (5.22) and hence of eq. (5.23) requires the knowledge or a good approximation of DF_* and ∂F_*. In the case of numerical simulations, they are accessible by the variational equation (5.18) for the discrete time steps of the stroboscopic map (5.12). As stated above, this is a hardly manageable part of the method for physical experiments. With respect to the initial conditions of eq. (5.11), it holds

$$DF(x_0, \mu) = \begin{pmatrix} \partial_{x^{(1)}} F^{(1)} & \partial_{x^{(2)}} F^{(1)} \\ \partial_{x^{(1)}} F^{(2)} & \partial_{x^{(2)}} F^{(2)} \end{pmatrix} (x_0, \mu) \tag{5.24a}$$

$$= \begin{pmatrix} \partial_{x^{(1)}} \zeta^{(1)} & \partial_{x^{(2)}} \zeta^{(1)} \\ \partial_{x^{(1)}} \zeta^{(2)} & \partial_{x^{(2)}} \zeta^{(2)} \end{pmatrix} (x_0, \mu; T) = \partial_{x_0} \zeta(T; x_0, \mu) \tag{5.24b}$$

$$= Y(T; x_0, \mu)\,, \tag{5.24c}$$

where Y is the fundamental matrix of the variational equation

$$\frac{\mathrm{d}}{\mathrm{d}t}(\delta x) = Df(x_*, \mu; t) \cdot \delta x$$

of eq. (5.11). Here, the superscript indices in brackets of $x^{(k)}$ denote the k-th entry of x with respect to the dimension in space. For legibility reasons, the argument (x_0, μ) or $(x_0, \mu; T)$ is denoted only once behind the matrix DF or Y, respectively. However, the matrices in eq. (5.24) all contain entries with values of the respective functions evaluated at $(x_0, \mu; T)$. Additionally, the derivative of the variational equation (5.18) with respect to the initial condition is

$$\frac{\mathrm{d}}{\mathrm{d}t} Y(t; x_0, \mu) = \frac{\mathrm{d}}{\mathrm{d}t} \begin{pmatrix} \partial_{x^{(1)}} \zeta^{(1)} & \partial_{x^{(2)}} \zeta^{(1)} \\ \partial_{x^{(1)}} \zeta^{(2)} & \partial_{x^{(2)}} \zeta^{(2)} \end{pmatrix} (t; x_0, \mu)\,. \tag{5.25}$$

According to eq. (5.11), a single entry of the right-hand side of eq. (5.25) with $k, l = 1, 2$ has the form

$$\frac{\mathrm{d}}{\mathrm{d}t}\zeta^{(l)}(t; x_0, \mu) = f^{(l)}(\zeta(t; x_0, \mu), \mu; t)\,, \quad \text{and} \tag{5.26a}$$

$$\begin{aligned}(Y(t; x_0, \mu))_{k,l} &= \frac{\mathrm{d}}{\mathrm{d}t}\left(\partial_{x_0^{(l)}}\zeta^{(k)}(t; x_0, \mu)\right) \\ &= \partial_{x^{(2)}} f^{(k)}(\zeta(t; x_0, \mu), \mu, t) \cdot \partial_{x_0^{(l)}}\zeta^{(2)}(t; x_0, \mu) \\ &\quad + \partial_{x^{(1)}} f^{(k)}(\zeta(t; x_0, \mu), \mu, t) \cdot \partial_{x_0^{(l)}}\zeta^{(1)}(t; x_0, \mu)\,.\end{aligned} \tag{5.26b}$$

In matrix notation, eq. (5.26b) reads

$$\frac{\mathrm{d}}{\mathrm{d}t}Y(t; x_0, \mu) = Df(\zeta(t; x_0, \mu), \mu; t) \cdot Y(t; x_0, \mu)\,, \tag{5.27}$$

which is a differential equation differentiated with respect to the initial conditions. According to eq. (5.24) it holds $DF(x_0, \mu) = Y(T; x_0, \mu)$. Inserting the initial conditions of eq. (5.11) leads to

$$\begin{aligned}Y(0; x_0, \mu) &= \begin{pmatrix} \partial_{x_0^{(1)}}\zeta^{(1)} & \partial_{x_0^{(2)}}\zeta^{(1)} \\ \partial_{x_0^{(1)}}\zeta^{(2)} & \partial_{x_0^{(2)}}\zeta^{(2)} \end{pmatrix}(0; x_0, \mu) \\ &= \begin{pmatrix} \partial_{x_0^{(1)}} x_0^{(1)} & \partial_{x_0^{(1)}} x_0^{(2)} \\ \partial_{x_0^{(2)}} x_0^{(1)} & \partial_{x_0^{(2)}} x_0^{(2)} \end{pmatrix} = \begin{pmatrix} 1 & 0 \\ 0 & 1 \end{pmatrix} = \mathbb{1}_{2\times 2}\,.\end{aligned} \tag{5.28}$$

In cases like e. g. the above-presented AFM model (5.8) where the parameter μ is the driving frequency ω, the period length $T = \frac{2\pi}{\omega}$ depends on the parameter. This will be used in the following. At first, we define

$$\begin{aligned}\eta(T; x_0, \mu) &\coloneqq \partial_\mu \zeta(T; x_0, \mu)\,, \quad \text{and so} \\ \eta(t; x_0, \mu) &= \partial_\mu \zeta(t; x_0, \mu)\,.\end{aligned}$$

Following a similar scheme, for a fixed T, it is

$$\partial_\mu F(x_0, \mu) = \partial_\mu \zeta(T; x_0, \mu) + \partial_T \zeta(T; x_0, \mu) \cdot \partial_\mu T(\mu) \tag{5.29a}$$

$$= \eta(T; x_0, \mu) + f(F(x_0, \mu), \mu; T) \cdot \partial_\mu T \tag{5.29b}$$

under the usage of eq. (5.11). The terms $f(\zeta(T; x_0, \mu), T) = \partial_T \zeta(T; x_0, \mu)$ and $\partial_\mu T(\mu)$ can be computed at least numerically. So, eq. (5.29) is generally accessible. Using eq. (5.11) results in the derivative

$$\frac{\mathrm{d}}{\mathrm{d}t}\left(\partial_\mu \zeta(t; x_0, \mu)\right) = \partial_\mu f(\zeta(t; x_0, \mu), \mu, t) + Df(\zeta(t; x_0, \mu), \mu; t) \cdot \frac{\mathrm{d}}{\mathrm{d}t}\left(\zeta(t; x_0, \mu)\right)\,.$$

So, it follows for eq. (5.29) that the derivative η of the solution ζ obeys

$$\frac{\mathrm{d}}{\mathrm{d}t}\left(\eta(t; x_0, \mu)\right) = Df(\zeta(t; x_0, \mu), \mu; t) \cdot \eta(t; x_0, \mu) + \partial_\mu f(\zeta(t; x_0, \mu), \mu; t) \tag{5.30}$$

with initial condition

$$\eta(0; x_0, \mu) = \partial_\mu \zeta(0; x_0, \mu) = \partial_\mu x_0 = 0\,. \tag{5.31}$$

Integrating eqs. (5.27) and (5.30) with initial conditions (5.28) and (5.31), respectively, results in the stroboscopic map (5.12) and eqs. (5.24) and (5.29) by the important derivatives. Thus, the optimal control gains (5.22) are computable for the noise-free case. Since the eq. (5.22) requires the knowledge of the derivatives inside the fixed point, the optimal control is only accessible for already known fixed points which is not generally the case. The following section 5.5.3 presents an approach for tracking the branch of periodic orbits without prior knowledge of the exact positions.

5.5.3 *Tracking of periodic orbits*

As already stated, the access to the optimal control gains (5.22) depends on the knowledge of the fixed points. Since the tracking and stabilization of these points is exactly the aim of the presented method, the fixed points are rarely given in applications where the control (5.15) might be useful. A practical approach similar to the ones presented in chapters 2 to 4 is to take in every control step the control gains from the previous one and recompute new values for $\xi \in \mathbb{R}^2$ after each step. Again, it is assumed that $F(x_0, \mu)$, $DF(x_0, \mu)$, and $\partial F(x_0, \mu)$ are at least numerically accessible.
For the search of a new fixed point (5.17), the reference values are favorably chosen as

$$x_R = x_* \quad \text{and} \quad \mu_R = \mu_* \,,$$

or in the close neighborhood. An approach for (x_*, μ_*) can be made by, e. g., secant methods if previous fixed points are already known. Since stable periodic orbits are accessible by running the experiment even without control, we can assume that the starting point of the branch of periodic states is known. Hence, a good approximation for (x_R, μ_R) is available. For the case of small changes along the trajectory, i. e. small variations

$$(x_* + \delta x) \text{ for } x_* \quad \text{and} \quad (\mu_* + \delta\mu) \text{ for } \mu_* \,,$$

the variational equation (5.18) becomes

$$\begin{aligned} x_* + \delta x &= F(x_* + \delta x, \mu_* + \delta\mu) \\ &= F(x_*, \mu_*) + \partial_\mu F(x_*, \mu_*)\delta\mu + DF(x_*, \mu_*)\delta x \,. \end{aligned} \tag{5.32}$$

Fulfilling the variational equation (5.32) leads to the condition

$$0 = \partial_\mu F(x_*, \mu_*) \cdot \delta\mu + (DF(x_*, \mu_*) - \mathbb{1}_{2\times 2}) \cdot \delta x$$

for the vector $(\delta x, \delta\mu)^T \in \mathbb{R}^3$. Hence, the reference values should be chosen such that

$$\begin{aligned}
\begin{pmatrix} \delta x_R \\ \delta\mu_R \end{pmatrix} &\sim \begin{pmatrix} -(DF(x_*,\mu_*) - \mathbb{1}_{2\times2}) \cdot \partial_\mu F(x_*,\mu_*) \cdot \delta\mu_* \\ \delta\mu_* \end{pmatrix} \\
&\sim \begin{pmatrix} -(DF(x_*,\mu_*) - \mathbb{1}_{2\times2})^{-1} \cdot \partial_\mu F(x_*,\mu_*) \\ 1 \end{pmatrix} \\
&\sim \det(DF(x_*,\mu) - \mathbb{1}_{2\times2}) \cdot \begin{pmatrix} -(DF(x_*,\mu_*) - \mathbb{1}_{2\times2})^{-1} \cdot \partial_\mu F(x_*,\mu_*) \\ 1 \end{pmatrix} \\
&= \begin{pmatrix} -\mathrm{adj}(DF(x_*,\mu_*) - \mathbb{1}_{2\times2}) \cdot \partial_\mu F(x_*,\mu_*) \\ \det(DF(x_*,\mu_*) - \mathbb{1}_{2\times2}) \end{pmatrix} \qquad (5.33)
\end{aligned}$$

is fulfilled, where $a \sim b$ means that a and b are proportional. For the last step of the reformulation (5.33), it was used that

$$M^{-1} = \frac{1}{\det(M)} \cdot \mathrm{adj}(M)$$

holds for the adjugate of a matrix M. Note that the adjugate matrix in eq. (5.33) is well-defined even if $(DF(x_*,\mu_*) - \mathbb{1}_{2\times2})$ is not regular. So, the steps are only made along the trajectory. Thus, the control algorithm only fails if the controllability condition concerning the linear independence of ∂F_* and $DF_* \cdot \partial F_*$ is violated.
Even though it is, in theory, always possible to state the reference values for each fixed point analytically, the region of attraction for the stabilized periodic orbits can be very small. For physical and numerical experiments, this could be challenging. Additionally, the above-described tracking of periodic orbits is only possible when no significant changes in the period length T take place. If the frequency ω is the parameter μ, changes in μ cause changes in the period length $T = \frac{2\pi}{\omega}$. This is another significant limitation of the stroboscopic control method.

5.5.4 *Results for the mathematical example of the Toda oscillator*

Similar to the previously presented control methods, we test the continuation with the stroboscopic control (5.15) and (5.16) on a mathematical example. For reasons of clarity and simplicity, the one-dimensional motion of a particle x is considered in an external potential V under damping c and a periodic harmonic drive with amplitude A and frequency ω of the following form

$$\dot{x} = v, \quad \dot{v} = -cv - V'(x) - A \cdot \cos(\omega t)\,.$$

Due to its simplicity and nonlinear behavior, the Toda oscillator [111] is a popular example to study the phenomenon of self-pulsation for solid-state lasers and an appropriate model for our purpose. Its potential is defined as

$$V(x) = \exp(-x) + x - 1\,.$$

The numerical simulation of this model was done in non-dimensional units and with the parameter values $c = 10^{-1}$, $A = 8 \cdot 10^{-3}$, and $\omega = \frac{2\pi}{T}$ with the period

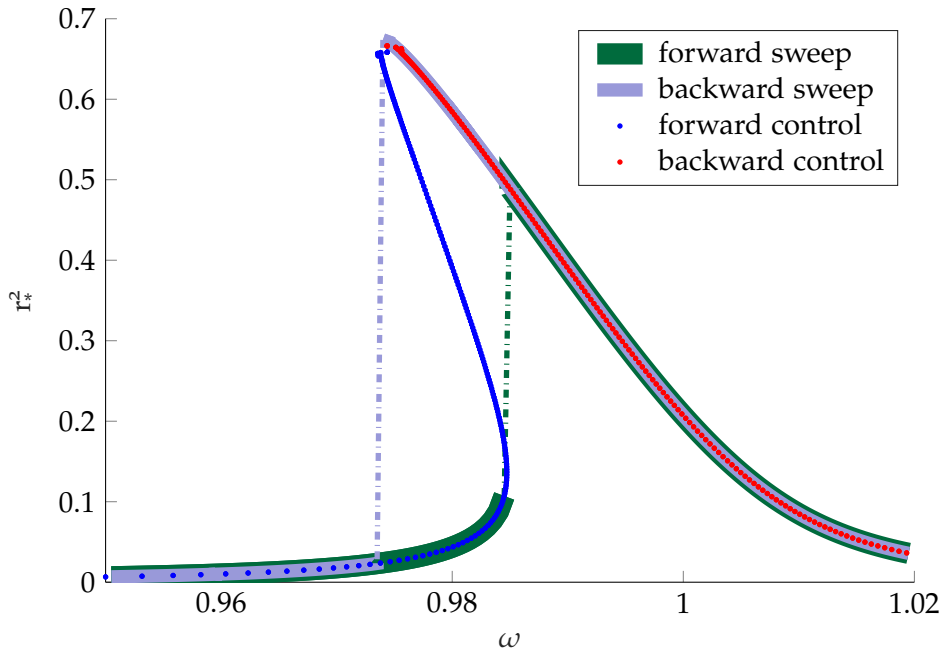

(a) Stationary amplitude $r_*^2 = x_*^2 + \frac{v_*^2}{\omega^2}$

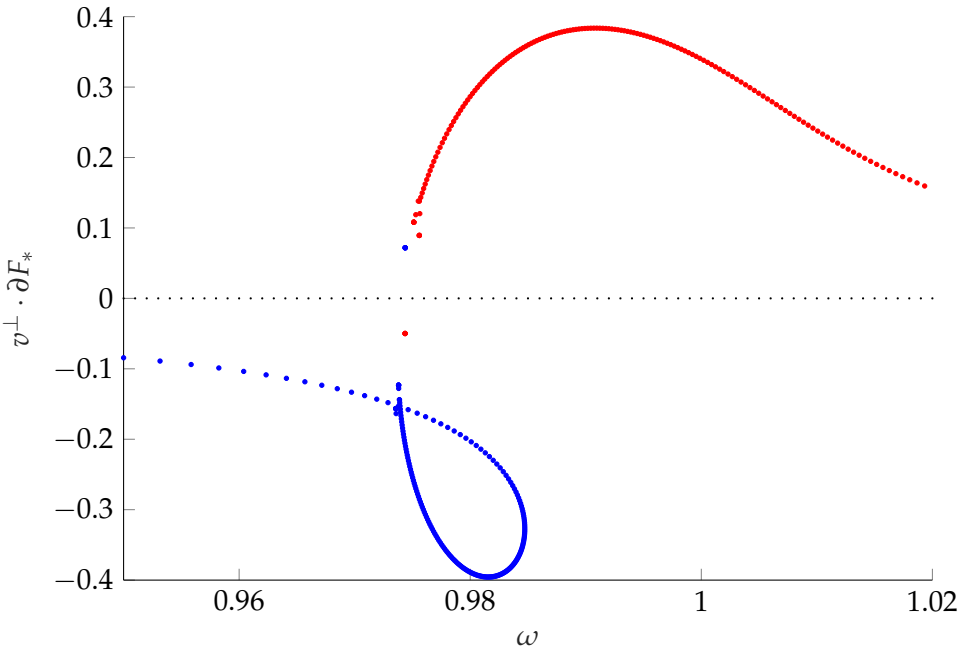

(b) Denominator $v^\perp \cdot \partial F_*$ of the optimal control gains in eq. (5.22)

Figure 5.6: Stroboscopic control of the Toda oscillator with (a) the stationary amplitude and (b) the denominator of the optimal control gains. The uncontrolled sweep is depicted in dark green for the forward sweep and lilac for the backward sweep. The forward control is shown by blue dots, and red dots show the control in the backward direction. Simulations were done by Wolfram Just and can be found in [27].

length T. The results are shown in fig. 5.6. The value of the stationary amplitude $r_*^2 = x_*^2 + \frac{v_*^2}{\omega}$ shows a bistable behavior in dependence of the driving frequency ω. The bistability and the stabilized unstable branch are depicted in fig. 5.6a. Since the control gains are optimized in every step by eq. (5.22), their dependence on the parameter ω is of great interest. It can be seen in fig. 5.6b that the denominator $v^\perp \cdot \partial F_*$ is vanishing in the neighborhood of a certain point with $\omega \approx 0.9756$. Similar to the results of the continuation with PD control presented in fig. 5.5, a breakdown of the control can be observed in fig. 5.6a at this specific point. This breakdown is caused by the violation of the controllability conditions. Thus, we may presume that a similar lack of controllability causes the breakdown of the PD control described in section 5.4.

6 CONCLUSION AND OUTLOOK

In this dissertation, several noninvasive feedback control-based methods were presented. For physical systems, explicit descriptions of the dynamics are rarely given. So, techniques for data-based stability analysis were introduced. They allow for obtaining complete bifurcation diagrams, including stability information for simulated systems and laboratory experiments.
The proportional control combined with the state observer presented in chapter 2 is easy to implement. The dynamic adaption (2.3b) of the target y for the next equilibrium allows for tracking a branch of either stable or unstable states. Since the sign of the control parameter α_2 for the target depends on the stability of the searched stationary point, the continuation of equilibrium points over fold bifurcation points is not possible by this method. By adding a supplementary control (2.11c) for the parameter α_1 of the proportional control for the state x, the value of α_1 is adapted according to the derivative information g_x of the controlled system. When the system has settled at a stationary point, the value of α_1 contains information about the equilibrium's stability. The idea of adaptive control, especially for the proportional case, dates back to the 1950s. See [126] and the references cited therein for a summary of the first adaptive-control approaches. But instead of more stability, the extended proportional control (2.11) aims for stability information. As already stated, the continuation over fold points is not possible by proportional control. Since the stability information is available with the extended proportional control, one could think of a continuation that skips the neighborhood of a bifurcation, i. e. when the absolute value of the derivative f_x of the original system is close to zero. Another alternative could be an additional control for the second control parameter α_2 inducing a change of sign in the bifurcation point. A second limitation of this method is due to the choice of parameter values. The theoretical limits for the values of the control parameters given in sections 2.1 and 2.2 are nonvanishing except for bifurcation points. In real-world systems these values are often not realizable due to physical restrictions. Hence, more elaborate control methods must be chosen.
The PD control has a broader field of applications since it takes the derivative information additionally into account. In chapter 3 this is used to construct a full bifurcation diagram, including the fold bifurcation points for the laboratory experiment of the Zeeman catastrophe machine. The motion data of the controlled system serve for the stability analysis of the originally uncontrolled system. A least-squares method applied *a posteriori* provides the linear stability information. Traditionally, stability analysis based on data is only possible by switching off the control [18] or perturbation of the controlled system [6]. Both invasion types are not necessary for the method presented in chapter 3. So far, this stability analysis was only applied to systems with stationary points. Generally, an adaption on periodic orbits should be possible since they appear as equilibrium points in Fourier space. Future works could also consider the stability analysis with higher-order terms

for other types of bifurcations and the identification of the relevant macroscopic variables in experimental setups.
The data-based stability information introduced in chapter 3 is used for the two-parameter continuation of bifurcation points in systems with an additional dynamic parameter. In chapter 4, the results of the implementation of the additional proportional control on the second bifurcation parameter λ are shown for simulated and laboratory experiments. Bifurcation points are of great interest in dynamical systems theory since they indicate changes in qualitative behavior. The presented method could help to identify the borders between stable and unstable regions for systems where free evolution might harm the experimental setup. Since the tracking of bifurcation points relies only on the data-based stability information, the investigation of points with other desired stability properties is generally possible, too. Producing backbone curves like in [7, 93, 94] are objects of interest for potential extensions of the continuation routine.
As mentioned above, periodic orbits appear as equilibrium points in Fourier space. So, the PD control presented in chapter 3 was adapted for the stabilization of periodic orbits in a model of an Atomic Force Microscope in chapter 5. The continuation of these points was possible for the simulated model but only with adapted control gains after a few found stationary points. Hence, the stabilization of periodic orbits in the laboratory experiment of an AFM might be hard to apply, and more elaborate methods should be considered that take, e. g., the integral part of the motion data into account. The stabilization of the unstable branch for the AFM could potentially increase the measurement quality of the AFM in the bistable regime. Another potential topic of future work is the adaption of data-based stability information introduced in chapter 3 on periodic orbits. For cases where stability information is at least numerically available, the stroboscopic map introduced in section 5.5 is an alternative. In contrast to already existing methods like OGY [78], the control parameters are kept constant for the length of whole periods. Since no indirect quantities like the phase for the AFM are needed, the stroboscopic control is easily implemented and provides simple access to the quantities of interest. But if the bifurcation parameter is the frequency, the changes in the period length must be small compared to other quantities involved. On the other hand, the noise of experimental data might cause major difficulties for the implementation, whereas, for PD control-based continuation, data with small noise might be manageable after filtering. Hence, the PD control with supplements is much closer to an experimental realization. As shown in section 5.4, singularities in the controlled systems can cause discontinuities. Generally, this is possible for the stroboscopic control, too.
Altogether, it has been shown that linear stability analysis of controlled systems is principally possible without knowledge of the underlying uncontrolled dynamics. The successful implementation in experiments proves the applicability, at least for simple laboratory dynamical systems. Additionally, its usage for the continuation of bifurcation points emphasizes the reliability of the gained stability information. The periodic orbits were stabilized by methods similar and different to the ones used for the stationary points within this dissertation. So, for future work considering the original stability of periodic orbits, several approaches are conceivable.

A

TECHNICAL DETAILS FOR THE LABORATORY EXPERIMENTS WITH THE ZEEMAN CATASTROPHE MACHINE

The present technical description is taken from Appendix A of [26] and was rephrased and adapted where necessary. Wherever a nontrivial formulation of a sentence or a paragraph was taken close to literally, this is identified by "([26])".
The experimental implementation of the laboratory experiments with the Zeeman catastrophe machine is based on a commercial low-cost laser engraver kit (ETE ETMATE). The necessary mechanical parts for 2-dimensional motion are included. Besides belt-driven linear stages and stepper motors, a controller board is contained, which facilitates stepper drivers and a microcontroller. The motion path is generated by the software based on the open-source firmware Grbl [35] implemented on the microcontroller. The codes for the Zeeman control algorithm (3.18) and the continuation (4.6) of bifurcation points are implemented in Python on a Raspberry Pi (RPi) single-board computer (Raspberry Pi 4 model B, 4 GB RAM). The RPi and the Grbl controller are connected by a universal serial bus (USB) interface operating as a virtual serial port ([26]). So, the motion of the stepper motor can be controlled via G-Code commands that consist of text strings and coding motion commands. The alterations of the angle ϕ are measured by an incremental rotary encoder (Sendix 5000, Fritz Kübler GmbH, 5000 steps per revolution [32]). The rotary encoder communicates via a two-channel digital signal (5 V, TTL compatible), which results in two quadrature square waves. A change in the angular state provokes a voltage level transition on both channels which allows for unambiguously determining the angular change direction from the quadrature phase. A voltage divider enables communication between the rotary encoder and the RPi since the RPi input pins can only process low-voltage TTL (LVTTL, 3.3 V) signals. Once the signal corresponding to a change of the angle is detected, the program for the control updates the stored angle. Note that in this sensor-readout setup, the value of the angle is not absolute. This means that before each sweep, the mechanics of the Zeeman machine must be homed into a starting position where the absolute value is known ([26]). The rotary encoder is attached to a 3-dimensional-printed plastic holder made from polylactic acid (PLA) to bring the points A, B, and P to the same height so that the system is nearly planar. For a basis of the point P, a measuring wheel with a radius of 79.6 mm (type 8000, Fritz Kübler GmbH [31]) is fastened directly to the rotary encoder. Since the pin for the point P cannot be mounted on the edge of the disk, the actual distance is $\rho = 65\,\mathrm{mm}$. Besides a planar basis for the experiment, the wheel supplies enough inertia to slow down the mechanical speed such that real-time processing of the data and communication are possible ([26]). The point P is connected with the two pins corresponding to the points A and B and mounted on a 3-dimensional-printed PLA holder and a 3-dimensional-printed PLA bracket attached to the engraver head, respectively. The connections consist of two helical tension springs, each with tensionless length $L_0 = 55\,\mathrm{mm}$ and a spring constant

$k = 5\,\mathrm{N/m}$. The point A has a distance of 244 mm to the origin, and the point B has a vertical distance λ of 230 mm to the origin in the case of the PD control (3.2). For the bifurcation-point continuation (4.3), the parameter λ is variable, too. The friction at the pins is reduced by greasing them with oil for bicycle chains.
As stated above, the speed of communication and measuring, particularly the angle readout, are crucial for sufficiently prompt control of the Zeeman machine. Therefore, the Python script for overseeing the rotary encoder state makes use of threaded callbacks and event detection, similar to the interruption of routines in microcontroller-based sensor applications. This technique keeps the response speed fast, and the computation load stays low ([26]). This approach is necessary for the described experiments since the determined limits for acceleration and velocity of the stepper motor are already at the mechanical limits. The angular velocity $\dot{\phi}$ is not measured directly but estimated numerically by a difference quotient with time-step size $\Delta t = 1/70\,\mathrm{s}$ since this is the inverse of the update rate of the angle. A state is considered stationary for the bifurcation-point continuation (4.3) when the tolerance for the distance $|\phi^* - \phi|$ between the measured angle and the target is $0.00175\,\mathrm{rad}$ ($\approx 0.1\,^\circ$), the tolerance limit for the absolute angular velocity is $0.00122\,\frac{\mathrm{rad}}{\mathrm{s}}$ ($\approx \frac{0.001^\circ}{0.0143\,\mathrm{s}}$), and the limit of the tolerance for the absolute angle acceleration $\ddot{\phi}$ is $0.00122\,\frac{\mathrm{rad}}{\mathrm{s}^2}$ ($\approx \frac{0.001^\circ \cdot \mathrm{s}^{-1}}{0.0143\,\mathrm{s}}$). Then, the next control target $(\phi^*)_{k+1} = (\phi^*)_k + 0.0349\,\mathrm{rad}$ ($\approx (\phi^*)_k + 2^\circ$) is set. For the bifurcation-point continuation (4.6), a state is considered to be a bifurcation point when additionally, the computed largest absolute value of the eigenvalues' real parts is $|\nu| < 0.5$. A new control target is set to $(\phi^*)_{k+1} = (\phi^*)_k + 0.0873\,\mathrm{rad}$ ($\approx (\phi^*)_k + 5^\circ$).

B

LINEARIZATION FOR THE CONTINUATION OF BIFURCATION POINTS FOR THE ZEEMAN CATASTROPHE MACHINE

From eq. (4.5) we know that the linearization matrix of the bifurcation-point control (4.3) has the following short-notation form

$$D\check{h} = \begin{pmatrix} 0 & 1 & 0 & 0 \\ \partial_{x_1} f_2 & \partial_{x_2} f_2 & \partial_\mu f_2 & \partial_\lambda f_2 \\ -K_P & -K_D & 0 & 0 \\ -K_B \cdot \partial_{x_1} \nu & -K_B \cdot \partial_{x_2} \nu & -K_B \cdot \partial_\mu \nu & -K_B \cdot \partial_\lambda \nu \end{pmatrix}.$$

For the model (3.19) of the Zeeman catastrophe machine, it holds

$$\partial_\phi L_1 = \frac{-a \cdot \rho \cdot \sin\phi}{L_1},$$
$$\partial_\phi L_2 = \frac{\rho \cdot (\lambda \cdot \sin\phi - \mu \cdot \cos\phi)}{L_2},$$

for eqs. (3.21) and (3.22), $\partial_\phi f_2 = -d$, and

$$\partial_\lambda f_2 = \frac{k}{m\rho}\left(\frac{L_0 \cdot \left(\lambda \cdot \mu \cdot \cos\phi - \lambda^2 \cdot \sin\phi - \mu \cdot \rho \cdot \cos^2\phi + \lambda \cdot \rho \cdot \sin\phi \cdot \cos\phi\right)}{\left(L_2\right)^{5/2}} - \frac{(L_2 - L_0) \cdot \sin\phi}{L_2} \right). \tag{B.1}$$

The largest real part ν of the eigenvalues of the linearization matrix

$$Df = \begin{pmatrix} 0 & 1 \\ \partial_\phi f_2 & -d \end{pmatrix}$$

of the original system $\dot{x} = f(x, \mu, \lambda)$ is

$$\nu = \begin{cases} -\frac{d}{2} + \sqrt{\frac{d^2 + 4 \cdot \partial_\phi f_2}{4}} & , \text{ if } \partial_\phi f_2 > -4d^2 \\ -\frac{d}{2} & , \text{ else.} \end{cases}$$

Since $d > 0$, the case $\nu = -\frac{d}{2}$ implies the stationary point is originally stable, we focuse on the case $\partial_\phi f_2 > -4d^2$. So, it holds for the partial derivatives of ν:

$$\partial_\phi \nu = \frac{1}{2} \cdot \left(\frac{d^2 + 4 \cdot \partial_\phi f_2}{4} \right)^{-1/2} \cdot \partial_\phi(\partial_\phi f_2),$$

with

$$\begin{aligned}\partial_\phi(\partial_\phi f_2) = \frac{k}{m\rho}\cdot\Bigg(&\frac{3\cdot a^2\cdot\rho\cdot L_0\cdot\sin^2\phi\cdot(\lambda\cdot\sin\phi-\mu\cdot\cos\phi)}{(L_1)^5}\\&-\frac{\cos\phi\cdot(2+a^2\cdot\rho\cdot L_0\cdot\sin\phi)}{(L_1)^3}+\frac{a\cdot L_0\cdot\sin\phi}{L_1}\\&+\frac{3\cdot\rho^2\cdot L_0\cdot(\lambda\cdot\sin\phi-\mu\cdot\cos\phi)^3}{(L_2)^5}\\&+\frac{(\rho\cdot L_0\cdot(\mu\cdot\cos\phi-\lambda\cdot\sin\phi)-1)\cdot(\lambda\cdot\cos\phi+\mu\cdot\sin\phi)}{(L_2)^3}\\&+\frac{L_0\cdot(\mu\cdot\cos\phi-\lambda\cdot\sin\phi)}{L_2}+(\lambda-a)\cdot\sin\phi-\mu\cdot\cos\phi\Bigg),\end{aligned}$$

$$\partial_{\dot\phi}\nu = 0\,,$$

$$\partial_\mu\nu = \frac{1}{2}\cdot\left(\frac{d^2+4\cdot\partial_\phi f_2}{4}\right)^{-1/2}\cdot\partial_\mu(\partial_\phi f_2)\,,$$

with

$$\begin{aligned}\partial_\mu(\partial_\phi f_2) = \frac{k}{m\rho}\Bigg(&\frac{\rho\cdot L_0\cdot(\mu-\rho\cdot\sin\phi)\cdot(\lambda\cdot\sin\phi-\mu\cdot\cos\phi)^2}{(L_2)^5}\\&+\frac{2\cdot\rho\cdot L_0\cdot\cos\phi\cdot(\lambda\cdot\sin\phi-\mu\cdot\cos\phi)}{(L_3)^2}\\&-\frac{L_0\cdot(\mu-\rho\cdot\sin\phi)\cdot(\mu\cdot\sin\phi+\lambda\cdot\cos\phi)}{(L_2)^{5/2}}-\frac{(L_2-L_0)\cdot\sin\phi}{L_2}\Bigg),\end{aligned}$$

where

$$\partial_\mu\left(\frac{L_2-L_0}{L_2}\right) = \frac{L_0}{(L_2)^{5/2}}\cdot(\mu-\sin\phi)\,,$$

$$\partial_\mu\left((L_2)^3\right) = 3\cdot L_2\cdot(\mu-\rho\cdot\sin\phi)\,,$$

and

$$\partial_\lambda\nu = \frac{1}{2}\cdot\left(\frac{d^2+4\cdot\partial_\phi f_2}{4}\right)^{-1/2}\cdot\partial_\lambda(\partial_\phi f_2)\,,$$

with

$$\begin{aligned}\partial_\lambda(\partial_\phi f_2) = \frac{k}{m\rho}\Bigg(&\frac{3\cdot\rho\cdot L_0\cdot(\lambda-\rho\cdot\cos\phi)\cdot(\lambda\cdot\sin\phi-\mu\cdot\cos\phi)}{(L_2)^5}\\&-\frac{2\cdot\rho\sin\phi\cdot(\lambda\cdot\sin\phi-\mu\cdot\cos\phi)}{(L_2)^3}\\&-\frac{L_0\cdot(\lambda-\rho\cdot\cos\phi)\cdot(\lambda\cdot\sin\phi-\mu\cdot\cos\phi)}{(L_2)^{5/2}}-\frac{(L_2-L_0)\cdot\cos\phi}{L_2}\Bigg),\end{aligned}$$

where

$$\partial_\lambda \left(\frac{L_2 - L_0}{L_2} \right) = \frac{L_0 \cdot (\lambda - \rho \cdot \cos\phi)}{(L_2)^{5/2}}$$
$$\partial_\mu \left((L_2)^3 \right) = 3 \cdot L_2 \cdot (\lambda - \rho \cdot \cos\phi) \ .$$

A numerical evaluation shows that the real parts of the eigenvalues of $D\check{h}$ are negative in a neighborhood around the bifurcation points for $K_P = -1 \frac{\text{mm}}{^\circ}$, $K_D = -1.5 \frac{\text{mm}\cdot\text{s}}{^\circ}$, and $K_B = 0.002\,\text{mm}$. For details see section 4.3.

C

CONTROL PARAMETER VALUES FOR PD CONTROL ON THE AFM MODEL

An overview of the found periodic orbits of the AFM model (5.8) with the corresponding values for the control parameters of the PD control (5.9) can be found in tables C.1 and C.2. The values of the first targets φ^* are chosen such that they have a distance of 0.02 rad to the phase corresponding to the previously found periodic orbit.
The target distance is decreased to 0.01 rad for the backward search after $\varphi^* = -1.1808$ for stability reasons.

Table C.1: Periodic orbits of AFM model (5.8) and control parameter values for the PD control (5.9) in forward direction (blue dots in fig. 5.5).

φ^* in rad	φ in rad	ω_{ex} in kHz	A in nm	K_P in s^2/rad	K_D in s/rad
−1.6229	−1.6229	51.147846	97.920	−10 000	8
−1.6429	−1.6438	51.147797	97.917	−10 000	8
−1.6629	−1.6624	51.135355	97.914	−10 000	8
−1.6829	−1.6836	51.134341	97.909	−10 000	8
−1.7029	−1.7023	51.120336	97.903	−10 000	8
−1.7229	−1.7235	51.113150	97.897	−10 000	8
−1.7429	−1.7395	51.080027	97.892	−10 000	7
−1.7629	−1.7614	51.074443	97.881	−10 000	7
−1.7829	−1.7892	51.049008	97.868	−10 000	7
−1.8029	−1.8021	51.027600	97.860	−12 000	9.5
−1.8229	−1.8225	51.008250	97.848	−12 000	9.5
−1.8429	−1.8412	50.971501	97.841	−12 000	9.5
−1.8629	−1.8640	50.937840	97.821	−12 000	9.5
−1.8829	−1.8854	50.905149	97.805	−12 000	9.5
−1.9029	−1.9035	50.874369	97.789	−12 000	10
−1.9229	−1.9227	50.841927	97.773	−12 000	10
−1.9429	−1.9431	50.794115	97.753	−5 000	12
−1.9629	−1.9595	50.807431	97.742	−4 000	12
−1.9829	−1.8977	50.689415	97.709	−6 000	12
−2.0029	−2.0019	50.691240	97.700	−6 000	12
−2.0229	−2.0263	50.572886	97.671	−6 000	12
−2.0429	−2.0422	50.560071	97.643	−6 000	12

φ^* in rad	φ in rad	ω_{ex} in kHz	A in nm	K_P in s^2/rad	K_D in s/rad
−2.0629	−2.0598	50.429818	97.648	−6 000	12

Table C.2: Periodic orbits of AFM model (5.8) and control parameter values for the PD control (5.9) in backward direction (red dots in fig. 5.5).

φ^* in rad	φ in rad	ω_{ex} in kHz	A in nm	K_P in s^2/rad	K_D in s/rad
−2.3208	−2.3202	49.981239	97.026	−10 000	6
−2.3008	−2.3000	49.986241	97.101	−10 000	6
−2.2808	−2.2809	49.990115	97.163	−10 000	6
−2.2608	−2.2616	50.003104	97.220	−9 000	10
−2.2408	−2.2400	50.038340	97.281	−6 000	11
−2.2208	−2.2215	50.073697	97.327	−8 000	12
−2.2008	−2.2018	50.115054	97.373	−6 500	12
−2.1808	−2.1814	50.170975	97.418	−10 000	12
−2.1708	−2.1701	50.200839	97.441	−6 500	12.5
−2.1608	−2.1617	50.224942	97.458	−6 500	12.5
−2.1508	−2.1505	50.286487	97.486	−8 000	12.75
−2.1408	−2.1417	50.274118	97.494	−6 000	12.75
−2.1308	−2.1299	50.192958	97.559	−6 000	13
−2.1208	−2.1218	50.425421	97.536	−4 000	13
−2.1108	−2.1121	50.334343	97.550	−5 500	12.9
−2.1008	−2.1005	50.398446	97.561	−6 000	12.9

D

TABLES OF SYMBOLS

A summary of symbols for variables and quantities used within the paper can be found in tables D.1 to D.5. The globally used symbols are listed in table D.1. The list of symbols for derivative-related quantities is table D.2. The specific variables for the models and experiments concerning the Zeeman catastrophe machine or the Atomic Force Microscope can be found in tables D.3 and D.4. The specific symbols used for the theory for the stroboscopic control are itemized in table D.5.

Table D.1: Globally used symbols

Symbol	Description
$\mathbf{o}$	matrix with only zero-entries
$\mathbb{1}$	identity matrix
$\alpha_1, \alpha_2, \alpha_3$	parameters for proportional control and extended proportional control
C	state matrix
D	input matrix
Df	linearization matrix of original dynamical system
F	discrete map (stroboscopic map in section 5.5)
f	continuous-time dynamical system
G	least-squares linearization matrix
g	dynamical system controlled by continuous-time proportional-control
Γ	coefficient matrix in least-squares method
Γ^+	Moore-Penrose pseudoinverse of Γ
$H_1,\ H_2,\ H_3$	Hurwitz determinants
K	feedback gain
K_B	bifurcation control parameter
K_D	differential control parameter
K_P	proportional control parameter
μ	bifurcation parameter
ν	eigenvalue
n	dimension of dynamical system
$p(\nu)$	characteristic polynomial
q	number of data points
R	controllability matrix
T	period length
t	time

Symbol	Description
t_0	initial time
u	input (control) vector
v	state vector
x	state of dynamical system
x^*	control target for x
$\bar{x}$	stationary point
x_0	initial value
y	target for the proportional control
$\hat{Z}$	collection of data points
$\hat{z}$	measured data of controlled dynamical system
ζ	solution of an initial value problem
Ψ	least-squares solution of $\dot{\hat{Z}} = \Psi\Gamma$
$(\bar{x}, \bar{\mu})$	stationary point of controlled system
$(\overline{\overline{x}}, \overline{\overline{\mu}}, \overline{\overline{\lambda}})$	bifurcation point of controlled system
$\|\cdot\|_F$	Frobenius norm

Table D.2: List of derivative-related symbols

Symbol	Description
$\frac{\mathrm{d}}{\mathrm{d}t}$	derivative with respect to time
$\dot{x}$	derivative of x with respect to time
$\partial_x f$	partial derivative of f with respect to x
$f_\mu,\ f_\lambda$	gradient of f with respect to μ or λ
Df	Jacobian of f

Table D.3: List of variables and quantities used for the model (3.19) of the Zeeman catastrophe machine

Parameter	Description	Values
A	fixed end of spring	$(-a, 0)$
a	negative x-coordinate of A	24.4 mm
B	movable end of spring	(λ, μ)
d	factor in damping constant δ	$1\,\mathrm{s}^{-1}$
δ	damping constant	$d \cdot m$
ϕ	angle	$(0, 2\pi)$

Symbol	Description	Values
ϕ^*	control target for ϕ	$(0, 2\pi)$
k	spring constant	$5\,\mathrm{N/m}$ and $1\,\mathrm{N/m}$
L_0	length of springs without tension	55 mm
L_1	length of spring to fixed end A	
L_2	length of spring to movable end B	
λ	x-coordinate of B	$[200, 280]$ mm
m	equivalent point mass of the disk	0.3 kg or 0.1 kg
μ	y-coordinate of B	$[-200, 200]$ mm
O	origin	$(0, 0)$
P	fixed point on edge of circular disk	
ρ	distance from P to O	65 mm
Δt	time step for update	$1/70$ s or 0.002 s

Table D.4: List of variables and quantities used for the model (5.8) of the Atomic Force Microscope

Parameter	Description	Values
a	acceleration of cantilever tip's position	
A_0	free amplitude	250 nm
A_{ex}	driving amplitude	
F_{ex}	excitation force	
F_{od}	oscillation damping force	
F_{sd}	sample damping force	
F_{sf}	surface force	
F_{sp}	spring force	
F_{tot}	total force	
ϕ	phase	
ϕ_{ex}	phase of driving signal	
ϕ_z	phase of cantilever tip	
φ	phase (shift)	$\phi_{ex} - \phi_z$
k	spring constant	$0.7\,\mathrm{N/m}$
m	mass of cantilever tip	
r	distance between atoms	
r_0	minimizer of V_{LJ}	2.8 nm
Q	quality factor	400
s	damping factor	$7 \cdot 10^{-4}\,\mathrm{nN \cdot nm^2 \cdot s}$

Symbol	Description	Values
σ	distance between atoms with $V_{LJ}(\sigma) = 0$	2.5 nm
V_0	depth of the potential well	$4.2 \cdot 10^{-18}$ J
V_{LJ}	Lennard-Jones potential	
v	cantilever's position velocity	
x	system's position	$(z, v)^T$
z	cantilever's actual position	
z_0	cantilever's equilibrium position	100 nm
Δz	softening parameter to avoid singularities	0.5 nm
ω_0	free resonance frequency	50 kHz
ω_{ex}	driving frequency	[48, 52] kHz

Table D.5: List of variables and symbols used for the stroboscopic control

Symbol	Description
DF_*	$DF(x_*, \mu_*)$ inside a fixed point
∂F_*	$\partial_\mu F(x_*, \mu_*)$ inside a fixed point
η	partial derivative $\partial_\mu \zeta$
F	stroboscopic map
$x_R,\ \mu_R$	reference values for the stroboscopic control
Ξ	linearization matrix of variational equation of stroboscopic control
ξ	control gain for the stroboscopic control
Y	fundamental matrix of variational equation of eq. (5.11)

BIBLIOGRAPHY

[1] E. H. Abed, H. O. Wang, and R. C. Chen. "Stabilization of period doubling bifurcations and implications for control of chaos." In: *Physica D: Nonlinear Phenomena* 70 (1) (1994), pp. 154–164. DOI: 10.1016/0167-2789(94)90062-0.

[2] M. Ashhab, M. V. Salapaka, M. Dahleh, and I. Mezić. "Control of Chaos in Atomic Force Microscopes." In: *Proceedings of the 1997 American Control Conference (Cat. No.97CH36041)*. Vol. 1. 1997, pp. 196–202. DOI: 10.1109/ACC.1997.611784.

[3] M. Ashhab, M. V. Salapaka, M. Dahleh, and I. Mezić. "Melnikov-Based Dynamical Analysis of Microcantilevers in Scanning Probe Microscopy." In: *Nonlinear Dynamics* 20 (3) (1999), pp. 197–220. DOI: 10.1023/A:1008342408448.

[4] M. Ashhab, M. V. Salapaka, M. Dahleh, and I. Mezić. "Dynamical analysis and control of microcantilevers." In: *Automatica* 35 (10) (1999), pp. 1663–1670. DOI: 10.1016/S0005-1098(99)00077-1.

[5] J. M. Balthazar, A. M. Tusset, and Á. M. Bueno. "TM-AFM nonlinear motion control with robustness analysis to parametric errors in the control signal determination." In: *Journal of Theoretical and Applied Mechanics* 52 (1) (2014), pp. 93–106. URL: http://www.ptmts.org.pl/jtam/index.php/jtam/article/view/v52n1p93.

[6] D. A. W. Barton. "Control-based continuation: Bifurcation and stability analysis for physical experiments." In: *Mechanical Systems and Signal Processing* 84 (2017), pp. 54–64. DOI: 10.1016/j.ymssp.2015.12.039.

[7] D. A. W. Barton and J. Sieber. "Systematic experimental exploration of bifurcations with noninvasive control." In: *Physical Review E* 87 (5) (2013), p. 052916. DOI: 10.1103/PhysRevE.87.052916.

[8] V. Belevitch. *Classical Network Theory*. San Francisco: Holden-Day, 1968.

[9] R. Bellman. "The stability of solutions of linear differential equations." In: *Duke Mathematical Journal* 10 (4) (1943), pp. 643 –647. DOI: 10.1215/S0012-7094-43-01059-2.

[10] P. R. Bevington and D. K. Robinson. *Data reduction and error analysis for the physical sciences*. 3rd ed. Boston: McGraw-Hill, 2003.

[11] G. Binnig, C. F. Quate, and C. Gerber. "Atomic Force Microscope." In: *Physical Review Letters* 56 (9) (1986), pp. 930–933. DOI: 10.1103/PhysRevLett.56.930.

[12] G. Binnig, H. Rohrer, C. Gerber, and E. Weibel. "Tunneling through a controllable vacuum gap." In: *Applied Physics Letters* 40 (2) (1982), pp. 178–180. DOI: 10.1063/1.92999.

[13] G. Binnig, H. Rohrer, C. Gerber, and E. Weibel. "Surface Studies by Scanning Tunneling Microscopy." In: *Physical Review Letters* 49 (1) (1982), pp. 57–61. DOI: 10.1103/PhysRevLett.49.57.

[14] G. Binnig, H. Rohrer, C. Gerber, and E. Weibel. "7 × 7 Reconstruction on Si(111) Resolved in Real Space." In: *Physical Review Letters* 50 (2) (1983), pp. 120–123. DOI: 10.1103/PhysRevLett.50.120.

[15] B. Birnir. *Dynamical Systems Theory*. University of California, Santa Barbara, 2008. URL: https://birnir.math.ucsb.edu/files/bjorn/class-documents/main.pdf (visited on May 23, 2023).

[16] S. Bosch. *Lineare Algebra: Ein Grundkurs mit Aufgabentrainer*. 6th ed. Berlin: Springer Spektrum, 2021. DOI: 10.1007/978-3-662-62616-0.

[17] S. L. Brunton, J. L. Proctor, and J. N. Kutz. "Discovering governing equations from data by sparse identification of nonlinear dynamical systems." In: *PNAS* 113 (15) (2016), pp. 3932–3937. DOI: 10.1073/pnas.1517384113.

[18] E. Bureau, F. Schilder, M. Elmegård, I. F. Santos, J. J. Thomsen, and J. Starke. "Experimental bifurcation analysis of an impact oscillator - Determining stability." In: *Journal of Sound and Vibration* 333 (21) (2014), pp. 5465–5474. DOI: 10.1016/j.jsv.2014.05.032.

[19] E. Bureau, F. Schilder, I. F. Santos, J. J. Thomsen, and J. Starke. "Experimental bifurcation analysis of an impact oscillator - Tuning a non-invasive control scheme." In: *Journal of Sound and Vibration* 332 (22) (2013), pp. 5883–5897. DOI: 10.1016/j.jsv.2013.05.033.

[20] A. Cayley. "A Memoir on the Theory of Matrices." In: *Philosophical Transactions of the Royal Society of London* 158 (1858), pp. 17–37. URL: https://www.jstor.org/stable/pdf/108649.

[21] A. Cazzolli, D. Misseroni, and F. Dal Corso. "Elastica catastrophe machine: theory, design and experiments." In: *Journal of the Mechanics and Physics of Solids* 136 (2020), p. 103735. DOI: 10.1016/j.jmps.2019.103735.

[22] A. Chandrashekar, P. Belardinelli, M. A. Bessa, U. Staufer, and F. Alijani. "Quantifying nanoscale forces using machine learning in dynamic atomic force microscopy." In: *Nanoscale Advances* 4 (2022), pp. 2134–2143. DOI: 10.1039/d2na00011c.

[23] H. Cho, M.-F. Yu, A. F. Vakakis, L. A. Bergman, and D. M. McFarland. "Dynamics of microcantilever integrated with geometric nonlinearity for stable and broadband nonlinear atomic force microscopy." In: *Surface Science* 606 (17) (2012), pp. L74–L78. DOI: 10.1016/j.susc.2012.05.009.

[24] J. P. Cleveland, B. Anczykowski, A. E. Schmid, and V. B. Elings. "Energy dissipation in tapping-mode atomic force microscopy." In: *Applied Physics Letters* 72 (20) (1998), pp. 2613–2615. DOI: 10.1063/1.121434.

[25] D. Davidovikj, F. Alijani, S. J. Cartamil-Bueno, H. S. J. van der Zant, M. Amabili, and P. G. Steeneken. "Nonlinear dynamic characterization of two-dimensional materials." In: *Nature Communications* 8 (1) (2017). DOI: 10.1038/s41467-017-01351-4.

[26] A. Dittus, N. Kruse, I. Barke, S. Speller, and J. Starke. "Detecting Stability and Bifurcation Points in Control-Based Continuation for a Physical Experiment of the Zeeman Catastrophe Machine." In: *SIAM Journal on Applied Dynamical Systems* 22 (2) (2023), pp. 1275–1299. DOI: 10.1137/22M1503245.

[27] A. Dittus, N. Kruse, H. Wallner, L. Böttcher, I. Barke, S. Speller, J. Starke, and W. Just. "Stroboscopic control and tracking of periodic states." In: *Nonlinear Dynamics* (2023). DOI: 10.1007/s11071-023-09105-2.

[28] E. Doedel, H. B. Keller, and J. P. Kernévez. "Numerical Analysis and Control of Bifurcation Problems (I): Bifurcation in Finite Dimensions." In: *International Journal of Bifurcation and Chaos* 1 (3) (1991), pp. 493–520. DOI: 10.1142/S0218127491000397.

[29] E. Doedel, H. B. Keller, and J. P. Kernévez. "Numerical Analysis and Control of Bifurcation Problems (II): Bifurcation in Finite Dimensions." In: *International Journal of Bifurcation and Chaos* 1 (4) (1991), pp. 745–772. DOI: 10.1142/S0218127491000555.

[30] R. Eisenschitz and F. London. "Über das Verhältnis der van der Waalschen Kräfte zu den homöopolaren Bindungskräften." In: *Zeitschrift für Physik* 60 (7–8) (1930), pp. 491–527. DOI: 10.1007/BF01341258.

[31] Fritz Kübler GmbH. *Measuring wheels*. URL: https://www.kuebler.com/en/products/measurement/linear-measuring-systems/product-finder/product-details/Measuring_wheels (visited on June 27, 2023).

[32] Fritz Kübler GmbH. *Sendix 5000*. URL: https://www.kuebler.com/en/products/measurement/encoders/product-finder/product-details/5000 (visited on June 10, 2022).

[33] F. G. Frobenius. "Ueber lineare Substitutionen und bilinear Formen." In: *Journal für die reine und angewandte Mathematik (Crelles Journal)* 1878 (84) (1878), pp. 1–63. DOI: 10.1515/crelle-1878-18788403.

[34] E. G. Gilbert. "Controllability and observability in multivariable control systems." In: *Journal of the Society for Industrial and Applied Mathematics Series A Control* 1 (2) (1963), pp. 128–151. DOI: 10.1137/0301009.

[35] GitHub. *Grbl*. Version 1.1h. 2019. URL: https://github.com/grbl/grbl (visited on June 10, 2022).

[36] P. Gleyzes, P. K. Kuo, and A. C. Boccara. "Bistable behavior of a vibrating tip near a solid surface." In: *Applied Physics Letters* 58 (25) (1991), pp. 2989–2991. DOI: 10.1063/1.104690.

[37] E. I. Green. "The Story of Q." In: *American Scientist* 43 (4) (1955), pp. 584–594. URL: http://www.jstor.org/stable/27826701 (visited on June 5, 2023).

[38] D. M. Grobman. "Homeomorphism of systems of differential equations." In: *Doklady Akademii Nauk SSSR* 128 (5) (1959), pp. 880–881.

[39] T. H. Gronwall. "Note on the Derivatives with Respect to a Parameter of the Solutions of a System of Differential Equations." In: *Annals of Mathematics* 20 (4) (1919), pp. 292 –296. DOI: 10.2307/1967124.

[40] J. Guckenheimer. "The Cusps of Zeeman's Catastrophe Machine." In: *Topology* 16 (2) (1977), pp. 177–180. DOI: 10.1016/0040-9383(77)90016-7.

[41] W. Hahn. *Stability of Motion*. Berlin, Heidelberg: Springer, 1967. DOI: 10.1007/978-3-642-50085-5.

[42] J. K. Hale and H. Koçak. *Dynamics and Bifurcations*. New York, NY: Springer New York, 1991. DOI: 10.1007/978-1-4612-4426-4_1.

[43] W. R. Hamilton. "On a New and General Method of Inverting a Linear and Quaternion Function of a Quaternion." In: *Proceedings of the Royal Irish Academy* 8 (1862), pp. 182–184. URL: https://www.jstor.org/stable/20488818.

[44] W. R. Hamilton. "On the Existence of a Symbolic and Biquadratic Equation which is satisfied by the Symbol of Linear or Distributive Operation on a Quaternion." In: *The London, Edinburgh, and Dublin Philosophical Magazine and Journal of Science* 24 (1862), pp. 127–128.

[45] W. R. Hamilton. "On the Existence of a Symbolic and Biquadratic Equation, which is satisfied by the Symbol of Linear Operation in Quaternions." In: *Proceedings of the Royal Irish Academy* 8 (1864), pp. 190–191.

[46] J. Han, N. M. Pugno, and S. Ryu. "Nanoindentation cannot accurately predict the tensile strength of graphene or other 2D materials." In: *Nanoscale* 7 (38 2015), pp. 5672–15679. DOI: 10.1039/C5NR04134A.

[47] P. Hartman. "A Lemma in the Theory of Structural Stability of Differential Equations." In: *Proceedings of the American Mathematical Society* 11 (4) (1960), pp. 610–620. DOI: 10.2307/2034720.

[48] M. A. Hassouneh, H.-C. Lee, and E. H. Abed. "Washout Filters in Feedback Control: Benefits, Limitations and Extensions." In: *Proceedings of the 2004 American Control Conference*. Vol. 5. 2004, pp. 3950–3955. DOI: 10.23919/ACC.2004.1383925.

[49] G. Haugstad. *Atomic Force Microscopy: Understanding Basic Modes and Advanced Applications*. Hoboken, New Jersey: Wiley, 2012. DOI: 10.1002/9781118360668.

[50] M. L. J. Hautus. "Controllability and observability condition of linear autonomous systems." In: *Proceedings of the Koninklijke Nederlandse Akademie van Wetenschappen, Series A* 72 (1969), pp. 443–448.

[51] M. W. Hirsch and S. Smale. *Differential Equations, Dynamical Systems, and Linear Algebra*. New York, San Francisco, London: Academic Press, 1974. URL: https://www.sciencedirect.com/bookseries/pure-and-applied-mathematics/vol/60/suppl/C.

[52] A. Hurwitz. "Über die Bedingungen, unter welchen eine Gleichung nur Wurzeln mit negativen reellen Theilen besitzt." In: *Mathematische Annalen* 46 (1895), pp. 273–284. DOI: 10.1007/BF01446812.

[53] L. Illing, D. J. Gauthier, and J. N. Blakely. "Controlling Fast Chaos in Optoelectronic Delay Dynamical Systems." In: *Handbook of Chaos Control*. Ed. by E. Schöll and H. G. Schuster. Weinheim: Wiley-VCH, 2007. Chap. 19, pp. 405–425. DOI: 10.1002/9783527622313.ch19.

[54] J. E. Jones. "On the determination of molecular fiedls. - I. From the variation of the viscosity of a gas with temperature." In: *Proceedings of the Royal Society London A* 106 (738) (1924), pp. 441–462. DOI: 10.1098/rspa.1924.0081.

[55] J. E. Jones. "On the determination of molecular fields. —II. From the equation of state of a gas." In: *Proceedings of the Royal Society London A* 106 (738) (1924), pp. 463–477. DOI: 10.1098/rspa.1924.0081.

[56] E. I. Jury. "A Simplified Stability Criterion for Linear Discrete Systems." In: *Proceedings of the IRE* 50 (6) (1962), pp. 1493–500. DOI: 10.1109/JRPROC.1962.288193.

[57] R. E. Kalman. "Contributions to the Theory of Optimal Control." In: *Boletin de la Sociedad Matematica Mexicana* 5 (2) (1960), pp. 102–119.

[58] H. B. Keller. "Numerical Solution of Bifurcation and Nonlinear Eigenvalue Problems." In: *Applications of Bifurcation Theory*. Ed. by P. H. Rabinowitz. New York: Academic Press, 1977, pp. 359–384.

[59] H. B. Keller. "Constructive methods for bifurcation and nonlinear eigenvalue problems." In: *Computing Methods in Applied Sciences and Engineering, 1977, I*. Ed. by R. Glowinski and J. L. Lions. Berlin, Heidelberg: Springer-Verlag, 1979, pp. 241–251. DOI: 10.1007/BFb0063623.

[60] I. Z. Kiss, Z. Kazsu, and V. Gáspár. "Tracking unstable steady states and periodic orbits of oscillatory and chaotic electrochemical systems using delayed feedback control." In: *Chaos: An Interdisciplinary Journal of Nonlinear Science* 16 (3) (2006), p. 033109. DOI: 10.1063/1.2219702.

[61] Y. A. Kuznetsov. *Elements of Applied Bifurcation Theory*. 2nd ed. Applied Mathematical Sciences 112. New York, Berlin, Heidelberg: Springer, 1998. DOI: 10.1007/b98848.

[62] H.-C. Lee and E. H. Abed. "Washout Filters in the Bifurcation Control of High Alpha Flight Dynamics." In: *1991 American Control Conference*. Evanston: American Automatic Control Council, pp. 206–211. DOI: 10.23919/ACC.1991.4791359.

[63] J. E. Lennard-Jones. "Cohesion." In: *Proceedings of the Physical Society* 43 (5) (1931), pp. 461–482. DOI: 10.1088/0959-5309/43/5/301.

[64] Y. Li and H. Dankowicz. "Adaptive control designs for control-based continuation in a class of uncertain discrete-time dynamical systems." In: *Journal of Vibration and Control* 26 (21–22) (2020), pp. 2092–2109.

[65] T. J. Litherland and A. Siahmakoun. "Chaotic behavior of the Zeeman Catastrophe Machine." In: *American Journal of Physics* 63 (5) (1995), pp. 426–431. DOI: 10.1119/1.17906.

[66] F. London. "Zur Theorie und Systematik der Molekularkräfte." In: *Zeitschrift für Physik* 63 (3–4) (1930), pp. 245–279. DOI: 10.1007/BF01421741.

[67] F. London. "The general theory of molecular forces." In: *Transactions of the Faraday Society* 33 (1937), pp. 8–26. DOI: 10.1039/TF937330008B.

[68] J. Lunze. *Regelungstechnik 2: Mehrgrößensysteme, Digitale Regelung*. 10th ed. Berlin: Springer Vieweg, 2020. DOI: 10.1007/978-3-662-60760-2.

[69] B. Marx and W. Vogt. *Dynamische Systeme. Theorie und Numerik*. Heidelberg: Spektrum Akademischer Verlag, 2011. DOI: 10.1007/978-3-8274-2448-8.

[70] S. Misra, H. Dankowicz, and M. R. Paul. "Event-driven feedback tracking and control of tapping-mode atomic force microscopy." In: *Proceedings of the Royal Society A: Mathematical, Physical and Engineering Sciences* 464 (2096) (2008), pp. 2113–2133. DOI: 10.1098/rspa.2007.0016.

[71] NANOSENSORS. *Special Developments List*. version 5.8. URL: https://www.nanosensors.com/pdf/SpecialDevelopmentsList.pdf (visited on Mar. 23, 2023).

[72] P. Nagy and P. Tasnádi. "Zeeman catastrophe machines as a toolkit for teaching chaos." In: *European Journal of Physics* 35 (1) (2014), p. 015018. DOI: 10.1088/0143-0807/35/1/015018.

[73] P. Nagy and P. Tasnádi. "Visualization of chaotic attractors in 3D as motivating tool for introductory physics course." In: *Journal of Physics: Conference Series* 1286 (1) (2019), p. 012028. DOI: 10.1088/1742-6596/1286/1/012028.

[74] H. Nakajima. "On analytical properties of delayed feedback control of chaos." In: *Physics Letters A* 232 (3) (1997), pp. 207–210. DOI: 10.1016/S0375-9601(97)00362-9.

[75] M. Net and J. J. Sánchez. "Continuation of Bifurcations of Periodic Orbits for Large-Scale Systems." In: *SIAM Journal on Applied Dynamical Systems* 14 (2) (2015), pp. 674–698. DOI: 10.1137/140981010.

[76] NobelPrize.org. *The Nobel Prize in Physics 1986*. 1986. URL: https://www.nobelprize.org/prizes/physics/1986/summary/ (visited on Mar. 1, 2023).

[77] R. Nozaki, J. M. Balthazar, A. M. Tusset, B. R. de Pontes, and Á. M. Bueno. "Nonlinear Control System Applied to Atomic Force Microscope Including Parametric Errors." In: *Journal of Control, Automation and Electrical Systems* 24 (3) (2013), pp. 223–231. DOI: 10.1007/s40313-013-0034-1.

[78] E. Ott, C. Grebogi, and J. A. Yorke. "Controlling chaos." In: *Physical Review Letters* 64 (11) (1990), pp. 1196–1199. DOI: 10.1103/PhysRevLett.64.1196.

[79] I. Panagiotopoulos, J. Starke, and W. Just. "Control of collective human behavior: Social dynamics beyond modeling." In: *Physical Review Research* 4 (4) (2022), p. 043190. DOI: 10.1103/PhysRevResearch.4.043190.

[80] I. Panagiotopoulos, J. Starke, J. Sieber, and W. Just. "Continuation with Non-invasive Control Schemes: Revealing Unstable States in a Pedestrian Evacuation Scenario." In: *SIAM Journal on Applied Dynamical Systems* 22 (1) (2023), pp. 1–36. DOI: 10.1137/22M1482032.

[81] W. Pauli. "Über den Zusammenhang des Abschlusses der Elektronengruppen im Atom mit der Komplexstruktur der Spektren." In: *Zeitschrift für Physik* 31 (1) (1925), pp. 765–783. DOI: 10.1007/BF02980631.

[82] A. Penner. "Characterization of bifurcations in the Zeeman catastrophe machine using singular value decomposition." In: *Chaos, Solitons & Fractals* 148 (2021), p. 111054. DOI: 10.1016/j.chaos.2021.111054.

[83] M. Planitz. "Inconsistent Systems of Linear Equations." In: *The Mathematical Gazette* 63 (425) (1979), pp. 181–185. DOI: 10.2307/3617890.

[84] V. M. Popov. *Hyperstability of Control Systems*. Berlin, Heidelberg: Springer, 1973.

[85] T. Poston and A. E. R. Woodcock. "Zeeman's Catastrophe Machine." In: *Mathematical Proceedings of the Cambridge Philosophical Society* 74 (2) (1973), pp. 217–226. DOI: 10.1017/S0305004100048003.

[86] W. H. Press, S. A. Teukolsky, W. T. Vetterling, and B. P. Flannery. *Numerical recipes in C: The art of scientific computing*. Cambridge: Cambridge University Press, 1986.

[87] K. Pyragas. "Continuous control of chaos by self-controlling feedback." In: *Physics Letters A* 170 (6) (1992), pp. 421–428. DOI: 10.1016/0375-9601(92)90745-8.

[88] K. Pyragas, V. Pyragas, I. Z. Kiss, and J. L. Hudson. "Stabilizing and Tracking Unknown Steady States of Dynamical Systems." In: *Physical Review Letters* 89 (24) (2002). DOI: 10.1103/PhysRevLett.89.244103.

[89] K. Pyragas, V. Pyragas, I. Z. Kiss, and J. L. Hudson. "Adaptive control of unknown unstable steady states of dynamical systems." In: *Physical Review E* 70 (2) (2004), p. 026215. DOI: 10.1103/PhysRevE.70.026215.

[90] A. Raman and D. Kiracofe. "Nonlinear dynamics of atomic force microscope microcantilevers in liquid environments - a review." In: *Nonlinear Theory and Its Applications, IEICE* 4 (3) (2013), pp. 184–197. DOI: 10.1587/nolta.4.184.

[91] A. Rauh, R. Dehnert, S. Romig, S. Lerch, and B. Tibken. "Iterative Solution of Linear Matrix Inequalities for the Combined Control and Observer Design of Systems with Polytopic Parameter Uncertainty and Stochastic Noise." In: *Algorithms* 14 (7) (2021). DOI: 10.3390/a14070205.

[92] G. Rega and V. Settimi. "Bifurcation, response scenarios and dynamic integrity in a single-mode model of noncontact atomic force microscopy." In: *Nonlinear Dynamics* 73 (1) (2013), pp. 101–123. DOI: 10.1007/s11071-013-0771-5.

[93] L. Renson, D. A. W. Barton, and S. A. Neild. "Experimental Tracking of Limit-Point Bifurcations and Backbone Curves Using Control-Based Continuation." In: *International Journal of Bifurcation and Chaos* 27 (1) (2017), p. 1730002. DOI: 10.1142/S0218127417300026.

[94] L. Renson, A. Gonzalez-Buelga, D. A.W. Barton, and S. A. Neild. "Robust identification of backbone curves using control-based continuation." In: *Journal of Sound and Vibration* 367 (2016), pp. 145–158. DOI: 10.1016/j.jsv.2015.12.035.

[95] E. J. Routh. *A Treatise on the Stability of a Given State of Motion, particulalry Steady Motion*. London: Macmilland and co., 1877.

[96] H. Salarieh and A. Alasty. "Stabilizing unstable fixed points of chaotic maps via minimum entropy control." In: *Chaos, Solitons & Fractals* 37 (3) (2008), pp. 763–769. DOI: 10.1016/j.chaos.2006.09.062.

[97] S. Santos, K. Gadelrab, C.-Y. Lai, T. Olukan, J. Font, V. Barcons, A. Verdaguer, and M. Chiesa. "Advances in dynamic AFM: From nanoscale energy dissipation to material properties in the nanoscale." In: *Journal of Applied Physics* 129 (13) (2021), p. 134302. DOI: 10.1063/5.0041366.

[98] F. Schilder, E. Bureau, I. F. Santos, J. J. Thomsen, and J. Starke. "Experimental bifurcation analysis - Continuation for noise-contaminated zero problems." In: *Journal of Sound and Vibration* 358 (2015), pp. 251–266. DOI: 10.1016/j.jsv.2015.08.008.

[99] V. Settimi, O. Gottlieb, and G. Rega. "Asymptotic analysis of a noncontact AFM microcantilever sensor with external feedback control." In: *Nonlinear Dynamics* 79 (4) (2015), pp. 2675–2698. DOI: 10.1007/s11071-014-1840-0.

[100] J. Sieber, A. Gonzalez-Buelga, S. A. Neild, D. J. Wagg, and B. Krauskopf. "Experimental continuation of periodic orbits through a fold." In: *Physical Review Letters* 100 (24) (2008), p. 244101. DOI: 10.1103/PhysRevLett.100.244101.

[101] J. Sieber and B. Krauskopf. "Control based bifurcation analysis for experiments." In: *Nonlinear Dynamics* 51 (3) (2008), pp. 365–377. DOI: 10.1007/s11071-007-9217-2.

[102] C. I. Siettos, I. G. Kevrekidis, and D. Maroudas. "Coarse bifurcation diagrams via microscopic simulators: a state-feedback control-based approach." In: *International Jorunal of Bifurcations and Chaos* 14 (1) (2004), pp. 207–220. DOI: 10.1142/S0218127404009193.

[103] T. Söderström and P. Stoica. *System identification*. New York et al.: Prentice-Hall, 1989.

[104] E. D. Sontag. *Mathematical control theory: deterministic finite dimensional systems*. 2nd ed. Texts in Applied Mathematics. New York, Heidelberg et al.: Springer Science & Business Media, 1998. DOI: 10.1007/978-1-4612-0577-7.

[105] R. W. Stark. "Bistability, higher harmonics, and chaos in AFM." In: *Materials Today* 13 (9) (2010), pp. 24–32. DOI: 10.1016/S1369-7021(10)70162-0.

[106] R. W. Stark and W. M. Heckl. "Fourier transformed atomic force microscopy: tapping mode atomic force microscopy beyond the Hookian approximation." In: *Surface Science* 457 (1) (2000), pp. 219–228. DOI: 10.1016/S0039-6028(00)00378-2.

[107] R. W. Stark, G. Schitter, and A. Stemmer. "Tuning the interaction forces in tapping mode atomic force microscopy." In: *Physical Review B* 68 (8) (2003), p. 085401. DOI: 10.1103/PhysRevB.68.085401.

[108] G. Strang. *Linear algebra and its applications*. 3rd ed. Fort Worth etc.: Harcourt Brave Jovanovich, 1988.

[109] S. H. Strogatz. *Nonlinear Dynamics and Chaos: With Applications to Physics, Biology, Chemistry, and Engineering*. 2nd ed. Boca Raton, London, New York: CRC Press Taylor & Francis Group, 2014.

[110] P. Thota, S. MacLaren, and H. Dankowicz. "Controlling bistability in tapping-mode atomic force microscopy using dual-frequency excitation." In: *Applied Physics Letters* 91 (9) (2007), p. 093108. DOI: 10.1063/1.2775031.

[111] M. Toda. "Studies of a non-linear lattice." In: *Physics Reports* 18 (1) (1975), pp. 1–123. DOI: 10.1016/0370-1573(75)90018-6.

[112] D. Vella and B. Davidovitch. "Indentation metrology of clamped, ultra-thin elastic sheets." In: *Soft Matter* 13 (11) (2017), pp. 2264–2278. DOI: 10.1039/C6SM02451C.

[113] B. Voigtländer. *Atomic Force Microscopy*. 2nd ed. NanoScience and Technology. Cham: Springer Nature Switzerland, 2019. DOI: 10.1007/978-3-030-13654-3.

[114] J. D. van der Waals. "Over de Continuiteit van den Gas- en Vloeistoftoestand." PhD thesis. Leiden, The Netherlands: Hoogeschool te Leiden, 1873.

[115] H. O. Wang and E. H. Abed. "Bifurcation control of a chaotic system." In: *Automatica* 31 (9) (1995), pp. 1213–1226. DOI: 10.1016/0005-1098(94)00146-A.

[116] L. Wang. "Analytical descriptions of the tapping-mode atomic force microscopy response." In: *Applied Physics Letters* 73 (25) (1998), pp. 3781–3783. DOI: 10.1063/1.122893.

[117] W. van de Water and J. Molenaar. "Dynamics of vibrating atomic force microscopy." In: *Nanotechnology* 11 (3) (2000), pp. 192–199. DOI: 10.1088/0957-4484/11/3/310.

[118] S. Wiggins. *Introduction to Applied Nonlinear Dynamical Systems and Chaos*. New York: Springer, 1990. DOI: 10.1007/978-1-4757-4067-7.

[119] K. Yagasaki. "Bifurcations and chaos in vibrating microcantilevers of tapping mode atomic force microscopy." In: *International Journal of Non-Linear Mechanics* 42 (4) (2007), pp. 658–672. DOI: doi.org/10.1016/j.ijnonlinmec.2007.01.009.

[120] K. Yamasue and T. Hikihara. "Control of microcantilevers in dynamic force microscopy using time delayed feedback." In: *Review of Scientific Instruments* 77 (5) (2006), p. 053703. DOI: 10.1063/1.2200747.

[121] K. Yamasue, K. Kobayashi, H. Yamada, K. Matsushige, and T. Hikihara. "Controlling chaos in dynamic-mode atomic force microscope." In: *Physics Letters A* 373 (35) (2009), pp. 3140–3144. DOI: 10.1016/j.physleta.2009.07.009.

[122] R. Young, J. Ward, and F. Scire. "The Topografiner: An Instrument for Measuring Surface Microtopography." In: *Review of Scientific Instruments* 43 (7) (1972), pp. 999–1011. DOI: 10.1063/1.1685846.

[123] E. C. Zeeman. "A catastrophe machine." In: *Biological Process in Living Systems*. Ed. by C. H. Waddington. Vol. 4. Toward a Theoretical Biology. Edinburgh: Edinburgh University Press, 1972, pp. 276–282. DOI: 10.4324/9781351297165.

[124] E. C. Zeeman. "Catastrophe theory." In: *Scientific American* 234 (4) (1976), pp. 65–83. URL: http://www.jstor.org/stable/24950329.

[125] E. C. Zeeman. "Catastrophe theory." In: *Structural Stability in Physics*. Ed. by W. Güttinger and H. Eikemeier. Berlin, Heidelberg: Springer, 1979, pp. 12–22. DOI: 10.1007/978-3-642-67363-4_3.

[126] K. J. Åström. "Adaptive feedback control." In: *Proceedings of the IEEE* 75 (2) (1987), pp. 185–217. DOI: 10.1109/PROC.1987.13721.

SELBSTSTÄNDIGKEITSERKLÄRUNG

Ich versichere eidesstattlich durch eigenhändige Unterschrift, die vorliegende Arbeit selbstständig und ohne fremde Hilfe verfasst zu haben. Dazu habe ich keine anderen als die angegebenen Hilfsmittel und Quellen verwendet. Alle Stellen, die wörtlich oder sinngemäß aus den genannten Werken entnommen sind, habe ich als solche kenntlich gemacht.
Aus Datenschutzgründen ist in dieser Online-Fassung keine Originalunterschrift enthalten.

Rostock, den

Anna Dittus